Hydrodynamic and water quality modelling of a shallow lake influenced by stormwater discharge from an active goldmine

A thesis presented to

The Faculty of Graduate Studies

of

Lakehead University

By

Michael D.B. St James

In partial fulfilment of the requirements

for the degree of

Master of Science in Biology

January 17th 2020

Abstract

Several mine-influenced lakes have become meromictic in Northwestern Ontario, a state in which complete turnover of the water column does not occur. Whether or not a lake experiences complete turnover has a significant impact on dissolved oxygen, nutrient cycling, available fish habitat and the production of potentially toxic compounds. Lower Unnamed Lake is the stormwater receiving body for Barrick Gold's Hemlo Gold mine. The mine-influenced water discharged into Lower Unnamed Lake is laden with a high concentration of total dissolved solids. Rather than freely mixing with the lake water, the mine influenced water sank to the bottom of the lake as a result of the density difference between the discharge and the lake water in the receiving body. It was of concern that stratification, induced by the density gradient, caused by the concentration of total dissolved solids had stabilized the lake and prevented turnover, causing Lower Unnamed Lake to become meromictic. This study used CE-QUAL W2 to create a hydrodynamic and water quality model of Lower Unnamed Lake, in order to evaluate mixing trends. Full turnover was predicted in the fall and two additional mixing events were produced by the model. The mixing events are evident in field observations of the lake outflow total dissolved solids, temperature and in-lake profiles of temperature, total dissolved solids and dissolved oxygen. It was determined that Lower Unnamed Lake was not meromictic. The location of stormwater discharge was relocated within the lake model in order to promote mixing of mine-influenced and natural lake water and prevent chemical stratification. Although modifying the discharge location did eliminate chemical stratification, it also resulted in increased total dissolved solids in the east basin of the lake and decreased concentration of hypolimnion dissolved oxygen and an increase in hypolimnion temperature in the west basin for a portion of the model run period. A model

was developed that eliminated discharge from Pond 102 and the results suggest that the proposed discharge location would result in similar hydrodynamics, temperature and dissolved oxygen as if Lower Unnamed Lake did not receive discharge from Pond 102. Model parameters were modified, and it was determined that the model with the current discharge location has the potential to become, while the model with the proposed discharge location did not. The model developed by this study can be used by Williams mine to determine if future discharge regimes will cause Lower Unnamed Lake to become meromictic, and if so, the location of Pond 102 discharge may be relocated to the proposed location, to inhibit chemical stratification and promote mixing.

Acknowledgements

I would like to thank my supervisor, Dr. Peter Lee, and my committee members; Dr Kam Leung, and Dr. Michael Rennie, for their guidance and patience throughout my thesis. Without their input, expertise and belief in me, this would not have been possible. Many thanks go out to my external examiner, Dr. Robert Stewart, who took time out of his busy schedule to review my thesis on short notice.

Thank you to the Lakehead University Environmental Laboratory, Johane Joncas & Julie Roberto for talking the time to teach me lab skills and techniques. The guidance I received from Daniel Brazeau & Susanne Walford was of vital importance in this journey. I would also like to thank my former office-mate, Kristi Dysievick for always being there to bounce ideas off and share a laugh. I would also like to thank my office mate, field assistant and one of my best friends, Adam Pun, who suffered along side me, through field work and behind the desk.

Thank you to Barrick Gold for supporting this research, and to Shane Hays and Jeremy Dart, who where very helpful in the collaboration.

I would like to thank my entire family for being there for me throughout my life and have been particularly supportive throughout this time. I couldn't imagine trying to get through life without such a supportive team behind me.

Lastly, but not least, I would like to thank Lakehead University and the entirety of the faculty and staff.

"All models are wrong, but some are useful"

-George Box

Table of Contents

List of Figures

List of Appendices

1 Literature Review

1.1 Stormwater Drainage

Gold mining requires the removal of non-economically viable ore to gain access to the precious veins hidden underground. Excavation results in large heaps of ore - herein referred to as *mine-rock*, which is stored on-site (Smith *et al.,* 2007). As mechanical and chemical weathering occurs, chemical constituents erode from the waste rock heaps, into the local watershed, as stormwater runoff (Winde & van der Walt, 2004). The chemical composition and subsequent risk of contamination from mine-rock can vary greatly, depending on regional geology, depositional morphology, climate and temporal factors (Khalil *et al.,* 2013). Contaminants - including heavy metals - are eroded and transported from the site, where they can generate secondary contamination in soil, water, and air (Moore and Luoma, 1990).

One key factor determining the composition of stormwater runoff is the sulfide/carbonate ratio of mine-rock. A high sulphide/carbonate ratio can lead to acid rock drainage (ARD) (Capanema & Ciminelli, 2003). If the mine rock contains a higher proportion of carbonates or silicates, the stormwater will have circumneutral pH and is termed neutral rock drainage (NRD) (Balistrieri *et al.,* 1999). The rate of chemical dissolution for each mineral varies according to pH, temperature, ORP, minerals present, and biological factors (Heikkinen *et al.,* 2009).

Sulfide oxidation produces H^+ ions, resulting in an acidic solution (Elberling, 1996). The predominant sulphide reaction, with regards to acid mine drainage, is the oxidation of the mineral pyrite (FeS_2), according to the following reaction:

(1) $$FeS_{2(s)} + (7/2)H_2O_{(l)} + (15/4)O_{2(aq)} \rightarrow Fe(OH)_{3(s)} + 2H_2SO_{4\,(aq)}$$

Under the presence of oxygen, pyrite reacts with water to form insoluble ferric hydroxide and sulphuric acid (Nordstrom, 1982). Acidic conditions increase solubility and bioavailability of metals and salts including Al, Fe, Mn, Ca, Mg, K, Na, Zn, Cu, Cd, Pb, Co, Ni, As, Sb and Se (MEND 2004). The low pH and high available metal concentrations can lead to an array of environmental issues and delayed remediation, as seen in the former Steeprock mine, near Atikokan (St James & Lee, 2015).

Neutral rock drainage, or NRD may result in environmental impacts beyond provincial and federal soil, sediment and water quality standards (Fraser, 1994). For example, NRD from the Rio Tinto mine in Quebec contains nickel concentrations that exceed regulatory limits (Plante *et al.,* 2014). Neutral rock drainage can alter the ecology, pedology and limnology of the receiving environment (Öhlander, 2012). Neutral drainage may occur under various conditions. If acidic mine drainage, as a result of sulphide oxidation is neutralized *in-situ* by carbonate and silicate minerals within the min-rock heaps, the discharge will have a circumneutral pH (Gahan, *et al.,* 2009). Additionally, if the molar ratio of sulfides/carbonates within the mine-rock is low enough, typically 1:2, or if the mine-rock is low in sulphides, typically > 1% w/w, chemical constituents that are soluble under circumneutral conditions will dissolve and become discharged into the environment (MEND, 2009). Mine-rock with sufficient carbonates can neutralize the ARD process is summarized with the following reaction (MEND, 2000):

(2) $FeS_{2(s)} + 2CaCO_{3(s)} + (15/4)H_2O_{(l)} + (3/2)O2_{(g)} \rightarrow Fe(OH)_{3(s)} + 2SO_4{}^{2-}{}_{(aq)} + 2Ca_{2(aq)} + 2CO_{2(g)}$

Under circumneutral conditions, metals including As, Cd, Cr, Mo, Ni, Sb, Se, and Zn may have the potential to leach in concentrations that are of concern (Clemente, 2000). Metals are released at neutral pH under two principal mechanisms: hydrolysis and the formation of oxyanion metals (Brown *et al.,* 1999). Metals such as Fe (II), Cd, Ni and Zn are weakly hydrolyzing, as they readily dissociate from their parent compounds in the presence of water (Lindsay, 2015). Oxyanions are formed in the presence of oxygen and water (Bowell, 1995). Metals including As, Cr, Mo and Sb form oxyanions in the form of AsO_3^{3-} (arsenite), AsO_4^{3-}(arsenate), CrO_4^{2-} (chromate), MoO_4^{2-} (molybdate), Sb $(OH)_4^-$ (antimoniate) and $Sb(OH)_6^-$ (antimonate) (Cornelis & Vandecasteele, 2010). Unlike most metals that carry a positive charge when dissolved, oxyanions are negatively charged under oxidizing conditions (MEND, 2004). Oxyanions are strongly sorbed in acid waters and are leached under circumneutral conditions (Jones, 1994).

Stormwater has the potential to impact the discharge receiving lakes. When precipitation is greater than evapotranspiration, stormwater containing elevated concentrations of the previously mentioned constituents seeps out of the foot of the mine-rock heaps (Peterson, 2014). The stormwater is then collected in stormwater ponds and subsequently discharged into the watershed. Because stormwater is laden with an elevated concentration of total dissolved solids (TDS), the stormwater discharge may be more dense than the natural waters in the receiving lake (Merriam, 2011). When discharge water is more dense than the water in the receiving lake, discharge water may sink to the bottom of the receiving lake, causing stratification and deters mixing (Uchtenhagen & Lee, 2015).

1.2 Lake Stratification

For much of the year, deep boreal lakes are stratified according to the thermal density gradient of the water column (Hakala, 2004). Turnover occurs when the density gradient within the water column erodes, and the water column circulates. Turnover mixes the water column, delivering oxygen to the depths and cycling nutrients to the surface (Kõiv et al., 2011).

Lakes in which complete turnover occurs are classified as holomictic. Holomictic lakes can be further classified into three types, according to turnover frequency: polymictic, dimictic and monomictic (Hutchinson, 1937). Polymictic lakes turnover many times throughout the ice-off period. Dimictic lakes turnover twice a year, once in the spring, and once in the fall, whereas monomictic lakes turnover once a year. Lewis & Cam (1993) illustrate the relationship between lake depth and latitude, with the predicted turnover behavior within a lake (Figure 1.1).

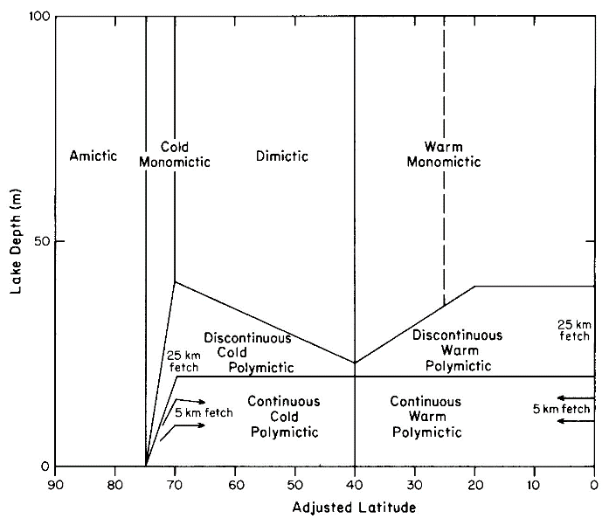

Figure 1.1: Lake turnover with relation to depth and latitude

Shallow lakes are expected to be polymictic, turning over throughout the year. Deeper, mid-latitude (0°-40°) lakes are expected to turn over once a year, while deep lakes within the latitudes of approximately 40° to 70° are expected to be dimictic (Figure 1.1) Lakes may have a density gradient that results in stratification that is sufficient to inhibit mixing, and turnover does not occur. Lakes in which no turnover occurs are deemed *meromictic* (Findeneeg, 1937). Turnover is initiated by wind and inhibited by the stabilization effect of a density gradient, stratifying the water column (Kittrell *et al.,* 1959).

The density gradient of water within a lake results in the development of layers that do not freely mix with each other. The terminology of these layers differs between holomictic and meromictic lakes. In holomictic lakes, three layers are present: the *epilimnion*, *metalimnion* and *hypolimnion* (Hutchinson, 1941). The uppermost, least dense layer is the epilimnion, which is well mixed. Beneath the epilimnion is the metalimnion, the middle layer in which a sharp density gradient is present. The bottommost layer is the hypolimnion, the densest layer of water. In meromictic lakes, the uppermost, least dense layer, that experiences mixing is the *mixolimnion*. The bottom layer, which is chemically different than the mixolimnion is the *monimolimnion.* A *chemocline* divides the mixolimnion and monimolimnion. A chemocline is characterized by a prominent chemical gradient (Hutchinson, 1957). In a meromictic lake, the monimolimnion does not mix with the mixolimnion. Classifying lakes according to mixing trends is a useful tool when developing an understanding of the hydrodynamic, biological and chemical process within a lake, in order to develop a management plan for discharge of mine water.

1.3 Meromictic Lake Properties

Whether or not turnover occurs impacts the hydrodynamics, biogeochemistry and ecology of a lake. Conditions that may be impacted include temperature, dissolved oxygen, distribution of nutrients and potentially toxic constituents, chemical speciation and habitat availability (Priscu *et al.,* 1982, Guerrero *et al.,* 1980, Meriläinen, 1970).

Holomictic lakes will turnover when the water column is isothermal. Meromictic lakes maintain a chemical density gradient sufficient to inhibit turnover (Boehrer & Schultz, 2008). Incoming solar radiation is absorbed by the upper layer of the lake, within the mixolimnion. Due to the extinction of solar radiation throughout the water column, the monimolimnion receives little heating in the form of solar radiation (Williams *et al.,* 1980). As a result, the monimolimnion is marked by a prominent temperature gradient and will be cooler than the mixolimnion in the ice-off months, further promoting stratification (Imboden & Wüest, 1995).

The temperature profile within a polymictic lake is near-isothermic, as the lake is almost constantly circulating and mixing (Zauke *et al.,* 1995). If a polymictic lake is made to be meromictic, a thermocline will form, with a cooler monimolimnion and warmer mixolimnion (Hausmann & Boehrer, 2006).

The concentration of dissolved oxygen (DO) plays a key role in nutrient cycling, available habitat for aquatic organisms, nutrient cycling and the production of potentially toxic constituents (Boehrer & Schultz, 2008; Hutchinson, 1957). DO can be expressed as the total concentration (mg/L), or as a function of percent saturation (%) of the theoretical maximum concentration of oxygen that can be dissolved in freshwater at a specific pressure and temperature (Cole & Wells, 2016). The gas solubility within water is governed by Henry's law, which states that the saturation concentration of dissolved gas in a liquid is proportional to its partial pressure and temperature (Henry, 1803). Greater atmospheric pressure results in the solubility of dissolved gas increasing. Temperature has an inverse relationship with gas solubility. Increased temperature decreases the solubility of gasses, as the enthalpy of dissolution is increased (van't Hoff, 1884). Cold water can facilitate a greater concentration of dissolved oxygen than warmer water. The saturation concentration of DO is decreased in warmer water, due to the increased kinetic energy of a warm system enabling dissolved gasses to be released in a gaseous form (Sander, 2015).

Dissolved oxygen is added to water through atmospheric diffusion and as a byproduct of photosynthesis. Dissolved oxygen is consumed through biological decomposition and released when DO saturated water is warmed (Wetzel, 1990). Atmospheric diffusion is the absorption of oxygen at the surface of the waterbody, interfacing with the atmosphere (Lyons, 1982). Because diffusion through a fluid is a slow process, convection currents are the mechanism that transports saturated DO from the surface, throughout the mixolimnion (Li *et al.*, 2001). Dissolution of DO is increased by wave action, exposing a greater surface area of the water surface to the atmosphere and increasing mixing of the mixolimnion (Bouffard *et al.*, 2014). During turnover, when the water column circulates, water throughout the lake is exposed to the atmosphere and becomes saturated with DO (Hutchenson, 1957). In a polymictic lake, where turnover occurs throughout the ice-off season, the water column DO will be near-saturation (Rueda & Schladow, 2003). The density gradient stratification between the mixolimnion and monimolimnion prevents dissolved oxygen from being transported below the chemocline (Cloern *et al.,* 1983).

Oxygen is produced by plants, algae, diatoms and photosynthetic bacteria (Pace & Prairie, 2005). Because the monimolimnion is often below the aphotic zone, photosynthesis does not occur, and oxygen is not produced (Tonolla *et al.,* 2005). Conversely, because meromictic lakes do not mix, they tend to build up detritus and nutrients, resulting in decomposition and oxygen consumption (Viollier *et al.,* 1955). For this reason, meromictic lakes often exhibit a hypoxic (DO < 2 mg/l) monimolimnion, low in dissolved oxygen (Charlton, 1980).

When turnover occurs, the lake exhibits uniform temperature, dissolved oxygen and concentration of TDS, nutrients and potentially toxic constituents (Imboden & Wüest, 1995). Turnover cycles nutrients and organic matter that have sunken to the hypolimnion throughout the water column (Lehman & Branstrator, 1994). When a lake does not turnover, nutrients do not cycle, and the productivity of the lake is reduced (Njuguna, 1988).

When high TDS water, containing potentially toxic constituents is discharged into a lake, the discharge can be incorporated into the monimolimnion (Molenda, 2014).

Without turnover to mix the lake, TDS accumulates at the bottom, concentrating potentially toxic compounds. Accumulation of high TDS can lead to the lake failing provincial water quality objectives (PWQO) standards (Uchtenhagan & Lee, 2015).

Redox potential is a measure of the tendency of an environment to oxidize or reduce chemical species. Positive values for redox potential indicate an oxidizing environment, while negative redox values indicate a reducing environment (Borch *et al.,* 2009). Because oxygen is an electron acceptor, environments with more oxygen will tend to oxidize chemical species. Environments with little oxygen will tend to reduce chemical species (Stumm & Morgan, 2011). The biogeochemical cycles for chemical speciation of elements are dependent on the oxidation state, driven by the redox environment (Sondergaard, 2009). Oxidation state alters the bioavailability, toxicity and mobility of both nutrients and potentially toxic compounds (Gambrell, 1994). The following figure illustrates the speciation of various chemical species when subject to varying redox potentials (E_h; Figure 1.2; Borch *et al.*, 2009).

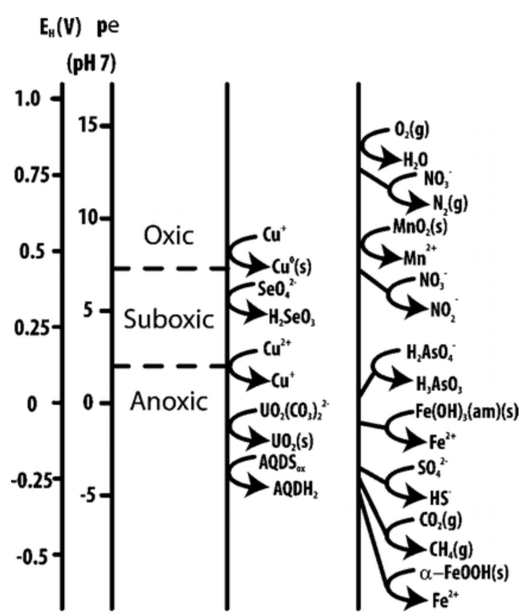

Figure 1.2. Redox ladder showing examples of environmentally relevant redox couples.

Meromictic lakes often exhibit a redox gradient (Balistrieri *et al.,* 1994). The oxygen-rich mixolimnion has a relatively high positive redox potential, compared to the negative redox potential within the oxygen-poor monimolimnion (Sondergaard, 2009). Due to the variation of the redox potential between the mixolimnion and monimolimnion, chemical speciation differs between layers (Hollibaugh *et al.,* 2005). One example is iron (Fe) speciation, which governs the biogeochemistry of several key nutrients and potentially toxic constituents (Maranger & Pullin 2003). Under circum-neutral pH and oxic conditions, Fe precipitates as Fe(III) (hydr)oxides (Taillefert *et al.,* 2000). The amorphous nature of solid Fe(III) (hydr)oxides provides absorption sites for toxic metals, such as As(V), thus reducing the bioavailability of As (Lui *et al.,* 2015). In a reducing environment, Fe(III) can be reduced by sulphide abiotically. The dissolution of the precipitate releases aqueous As into the water (Dos Santos Alfonso & Stumm, 1992).

When oxygen is not present, microbes must utilize an alternative electron acceptor (Küsel, 2003). Rather than utilizing oxygen for respiration, sulphur reducing bacteria in sediment reduce elemental sulfur to sulphide in the form of H_2S (Kondo, 2006). H_2S is toxic, as it effects auxin transport in plants (Zang *et al.*, 2017). H_2S is toxic to animals due to the impact on the central nervous system, as it binds with iron in the mitochondrial cytochrome enzymes, preventing cellular respiration (Lindenmann *et al.,* 2010).

Purple and green sulphur bacteria photosynthesis utilize sulphide, in the form of H_2S as an electron donor (van Niel, C. B. 1932). The purple and green sulphur bacteria are often present in the chemocline, where light is sufficient for photosynthesis to occur (Tonolla *et al.,* 2005). These organisms play a key role in phosphorus cycling in meromictic lakes. In the fall, when the mixolimnion depth deepens, and incorporates the upper region of the chemocline, the phosphorus-rich bacteria are upwelled and brought towards the oxygen rich surface, where they are consumed by heterotrophs and the phosphorus is made available (Overmann *et al.,* 1996).

Meromictic lakes influence habitat availability for aquatic organisms through increased mixolimnion temperature, decreased monimolimnion dissolved oxygen, reduced nutrient cycling and the presence of toxic chemical constituents (Wang *et al.,* 2015, Boehrer & Schultz, 2008).

1.4 Characterization of Stratification

Density gradients in boreal lakes are most often thermogenic, due to varying water temperatures but can also be influenced by biogenic and chemical gradients within the water column (Kraemer *et al.,* 2015). Understanding the mechanisms inducing stratification is vital when developing management plans to prevent lakes from becoming meromictic.

Thermogenic stratification in holomictic lakes is governed by a temperature gradient, with less dense water at the surface (epilimnion), and a more dense layer at the bottom (hypolimnion) (Boehrer & Schultz, 2008). Between the layers exists a section characterised by a sharp change in temperature, known as the thermocline (Hutchinson, 1957). During warm summer months, less dense, warmer water is at the top of the column, with the cooler denser water lying underneath. The reverse is true during the winter months, when less dense, cooler water overlays more dense, warmer water (Bertram, 1993). Variation in density is due to the density of water being greatest at approximately 4°C (Weiss *et al.,* 1991). The surface cooling effect of the winter months causes the epilimnion to cool below 4°C, making it less dense than the warmer hypolimnion (Hondzo & Stefan, 1991). The warming effect of the summer months causes the epilimnion to exceed 4°C, making it less dense than the hypolimnion. During the fall and spring, when the water column is isothermal, - with consistent temperature throughout the water column - the density gradient is reduced. With the thermal density gradient reduced, the force applied by the wind needed to turnover the lake is reduced, thus, turnover may occur (Hutchinson, 1957). Thermogenic stratification may lead to a meromictic condition in tropical lakes, where the atmospheric temperature does not fall below 4°C for a significant part of the year (Katsev *et al.,* 2017).

Biogenic stratification in meromictic lakes is caused by the decomposition of organic material. Organic material sinks to the monimolimnion, where decomposition then occurs. Decomposition then results in an increased electrolyte concentration, thus increasing hypolimnion density when compared to the mixolimnion (Hakala 2004). A high concentration of nutrients is required for biogenic stratification to impact the stability of the water column (Pasche *et al.,* 2009). The increased nutrients and organic carbon can lead to a hypoxic monimolimnion (Duthie & Carter, 1970). These nutrients may be ectogenic, flowing into the lake from another source, such as eutrophication from agricultural stormwater (Roland, 2017).

Chemogenic stratification is due to a gradient in total dissolved solids. When dissolved solids are added to water, the volume of water does not change, but the mass of the water increases proportionally to the mass of the dissolved solids added (Boehrer & Schultz*,* 2008). Thus, water with a higher concentration of total dissolved solids (TDS) is more dense (Sibert, 2015). Lakes exhibit chemogenic stratification when the concentration of TDS in the monimolimnion is greater than the concentration of TDS in the mixolimnion (Patterson, 1984). The chemocline divides the layers, characterized by a sharp gradient in the concentration of TDS (Hutchinson, 1957). Chemical gradients can be caused by ectogenic input of dilute TDS water entering a lake that has higher TDS concentration (Fisher, 2006). The dilute TDS, lower density inflow water acts as a cap, making up the mixolimnion, covering the more dense water in the monimolimnion (Espana *et al.,* 2009). Island Copper Mine Lake was formed from a decommissioned open pit from a copper mine, in Vancouver, British Columbia. The decommissioned open pit was flooded with high TDS seawater and capped with freshwater. In this case, a meromictic pit lake was purposely designed to prevent turnover and dissolved oxygen from interacting with the buried tailings (Fisher, 2002).

A chemogenic meromictic lake can occur when TDS-laden exogenic water enters a relatively lower TDS lake. The higher TDS discharge sinks to the bottom of the lake and is incorporated within the monimolimnion (Ficker *et al.,* 2011). Examples of sources of high TDS discharge causing a meromictic lake include mine tailings water, such as Frank Lake, in Hemlo, Ontario (Uchtenhagen & Lee, 2015), road salt runoff in Woods Lake, Michigan (Marsalek *et al.,* 2000) and mine water discharge in the Rontok Wielki Reservoir, Poland (Molenda, 2018).

Stratification is often due to a combination of thermogenic, biogenic and chemogenic factors inhibiting turnover and increasing water column stability. Stability of the water column is influenced by a variety of other factors including topographic sheltering, bathymetry, wind intensity, and storms, solar radiation/heating, precipitation/evaporation, and inflow/outflow location, volume and water quality (Boehrer & Schultz, 2008).

1.5 Factors Influencing Stratification

The temperature of the water column is governed by multiple factors, including the magnitude and wavelength of solar radiation reaching the water surface, how the radiation is attenuated within the water column and sediment temperature and remittance of radiation (Imboden and Wüest, 1995).

Solar radiation is the zenith angle, the perpendicular angle between the lake and the sun. A zenith angle of 0^{o} would indicate the sun is directly above the lake, where solar radiation would be greatest, while a zenith angle greater than 90^{o} would indicate that no direct solar radiation is reaching the water surface (Jacobson, 2005). The greater the zenith angle, the greater the amount of ozone and atmosphere the solar radiation must pass through, thus decreasing the solar radiation reaching the surface of the lake (Gonzalez *et al.,* 2015). Zenith angle is dependent on latitude, time of year and time of day (Woof, 1968). Equatorial regions will have a greater net solar irradiance, compared to regions further away from the equator (Lukianova *et al.,* 2017). The zenith angle of northern latitudes is greater in the winter and less in the summer, which is responsible for seasonal disparages in temperature. The zenith angle changes throughout the day, with noon being the smallest and dusk and dawn being the greatest (Gonzalez *et al.,* 2015).

Cloud cover will also impact the amount of solar radiation at the water surface. Clouds reflect shortwave radiation from the sun back out to space, thus decreasing the total shortwave radiation at the water surface (Svensmark & Friis-Christensen, 1997). In contrast, a portion of longwave radiation emitted by the Earth is remitted back to the Earth's surface as a part of the greenhouse gas effect. Other greenhouse gasses that increase longwave solar radiation at the Earth's surface include water vapour (H_2O), carbon dioxide (CO_2), methane (CH_3) and nitrous oxide (N_2O) (Rodhe, 1990). As the concentrations of the previously mentioned gasses increase, so will the amount of longwave radiation at the water surface.

The amount of and distribution of solar radiation within the water column is then governed by shading effects, albedo and the fraction of solar radiation absorbed by the water surface, the attenuation rate due to water, inorganic suspended solids and the fraction of radiation remitted from the sediment and sediment temperature (Cole & Wells 2016).

When solar radiation reaches the surface of the lake, a fraction of long-wave solar radiation is absorbed by the surface layer (β). β is a function of light extinction (λ) of the water column, and can be determined with the following formula, developed by Williams et al. (1980):

(3) $$\beta = 0.265\ln(\lambda) + 0.614$$

Greater β values indicate that a greater portion of longwave radiation is more readily absorbed, with a typical value of .45, or 45% (Tennessee Valley Authority, 1972). Shallow systems are more complicated as the light extinction coefficient changes as a function of depth and light wavelength (Cole & Wells 2016). As the radiation enters the water column, a series of extinction coefficients govern the distribution, summarized in the following equation (Cole & Wells 2016).

(4) $$\lambda = \lambda_{H2O} + \lambda_{ISS} + \lambda_{POM} + \lambda_{\alpha}$$

λ = net extinction coefficient, m^{-1}

λ_{H20} = extinction coefficient for water, m^{-1}

λ_{ISS} = extinction coefficient due to inorganic suspended solids, m^{-1}

λ_{POM} = extinction coefficient due to particulate organic matter, m^{-1}

λ_{α} = extinction coefficient due to algae, m^{-1}

The net light extinction coefficient (λ) is dependent on the extinction coefficient of the water (λ_{H20}), plus the light extinction due to inorganic suspended solids (λ_{ISS}), particulate organic matter (λ_{POM}), and algae (λ_{α}). Light extinction is a function of water transparency. Stained water, due to humic and fulvic acids will increase the light extinction of water (λ_{H2O}), as the dissolved substances within the water absorb light energy (Esfahani *et al.,* 2015). Increased algae, particulate organic matter and inorganic suspended solids will contribute to an increased light extinction (Kirk, 2011). As the previously mentioned factors absorb and scatter radiation, the water is heated, while blocking light energy from penetrating deeper (Esfahani *et al.,* 2015). Light absorption and reflection cause the water nearer to the surface to be heated, while the water nearer to the bottom receives less light and heat from solar radiation (Carpenter *et al.,* 2015).

Light extinction coefficients govern how deep below the surface solar radiation may penetrate. The uppermost layer, with enough solar radiation that allows oxygen-producing phytoplankton and plants is the euphotic zone (Lee *et al.,* 2007). Beneath the euphotic zone is the disphotic zone, in which light is still present, but not in sufficient amounts to allow for photosynthetic respiration (Tonolla *et al.,* 2005). Because little light penetrates the disphotic zone, oxygen is not produced (Tsai,*et al.,* 2016). In shallower, littoral zones, shortwave radiation from the sediment may be re-radiated back up to the water column (Cole & Wells, 2016).

Wind is the primary factor driving lake mixing through two mechanisms: direct wind stirring and shear-generated turbulence (Lorirai *et al.,* 2011; Etimead-Shadhidi & Imberger, 2001). Direct wind stirring causes turbulence at the water surface causes mixing of the epilimnion/mixolimnion. Wind influences surface heat exchange and concentration of dissolved oxygen (DO) through increasing surface roughness and mixing the epilimnion/mixolimnion, exposing a greater amount of the water to the surface of the lake and atmosphere over a given amount of time (Kittrell *et al.* 1959). A well-mixed epilimnion/mixolimnion will be both isothermal and isocheimal. Increased wind events will degrade the density gradient further, deepening the epilimnion/mixolimnion.

Shear-generated turbulence is the primary mechanism responsible for turnover (Etimead-Shadhidi & Imberger, 2001). Shear-generated turbulence originates within the boundary of the well-mixed epilimnion and the stratified metalimnion when the destabilizing effect of velocity-shear due to internal seiches overcomes the stabilizing effects of the density gradient (Kraus & Turner 1967). This phenomenon occurs particularly within long, narrow lakes when stratification is weak, often during late fall and early spring (Gorham & Boyce 1989). Internal seiching creates currents along the bottom of the lake, creating shear force along the boundary sufficient to destroy stratification (Lorrai et al. 2011).

Sheltered areas, such as mountainous regions can reduce wind velocity, while large, open spaces allow for higher wind velocities (Valerio, *et al.,* 2017). The amount of wind-shear force exerted on the lake depends on wind sheltering and fetch (Markfort, 2010). Lakes with longer fetch length, especially with regards to the direction of prevailing winds, will have a greater likelihood of turnover because energy from wind can be exerted to a greater surface area of the lake, contributing to greater surface roughness and force being transferred to the lake (Read *et al.,* 2012).

Bathymetry and basin morphology contribute to mixing dynamics. Shallower, continuous basins will be more susceptible to mixing due to the water body being able to transfer energy and momentum in the form of eddies and seiches (Boehrer & Schultz, 2008). In water bodies with multiple deep basins or sills, disconnected by shallower sections, eddy momentum and seiching throughout the lake are reduced, thus inhibiting mixing, such as Lake Whatcom, in Washington (Pickett and Hood 2008). In general, lakes with greater surface area to volume, with a more homogenous bathymetry are more prone to shear-induced mixing when compared to lakes with a lesser surface area to volume ratio with a heterogenous bathymetry (Gorham & Boyce 1989). Fetch is also a key factor in epilimnion depth and mixing potential. Lakes with a longer fetch will transfer more energy from the wind into the lake (Markfort, 2010).

Basin morphology also impacts the sediment temperature. In deep sections, sediment temperature can be assumed to be equal to the average annual temperature for the region (Cole & Wells, 2016). Sediment temperature will have a regulatory effect on the hypolimnion/monimolimnion water temperature (Bouffard & Wüest, 2019). Shallow sections, where shortwave solar radiation is readily absorbed and re-radiated by the sediment, will have a warming effect on the water column (Fang & Stefan, 1996).

Lakes with greater surface area will tend to have a deeper thermocline, compared to lakes with a smaller surface area. Gorham and Boyce (1989) describe the relationship between thermocline depth at the time of maximum heat content and surface area as:

(5) $$h = 2.0\ (t/g\Delta\rho)^{1/2} L^{1/2}$$

Where h is epilimnion thermocline depth (m), t is the wind stress associated with late summer storms, $\Delta\rho$ (g/L) is the , contrast between epilimnion and hypolimnion typical for lakes in the region, g is the gravitational constant due to gravity and L is the square root of the surface area (m^2) of the lake.

Water quality and rate of discharge, along with depth and location of discharge influence how readily discharge water will mix with lake water (Boeher & Schultz, 2008). When a fluid is moving through a system, two types of flow can occur: laminar and turbulent. Laminar flow occurs when fluid particles flow along a smooth path, along adjacent layers, with little or no mixing (Streeter, 1966). Eddies and cross currents perpendicular to flow are not produced (Geankoplis, 2003). Turbulent flow occurs when fluid particles flow along a chaotic and highly irregular path, producing eddies and cross currents, resulting in high diffusivity and mixing (Sullivan *et al*., 2000). When water of variable density is introduced to a system, the tendency to segregate under laminar flow, or mix under turbulent flow is dependent on the Reynolds number (Tansley *et al.,* 2001).

(6) $$Re = ud/v$$

Where *Re* is the Reynolds number, u is the fluid velocity, *d* is the characteristic dimension of the surface and v is the kinematic viscosity. Fluid velocity is expressed as velocity of the fluid, with respect to the boundary of the fluid parcel. The characteristic dimension is the surface area of the flow boundary of the fluid parcel. Kinematic viscosity is the measure of the inherent resistance of a fluid to flow. In the case of two fluids, kinematic viscosity acts as a buoyancy term, in the difference of density between the two fluids (Tansley *et al.,* 2001). A smaller Reynolds number suggests laminar flow, resulting in stratification, while a higher Reynolds suggests turbulent flow, resulting in mixing (Jabbari *et al.,* 2016). Increasing the density difference between the two fluids, along with decreasing surface area of the flow boundary and decreasing velocity of discharge will reduce the Reynolds number, inhibiting the two fluids from mixing (Galperin *et al.,* 2007).

1.6 Predicting Mixing Trends in Lakes

Due to the ecological significance of turnover, predicting turnover trends can be vital when managing lakes. The stability of a parcel of fluids in a stratified body in one layer, compared to another is described as the Richardson number and further refined by the Taylor-Goldstein equation (Huppert, 1973):

(7) $$\mathrm{Ri} = N^2 / (\mathrm{d}u/\mathrm{dz})^2$$

Where N is the Brunt–Väisälä frequency, which is a measure of buoyancy, u is horizontal velocity (m/s) and z is depth (m). The Richardson number takes into account differences in density, horizontal velocity, depth and acceleration due to gravity to determine stability (Howard, 1963). According to the Taylor-Goldstein equation, density gradients of greater depth require a greater horizontal velocity to mix (Huppert, 1973).

Although the Richardson number provides a metric for stability and is often used in meteorology, oceanography and limnology, more variables are required to investigate site-specific stability characteristics of the lake under investigation. To determine the stability of a lake, Schmidt included the surface area of the lake and area of the lake at variable depths (1915). Schmidt's stability equation sought to estimate the amount of work (J) required to mix a lake through comparing the location of the centre of mass in a stratified lake, versus the centre of mass if the lake was fully mixed through the following formula (Schmidt, 1915):

(8) $$S=1/A_0 \int_0^{zm} (Z-Z_g)\, A_z\, (\rho_Z - \rho_m)\, dZ \quad \text{[integral from 0 to } Z \text{ m]}$$

Where A_0 is the surface area of the lake (m^2), Z is the height above the bottom of the lake (m), Z_g is the centre of volume above the bottom of the lake (m), A_z is the area of the lake at depth Z (m^2), ρ_Z is the density of water at depth Z (kg/m^3) and ρ_m is the density at complete mixing (kg/m^3).

Although the Schmidt equation provides a more site-specific estimation than the Richardson number, factors including fetch, bathymetry, lake heterogeneity, and bottom friction are not accounted for. In order to include the previously mentioned variables, a simple equation is insufficient, and the use of computer modelling software is required.

The advancement of computer modelling allows for the integration of multiple factors that impact hydrodynamic and water quality within a specific lake, under specific conditions (Jorgensen, 2016). As models develop over time, they become more refined in their capabilities and reliability. With any model, results can only be obtained through accurate algorithms and carefully collecting and interpreting data. As the statistician George Box once remarked, "All models are wrong, but some are useful".

1.7 CE-QUAL W2

CE-QUAL W2 is a two-dimensional, hydrodynamic and water quality model, developed by Portland State University and the United States Army Corps of Engineers. CE-QUAL W2 has been utilized in hundreds of cases and the model has been demonstrated to predict both hydrodynamics and water quality, which can be used to optimize water management plans for lakes, reservoirs and rivers (Cole & Wells 2016). Due to the extensive nature of the model, this introduction will only include an explanation of the general mechanics of the model and inputs, found in the manual. Hundreds of the detailed stoichiometry and momentum equations governing the model can be found in the CE-QUAL W2 users manual (Cole & Wells, 2016).

Capabilities

The hydrodynamic properties CE-QUAL W2 is capable of predicting water surface elevations, longitudinal & vertical velocities, stratification, turnover and temperature. CE-QUAL W2 models over 100 water quality parameters. Key components include TDS, suspended solids, oxygen demand, organic matter, pH, alkalinity, and dissolved oxygen. CE-QUAL W2 allows the user to manipulate inputs into the waterbody to assess how changes will impact the hydrodynamics and water quality modelling output. For example, if the inflow rate, water quality and discharge location are modified, the model will predict how the waterbody will react. The user may also modify the meteorological data to assess how the waterbody will react to a variation in climate or extreme weather events.

Limitations

Limitations are inherent due to the complexity of modelling natural systems, as the system must be simplified. The chemical and biological interactions within a lake are quite complex. Because of this, the model must consist of factors that influence the system the greatest, possibly omitting factors that may have less impact, such as variability in sediment temperature. The model is only as good as the underlying mechanics and governing equations as well as the quality of the data collected. Limitations relevant to this study include that the fact that the model is laterally averaged throughout each cell, over a given area, the model will not account for lateral variations in shoreline, bathymetry and water quality within each cell. There is also variation and debate over which transport schemes and kinetics should be used in various situations, specifically with regards to eddy and turbulence equations. Sediment temperature, sediment heat exchange, eddy viscosity and diffusivity, and all other coefficients are space and time invariant within a waterbody, which may lead to issues if the waterbody contains a great amount of heterogeneity. Great care must be taken when constructing and calibrating any model; CE-QUAL W2 is no different.

Model input data is divided into five categories: *geometric data, boundary conditions, initial conditions, hydraulic parameters* and *kinetic parameters. Geometric data* in the model represents the bathymetry of the water body in a two-dimensional, laterally averaged finite-difference grid (Figure **X**). The grid is an approximation of the shoreline and bathymetry. An accurate bathymetric map must be used in order to compose an accurate model grid.

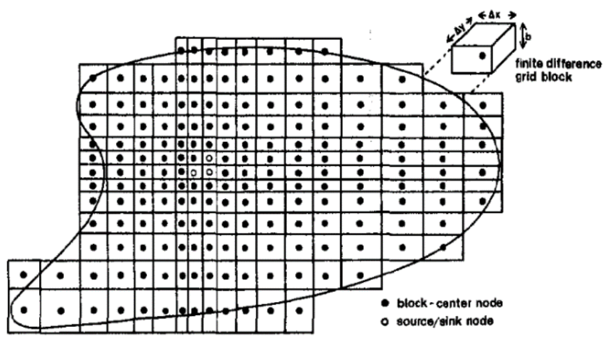

Figure 1.3: Finite difference grid (Mercer & Faust 1980)

The finite-difference grid consists of a series of rectangular cells, making up the horizontal segments and rectangular cells and vertical layers.

The model developer must determine appropriate segment lengths and layer heights. Smaller segment lengths and layer heights are more accurate, but more computationally intensive, taking up more time and memory to run the model. Run time is less of an issue with modern computers but can still vary drastically. Grid spacing should vary gradually, from segment to segment and layer to layer to minimize discretization errors. Areas of strong gradients and high slopes should have a grid resolution that is sufficiently fine in order to accurately model changes in the water.

Because the model is laterally averaged, the segment width must be calculated as a function of cell volume to account for bathymetric variation across the bottom of the lake and shoreline. Using bathymetric mapping software, such as Golden Software's SURFER 16, layer height and segment length can be input to determine the volume of the cell. The user then calculates the average segment width using cell volume, layer height and segment width in the following equation:

(9) segment width = cell volume / (layer height * segment length)

Segment lengths and widths are input into the model grid and are represented in a top view, as in Figure 1.4 and side view, as a cross-section (Figure 1.5), adapted from Cole & Wells (2016).

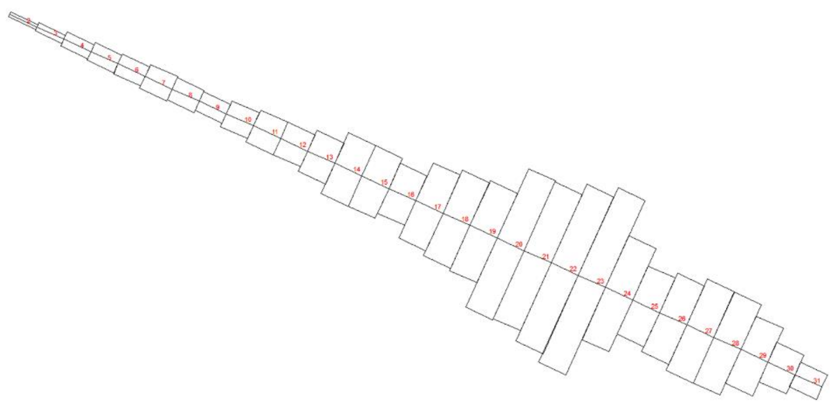

Figure 1.4: Top view of Degray Lake CE-QUAL W2 grid

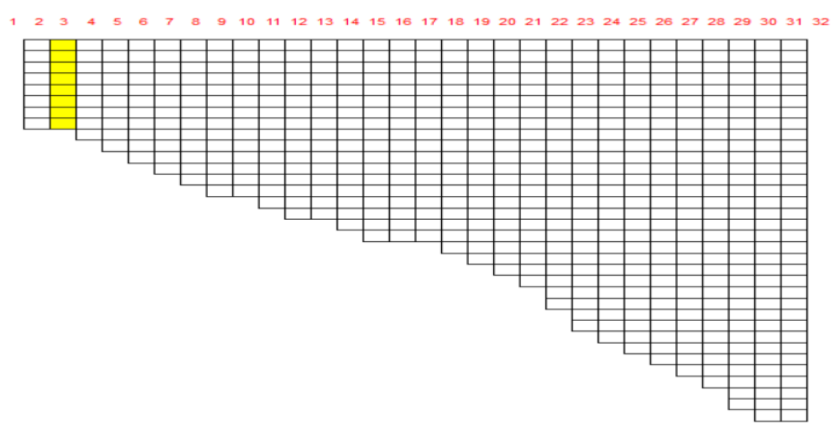

Figure 1.5: Longitudinal view of Degray Lake CE-QUAL W2 grid

Due to the two-dimensional nature of the model, each cell is evenly mixed within itself and interacts with the surrounding cells. Accurate bathymetry is vital when modelling the lake, as inaccurate bathymetry can impact sediment oxygen demand, water transport momentum and the volume-elevation curve (Williams, 2007).

Initial conditions represent the lake at the start of the model. The water surface elevation and vertical profile of temperature, dissolved oxygen, TDS and constituents of concern within the water column are input as independent values for each vertical row. Profiles are laterally averaged throughout the waterbody.

Boundary conditions are factors that are inputs and outputs within the water body, which include inflows/outflows, meteorological data, surface heat exchange and solar radiation absorption. The model developer determines which segment within the model grid inflows enter and outflows exit. The water column segment and layer are assigned to enter the water body through either a user-defined layer or the inflows enter a layer with a corresponding density. Conversely, inflows may be input as distributive tributaries, in which flows are distributed evenly throughout the waterbody. Within the flows, a variety of different water quality components can be input, depending on what outputs are required for the specific investigation. In order to predict stratification, turnover, temperature, dissolved oxygen and water level, the following inputs are required both within the waterbody and inflows to the waterbody: inflow and outflow rates, temperature, TDS, dissolved oxygen, pH, chlorophyll a, total organic carbon, dissolved/total phosphorus, nitrate + nitrite nitrogen, ammonium nitrogen & total Kjeldahl nitrogen, biological oxygen demand, Secchi depth, total inorganic carbon, total suspended solids, dissolved/total iron, dissolved/total manganese, dissolved/total silica.

Accurate meteorological data is also required and are a part of the boundary conditions. Meteorological data must include wind velocity and direction, shortwave solar radiation, cloud cover, temperature, dewpoint and precipitation. The manner in which meteorological forces interact with a lake depends on the bathymetry, wind sheltering and water quality, as previously mentioned.

Hydraulic parameters are the hydrodynamic equations governing the model. These include coefficients for vertical and horizontal momentum and temperature/constituent diffusivity, which are represented by longitudinal eddy viscosity and longitudinal eddy diffusivity (m^2/s). Large, weakly stratified lakes and reservoirs with a relatively low horizontal velocity have relatively low and predictable eddy viscosity and diffusivity. In stratified systems, with relatively high horizontal velocity, longitudinal eddy viscosity and diffusivity is more difficult to determine and can be as high as 10-30 m^2/s and 10-100 m^2/s, respectively.

A variety of turbulence models may be applied to the model as well. CE-QUAL W2 provides six vertical eddy viscosity formulations to be used, including: Nicuradse (Rodi, 1993), Parabolic (Engelund, 1976), W2 (Cole & Buchak, 1995), W2 with mixing length of Nickuradse (Cole & Buchak, 1995; Rodi, 1993), Renormalization group (Simoes, 1998) and Turbulent kinetic energy (Wells, 2003). The specific formulation equations can be found in Cole & Wells (2016). The Parabolic, Nicuradse and Renormalization group are appropriate for riverine and estuarine systems in which shear due to friction is dominant. Such systems are often heavily stratified with relatively high horizontal velocity. W2 is appropriate for systems, such as reservoirs and lakes, where wind shear is dominant. The turbulent kinetic energy formulation is considered a generalized formulation, designed to work for a variety of systems.

The interactions between the waterbody and sediment are within the hydraulic parameters. Bottom friction interacts with the eddy viscosity formulations to influence the momentum of water. The sediment also interacts with the water column to influence water temperature through the coefficient of bottom heat exchange ($W/m^2/^{o}C$), sediment temperature and proportion of shortwave radiation lost to sediment that is added back to the water column.

Kinetic parameters include more than 120 coefficients that impact constituent cycling, nutrient dynamics, decay rates, oxygen demand and respiration. In general, these parameters control the source-sink relationships within the waterbody. It is often the case that when calibrating the model for oxygen, one or more kinetic parameters is responsible for site-specific conditions.

Calibration data is required to ensure the model is sufficiently simulating the hydrodynamics and water quality of the waterbody. Calibration data parameters should be selected according to the constituents in question, depending on site-specific and project-specific requirements. Calibration parameters include: vertical profiles of temperature, TDS and dissolved oxygen and surface-level elevation. Outflow constituents, including flow rate, temperature and TDS are also useful to ensure the model is simulating the heat and mass balance. Field data, when compared to model output data, can be used to modify model parameters to more closely simulate properties of the waterbody under investigation.

Vertical profile calibration is based on the absolute mean error (AME) of the field data, compared to model output data. AME is a statistic based on the average variance between field and modelled data at each datapoint, or sample elevation within the profile. The equation for AME is as follows:

$$\text{AME} = \frac{\sum |\text{Predicted} - \text{Observed}|}{\text{Number of Observations}} \quad (10)$$

A lower AME is evidence of a more accurate model. As a rule, Cole and Wells (2016) state that AME should be <1°C for temperature and <1mg/L for dissolved oxygen. TDS is more difficult to make a general limit for, as there is great variation amongst waterbodies. Although there is no agreed-upon range for the AME of TDS, it should be within a justifiable range.

When modifying model coefficients and parameters, it is important to be able to explain and justify any changes made. Hundreds of parameters within CE-QUAL W2 can be modified in order to provide a more representative model of the waterbody. Some of the key calibration components are as follows: wind sheltering coefficient, bottom friction, longitudinal eddy viscosity/diffusivity, fraction of solar radiation absorbed by the surface layer, light extinction coefficients and inflow/outflow rate. The aforementioned list is by no means exhaustive but consists of calibration components most often adjusted by model developers.

2 Case Study

2.1 Mine Influenced Stormwater Discharge

Mining can have deleterious effects on the pedology, limnology and ecology of the environment (Mend, 2004). In order to minimise environmental impacts, the provincial government of Ontario, and the federal government of Canada have implemented regulations, including the regulation of stormwater discharge, under the *Metal Mining Effluent Regulations* (SOR/2002-222) and the Ontario *Water Resources Act* (R.S.O. 1990).

As precipitation and surface water flows through the mine-rock heaps on site, chemical constituents within the mine rock are eroded and ultimately discharged into the environment as stormwater (Winde & van der Walt, 2004). The mine's certificate of approval regulates maximum loadings allowable for several chemical constituents, and states that environmental impact must be minimized (COA 4-0075-92-967). Although there is no limit set for the maximum allowable concentration for total dissolved solids (TDS) in stormwater, environmental impact at the range of observed levels may occur (Minnow, 2013; Uchtenhagen & Lee, 2015).

Increasing the concentration of TDS within water increases density (Sibert, 2015). When high-TDS laden stormwater is discharged into a natural lake, with a low concentration of TDS, rather than the waters mixing, the stormwater and natural lakewater may stratify (Molenda, 2018). Chemogenic stratification - induced by discharging stormwater with elevated concentrations of TDS - causes a density gradient within the water column, which may prevent the lake from experiencing turnover, as in meromictic lakes (Espana *et al,* 2009). Turnover is a process in which the water column circulates, delivering dissolved oxygen to the depths, and nutrients to the surface

(Boehrer *et al*, 2008). A lake that does not turnover is classified as meromictic. Meromictic lakes consist of two distinct strata: the mixolimnion and monimolimnion (Hutchinson, 1957). The upper, surface layer is the mixolimnion. The mixolimnion experiences turnover and contains a relatively lower concentration of TDS and a higher concentration of dissolved oxygen water than the monimolimnion (Fisher & Lawrence, 2006). The monimolimnion is the lower layer, which does not experience turnover. The monimolimnion is characterized by relatively high concentrations of TDS, while typically having a low, often hypoxic concentration of dissolved oxygen (DO) (Ficker *et al,* 2011).

2.2 Lake Mixing Dynamics

Holomictic lakes, in which complete turnover occurs at least once a year is typical for boreal lakes (Hakala, 2004; IJC, 1977). Of 40 lakes surveyed in the Experimental Lakes Area, outside of Kenora, Ontario, only two were found to be naturally meromictic; two had occasional, incomplete mixing and 36 were holomictic (Schindler, 1971). Meromictic conditions may also arise due to anthropogenic influence. In some cases, meromixis are desired. Open-pit mines often contain a high concentration of sulphide minerals within the rock (MEND, 2000). When exposed to water and oxygen, sulphide minerals, such as pyrite can oxidise and produce acid rock drainage (Capanema & Ciminelli, 2003). The Island Lake Copper Mine in British Columbia flooded the decommissioned open pit with high-TDS seawater, then capped the lake with low-TDS freshwater, creating a meromictic pit lake (Fisher, 2002). In these cases, it is beneficial to flood the pit and establish a meromictic pit lake to prevent the lake from turning over and delivering dissolved oxygen to the pyrite, flooded beneath (McNaughton & Lee, 2010).

When dealing with lakes in a natural environment, meromixis often result in deleterious environmental impacts (Boehrer *et al*, 2008). Cleaver Lake, near Schrieber, Ontario is the receiving body for the former First Quantum Minerals Limited zinc and copper mine. Cleaver Lake had become meromictic, as the concentration of TDS from the mine discharge was higher than the concentration of TDS in Cleaver Lake's natural lake water. As a result of Cleaver Lake becoming meromictic, the monimolimnion became hypoxic and contained an elevated concentration of zinc and copper (Haapa-aho, 2004). These conditions reduced the available habitat for brook trout, and the species was extirpated from the lake (Denholm *et al,* 1995).

As of 2011, Frank Lake, the tailings water discharge lake for Barrick Gold's Hemlo gold mine, was meromictic. Under the meromictic state, the monimolimnion of Frank lake was hypoxic, with a concentration of dissolved oxygen of <1mg/L (Uchtenhagan & Lee, 2013). Barrick Gold Hemlo was undergoing Environmental Effects Monitoring (EEM), under the Ministry of Northern Development, Mines and Forestry, in order to obtain a Certificate of Approval, as required to expand their open-pit mining operation. Part of the obligations under the EEM is to ensure that impacted lakes do not become meromictic, and if they are, a plan is required for the lakes to be returned to a holomictic state (MNDM, unpublished memo, 2010).

Barrick Gold has expressed concern that Hemlo Williams mine stormwater receiving lake, Lower Unnamed Lake has become meromictic. The was expanding the open pit mining operation and was required to determine if the increased loadings being discharged will cause Lower Unnamed Lake to become meromictic. Williams mine was interested in whether relocating the location within Lower Unnamed Lake that Pond 102 is discharged will influence chemical stratification.

1.3 General Objectives

The objectives of this study were as follows:

A) Develop a CE-QUAL W2 model of Lower Unnamed Lake

B) Determine the mictic state of Lower Unnamed Lake, using the CE-QUAL W2 model and field observations

C) Modify the CE-QUAL W2 model by relocating the Pond 102 stormwater discharge location to the shallow channel, upstream of the west basin to prevent chemical stratification within Lower Unnamed Lake.

D) Modify the CE-QUAL W2 model to determine the hydrodynamics and water quality of Lower Unnamed Lake if stormwater from Pond 102 was not being discharged into the lake.

E) Modify the CE-QUAL W2 model to determine if Lower Unnamed Lake has the potential to become meromictic with the current and proposed Pond 102 discharge location.

It was hypothesized that:

A) A CE-QUAL W2 model will be effectively constructed and calibrated.

B) Lower Unnamed Lake was not meromictic.

C) Modifying the discharge location will promote mixing of the stormwater and lake water. Chemically induced stratification will be eliminated, thus reducing stability within Lower Unnamed Lake.

D) Elimination of Pond 102 discharge will eliminate chemically induced stability, causing Lower Unnamed Lake to become polymictic. The thermocline will be deeper and the concentration of hypolimnion dissolved oxygen will increase.

E) Lower Unnamed Lake has the potential to become meromictic with Pond 102 discharge in the current location, but not when discharged is released from the proposed location.

3 Methodology

3.1 Study Site

The Barrick Gold Hemlo Williams mine is 35 km east of Marathon Ontario. The site is an active open pit and underground gold mine. Since operations began in 1985, the Williams mine has produced 21 million ounces of gold (Cox *et al.,* 2017). In order to access the gold baring ore, the removal of approximately 27 million tonnes of non-economically waste rock was required. The waste rock is segregated into waste rock heaps on-site, according on the propensity of the waste rock to become acid-generating. Three stormwater ponds were constructed to capture the surface water runoff/infiltration from the waste rock heaps: Pond 102, Pond 400 A and Pond 300. Pond 300 discharges into Blueberry creek, while Ponds 102 and 400A discharge into Lower Unnamed Lake (LUL), located within the Little Black River watershed. The discharge volumes of the stormwater ponds vary year-to-year. In 2017, Pond 102 discharged 692 877 m^3, while Pond 400 A discharged 14 497 m^3 of stormwater into LUL. The average concentration of TDS of both discharge ponds was approximately 1250 mg/L, although substantial variation occurred over the year. In contrast, the discharge from Upper Unnamed Lake contains a relatively low concentration of TDS, averaging around 85 mg/L. Prior to this study, the inflow volume from Upper Unnamed Lake was unknown.

Strong gradients in the concentration of TDS, from the epilimnion to the hypolimnion have been previously observed in LUL (Minnow 2013).

3.2 Lower Unnamed Lake Model Input Data

The CE-QUAL W2 model was constructed using data collected in 2017. A detailed description of the model inputs can be found in Appendix *X*. The model was developed in 6 steps: 1) development of model bathymetry, 2) boundary conditions, 3) initial conditions, 4) parameters impacting dissolved oxygen, 5) calibration, 6) modification of stormwater discharge location.

Model Bathymetry

The model grid is an adaptation of the lake bathymetry. A bathymetric map of Lower Unnamed Lake was created using a LOWRANCE HDS5 LAKE INSIGHT depth sounder, equipped with GPS that produced dataset, consisting of longitude (x), latitude (y) and depth (z). Golden software's SURFER 16 programme was used to process the 3-dimensional bathymetric map with the x,y,z dataset (Figure 3.1; 3.2; 3.3).

CE-QUAL W2 requires a 2-dimensional, laterally averaged grid to represent the lake bathymetry. The bathymetric map was converted into a 2D grid, consisting of a series of cuboid cells. The cell length was dependent on the shoreline and bathymetric heterogeneity (Figure 3.1). Depth for all cells was set to 0.125 m. To account for the amorphous shoreline, cell width was calculated by creating a grid within SURFER of the cell location, length and depth. Surfer then produced a cell volume. Cell width was then calculated using the following equation:

(11) segment width = cell volume / (layer height * segment length)

Cell widths, lengths, heights and volumes were all kept within 50% of their neighbouring values to ensure numerical stability within the model.

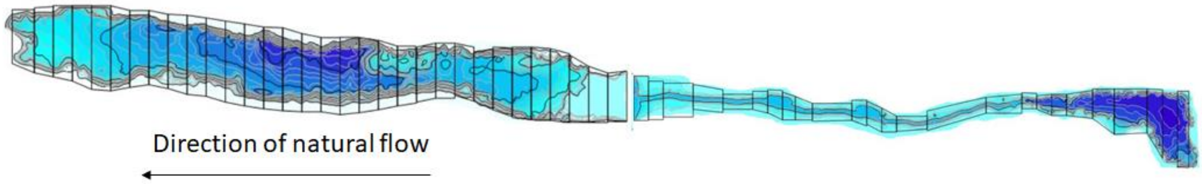

Figure 3.1: Top view of Lower Unnamed Lake bathymetry with model segments

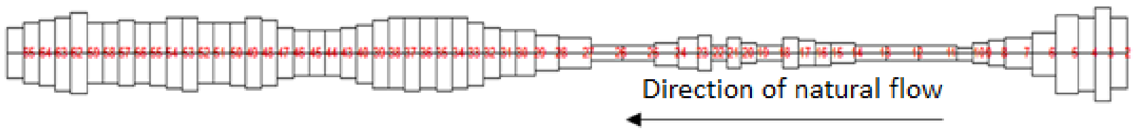

Figure 3.2: Top view of Lower Unnamed Lake model bathymetric grid

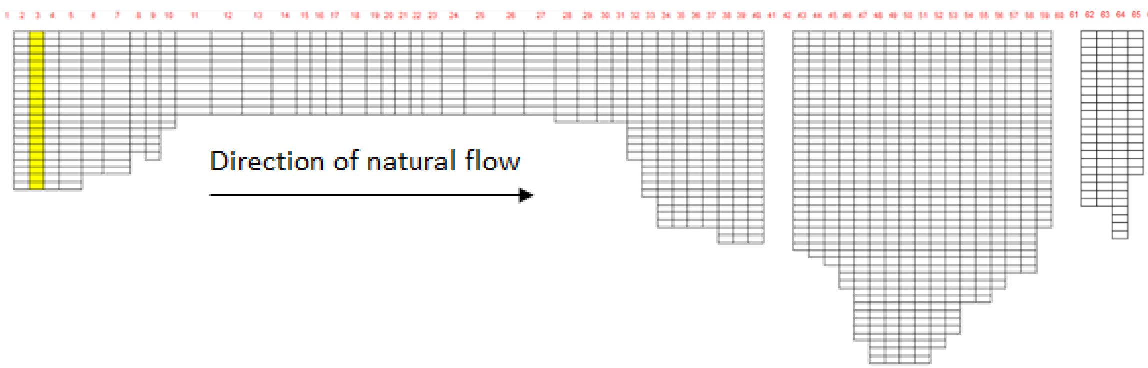

Figure 3.3: Longitudinal side view of Lower Unnamed lake model bathymetric grid

The natural watercourse flows from Upper Unnamed Lake, into segment 2 of the model grid. Water flows east to west and out of the lake at segment 65. The model was divided into three water bodies, segments 2-40, 43-59 and 62 to 65, to account for variations in sediment temperature (Fig. 3.3).

Initial Conditions

The initial water level was measured using the distance from the surface of the water to a set point marked on a cliff above the lake. An ONSET HOBO water level logger (P/N: U20L-040) was deployed within the lake to determine water depth every 30 minutes. A separate ONSET HOBO water level logger was deployed on land to compensate for variations in barometric pressure. A DATASOND HYDROLAB

SURVEYOR 4α (serial no. 32016) was used to determine dissolved oxygen, temperature, pH, specific conductivity, ORP, and turbidity. Readings for the HYDROLAB were taken every 0.5 meters in depth at two locations within the lake (Fig **3.4**).

Total dissolved solids (TDS), suspended solids, phosphate, ammonium, nitrate, iron, dissolved organic matter, chlorophyll α and alkalinity was determined by the ISO/IEC 17025:2005 accredited The Lakehead University Environmental Laboratory. Data collection for all aforementioned parameters was repeated each field trip, (18/3/2017, 12/5/2017, 7/6/2017, 25/6/2017, 14/7/2017, 4/8/2017, 9/6/2017, 10/5/2017and 30/10/2017. Meteorological data was provided by Barrick Hemlo, from their on-site weather station. Light extinction was determined using a Secchi disk.

Sediment Oxygen Demand

Sediment Oxygen demand was determined using *ex-situ* incubation of sediment cores, similar to the methods employed by Rong, *et al,* (2016). Nine Sediment cores from five locations within Lower Unnamed Lake (Figure 4) were collected. The 6 cm diameter cores were frozen and cut to 30 cm, with 10 cm of sediment depth, then allowed to thaw. The overlying water was removed and replaced with oxygen-saturated, distilled-deionized water. Sediment cores were incubated in the dark, at 25°C in a Sanyo MLR-350 H growth chamber. An ONSET HOBO dissolved oxygen logger (P/N: U26-001) was fixed to the top of the core, submerged in the water with an airtight seal. The concentration of dissolved oxygen was logged every 30 minutes for a period of 24 hours. The rate of oxygen consumption was calculated from the slope of DO *versus* time profiles. Sediment oxygen demand, expressed as g/(m^2/day), was determined by the area of the sediment-water interface and total oxygen consumed per volume of water in the column, using the following equation:

(12) $$\text{SOD} = (m^*\mathcal{V}) \,/\, A$$

Where m is the slope of concentration of dissolved oxygen consumed over 24 hours, $\mathcal{V}$ is the volume of water and A is the area of the sediment-water interface. Sediment oxygen demand is time-invariable within the model; therefore, SOD was only determined once. The model preforms internal temperature rate multipliers for sediment oxygen demand.

Biological Oxygen Demand

Biological oxygen demand (BOD) was determined by the Lakehead University Environmental Laboratory, using method code: WBOD5 (Joncas, 2019). Samples were collected in 500 ml FISHER high-density polyurethane bottles (Cat # 02-912-293A). Sample bottles were then immediately wrapped in tin foil and stored in a cooler full of ice when transported to the lab, where they were processed within 48 hours.

Processing BOD requires a solution of dilution water and a biological seed, consisting of a blend of microbial cultures that consume oxygen. Dilution water solution contained 1 ml/l of the following solutions: phosphate buffer (SCP Science, Cat # 250-110-100), magnesium sulphate solution (SCP Science, Cat # 250-110-400), calcium chloride solution (SCP Science, Cat # 250-110-200), and ferric chloride solution (SCP Science, Cat # 250-110-300). The seed solution was prepared by mixing one capsule of Poly-seeds from Fisher Scientific (Cat #LC1888050) with 400 ml of dilution water. BOD water samples were transferred into 500 ml Erlenmeyer flasks. 4 mL of seed solution was added to each sample. The quality control (QCWX) used 6.2 ml *Glutamic acid solution* from Fisher (Cat #3255-4), with 4 ml of seed solution and 489.8 mL of dilution water. A blank sample was prepared using 496 ml of dilution water and 4 ml of seed solution. Initial dissolved oxygen concentrations were read using a Mettler Toledo DO meter (Part # 51344621). All samples were incubated in a VWR Sheldon Model 2005 Low-Temperature Incubator, in the dark for five days at 20^{o}C. After five days, the dissolved oxygen concentration for all samples was determined using the DO meter. BOD_5 was then determined using the following formula:

$$BOD_5 \text{ mg/l} = (Di\text{-}Ff) \text{ / volume of sample water} \quad (13)$$

Where Di is the DO of the diluted sample before incubation and Df is the DO of the sample after incubation.

Flow Rate

Flow rate for the inflow and outflow of Lower Unnamed Lake was determined using the USGS method (2013), in which the stream is divided into transects (Turnipseed & Sauer 2010). The depth and width of each transect were measured. The velocity was determined using a Swoffer Model 2100 Series Current Meter. Transect dimensions and velocity were measured five times each and averaged. A water level logger captured stream depth every half hour. A separate water level logger was deployed on land to compensate for variations in barometric pressure. Stream depth was correlated to flow rate by creating a stream gauging rating curve, following a single-log-linear equation (Rantz *et al.*, 2013):

$$Q = K^*D^n$$

Where Q is the flow rate (m^3/s), D is stream depth, and K & n are derived from the trendline.

Barrick Hemlo provided flow rates and water quality for Pond 102 & Pond 400A discharge, which flows into Lower Unnamed Lake. Calculations for Unnamed Lake inflow and outflow rates are in Appendix A (**XX**)

Calibration Data

The volume-elevation relationship of the bathymetric map created using SURFER 16 (field bathymetry data) was compared to the volume-elevation (m^3 / MASL) of the constructed CE-QUAL W2 model bathymetric grid. The volume was compared at increments of 0.125 m.

Field data were compared to model output data for model calibration. The outflow temperature and conductivity were used for the model thermal and mass budget, using an ONSET HOBO conductivity and temperature logger (P/N: U24-001).

The lake depth was monitored using an ONSET hobo lake depth logger that recorded depth every hour.

Lake profiles were taken at the deepest part of the lake, at location *A* and near the inflow and at location *B* (Fig 4), on 18/3/2017 (Julian day 77), 12/5/2017 (Julian day 132), 7/6/2017 (Julian day 158), 25/6/2017 (Julian day 176), 14/7/2017 (Julian day 195), 4/8/2017 (Julian day 216), 9/6/2017 (Julian day 249), 10/5/2017 (Julian day 278) and 30/10/2017 (Julian day 303).

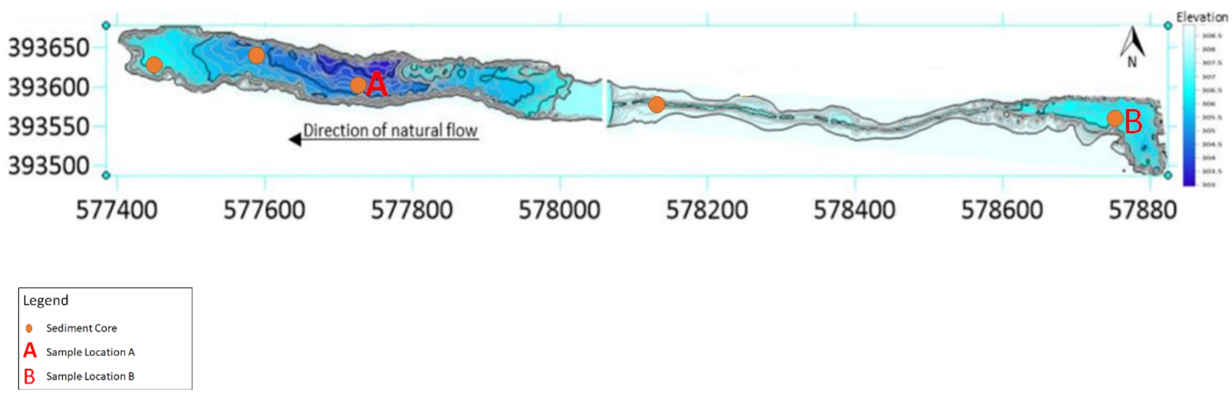

Figure 3.4: Location of calibration profiles and sediment cores in Lower Unnamed Lake

Model calibration

CE-QUAL W2 has several coefficients that often require modification to be better suited for the Lower Unnamed Lake during calibration. These coefficients include, wind sheltering coefficient, which was modified from 1.0 to 0.7 to account for sheltering of the lake. The wind sheltering coefficient was increased to 1.5 on October 28th to account for the high wind gusts, which were not incorporated into the model. Horizontal dispersion/diffusion was modified from 0.013 to 2.0 to account for stratification eddies in a stratified system. The vertical turbulence closure algorithm was set to *Parabolic*. The lake was divided into three waterbodies to account for variations in sediment temperature and the coefficient for bottom heat exchange. The lengths of the waterbodies, with respect to distance from the lake outflow were as follows: waterbody 1 was 0 – 60 m, waterbody 2 was 60 to 400 m and wb3 was 400 to 1400 m from the lake outflow. The sediment heat exchange for waterbody 1 & 2 was turned off, as the sediment temperature variation through the shallow regions negatively impacted model temperature accuracy. The sediment temperature in waterbody 2 was set to 5 ^{o}C, with a coefficient of bottom heat exchange of 0.3 W/m^{2}/^{o}C.

The water level in the uncalibrated model was greater than the field observed water level. The railway tracks, adjacent to LUL contained several ungauged culverts (Appendix X). To account for ungauged water flowing out of LUL, the outflow rate was increased to match the modelled water level with the observed. The outflow rate of the model had to be increased by varying rates throughout the year. The total outflow rate was 7 % greater than the calculated outflow. All flow calculations and calibration modifications are in Appendix A (Figure A.1 – A.12).

Lower Unnamed Lake contained an ungauged inflow in the east basin (16 U 578818 E 539559). The source of the ungauged inflow was a wetland area, located approximately 60 m east of LUL. The discharge rate was set to five times the precipitation rate, over the area of LUL. The discharge rate was chosen, as the mass balance of TDS was well calibrated. Setting the discharge rate as a function of precipitation rate allowed the model to be applied in years to come. The chemical constituents were set to the same as the inflow from UUL. Photos of the ungauged discharge are in Appendix A (Figure A.16.; A.17)

3.3 Model Output Data

Model output data analysed by this study included: Outflow rate, temperature & TDS, sediment temperature, in-pool water velocity vectors, profiles of temperature, TDS, dissolved oxygen & density. The density ratio and TDS ratio of the hypolimnion and epilimnion were also used to asses stratification and stability.

The difference in water density between the hypolimnion and epilimnion was plotted as a ratio of the hypolimnion density, divided by epilimnion density (0.5 m below water surface). A greater density ratio indicated the lake was more stable, inhibiting turnover. A density ratio of 1 indicates that there no density difference between the epilimnion and hypolimnion, therefore the lake is susceptible to turnover. The same process was applied with regards to TDS to assess chemical stratification.

Determination of turnover

Turnover was observed in the field with lake outflow temperature loggers, lake outflow conductivity loggers and in-lake profiles of temperature, TDS and dissolved oxygen. Turnover was observed in the model by analysing lake outflow temperature and TDS, momentum velocity vectors, temperature profiles, TDS profiles, oxygen profiles and density profiles

3.4 Proposed Scenario Model Development

Proposed Discharge Location Model

Once the model was sufficiently calibrated, the discharge point location for Pond 102 was relocated from the current location (N 577510, E 5393670), to a proposed discharge point (N 578440, E 5393560) (Fig. 4.5 & 4.6). The current location discharges near the deepest point in the lake (5 m). The proposed location is upstream, relative to the natural flow, with an average depth of approximately 1 m. The elevation of Pond 102 is 347 m above sea level. The proposed discharge location is 650 m from Pond 102, at an elevation of 310 m above sea level, resulting in a slope of approximately 5.7%. The initial conditions and calibration parameters from the calibrated model were unaltered, except for the coefficient of bottom heat exchange (CBHE), with was modified from 0.3 ($W/m^2/^oC$) to 1.0 ($W/m^2/^oC$). This was done to account for modifying the Pond 102 discharge temperature to the field determined hypolimnion temperature in the current location model and leaving the proposed discharge temperature as the field determined temperature.

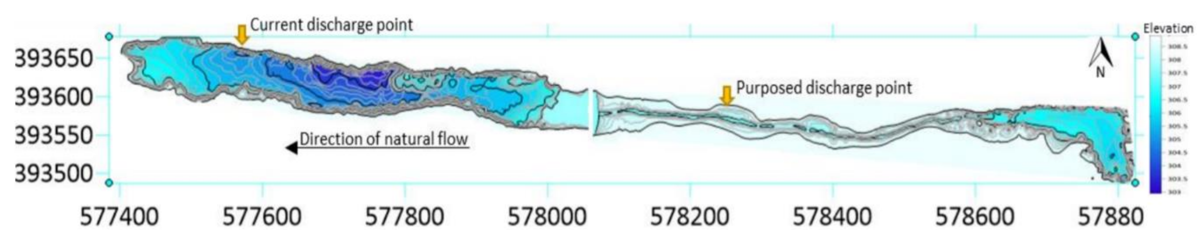

Figure 3.5: Current discharge point and purposed discharge point bathymetric map

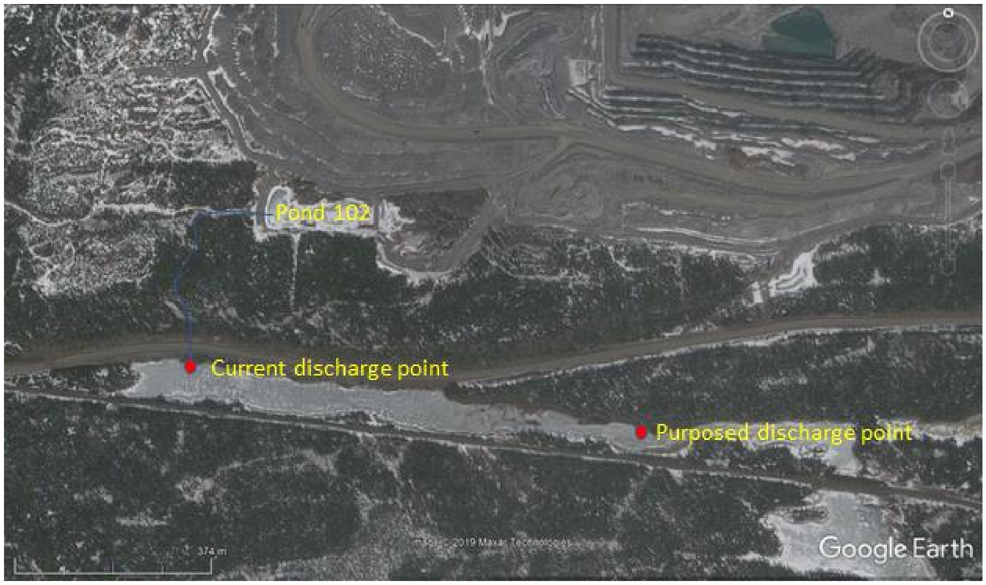

Figure 3.6: Current discharge point location and purposed discharge point location aerial view

Model with Pond 102 Discharge Eliminated

A model was developed of Lower Unnamed Lake, without Pond 102 discharge, using the same calibration parameters and initial conditions as the proposed 102 discharge location model. This was done to compare the effects of relocating the discharge location, with relation to Lower Unnamed Lake, if there was no discharge from Pond 102. Pond 400 A is still discharged within the model. A dynamic spillway was used to maintain the same water level in both models. The model that does not receive 102 discharge was referred to as the “unimpacted model”. Temperature, TDS and dissolved oxygen were plotted for both the proposed 102 discharge location and the unimpacted models. An explanation of all modifications is in Appendix C.2.

Meromictic Potential Model

Two models of Lower Unnamed Lake were developed to evaluate the potential for LUL to become meromictic. The following manipulations were made to the current and proposed location models:

a) Storm event intensity was reduced by adjusting the wind sheltering coefficient to 0.5 for all modelled days.

b) The concentration of TDS from Pond 102 discharge was set to 1950 mg/L throughout the year, which was the greatest TDS concentration observed from the discharge site.

c) The inflow rates from Pond 102, UUL inflow and added inflow were averaged and flow rates from each respective discharge were constant through the model year

d) A dynamic spillway was used to maintain the same water level as the original models.

3.5 Statistical analysis

Modelled outputs were compared to calibration data using mean error (ME), absolute mean error (AME), standard deviation (SD) and root mean square deviation (RSMD). RSMD is the mean of squares of the device and is used to compare the differences in two varying time series, expressed as:

(14) $$\sqrt{\sum \mathrm{n\ i} = 1 \frac{(\hat{y}i - yi)2}{n}}$$

Where $\hat{y}$ is the observed value, y is the predicted value, and n is the number of samples.

4.0 Results

4.1 Model Grid and Water Balance

The CE-QUAL W2 model produced the physical and chemical characteristics, outlined below.

4.1.1 Model Grid

The absolute mean error of the elevation increments was 6.1 ± 8.5%. The total volume of the CE-QUAL W2 bathymetric grid had 0.5% (700 m^3) less volume, compared to the Surfer 16 bathymetric model (Figure 4.1).

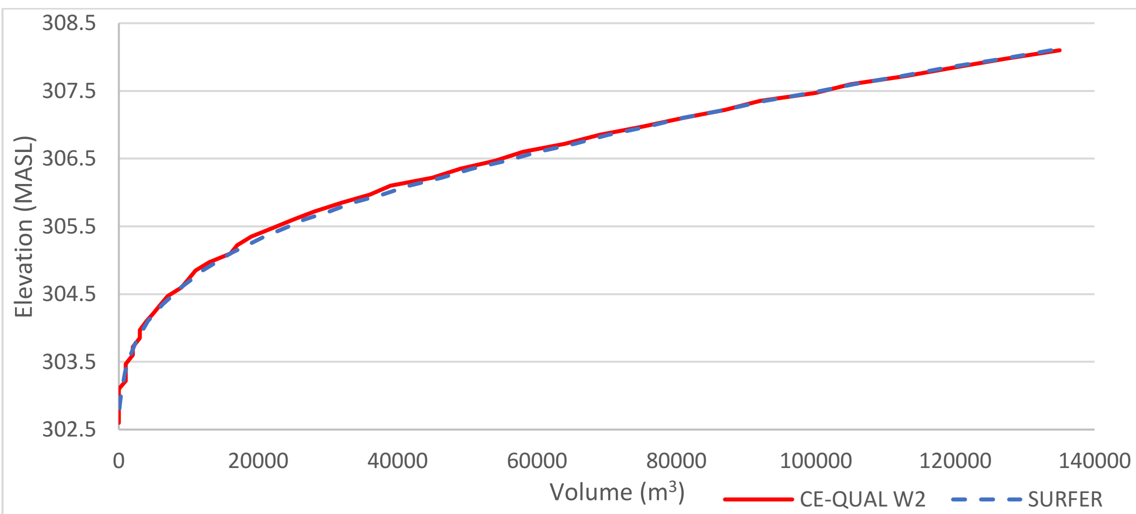

Figure 4.1: Volume-elevation curve for Lower Unnamed Lake bathymetry from Surfer 16 and CE-QUAL W2 grid

The total expected volume of water was compared to the volume of water within the CE-QUAL W2 grid and expressed as percent error. The deepest one meter of the lake (<304.5 MASL) had the greatest variation between field and modelled volumes. The minimum cell width resulted in an increased volume of water at the deepest cell, as the volume in Surfer was 92 m^3, as opposed to 112 m^3 in CE-QUAL. As the elevation and total volume increased, the deviation from the expected volume decreased (Figure 4.2).

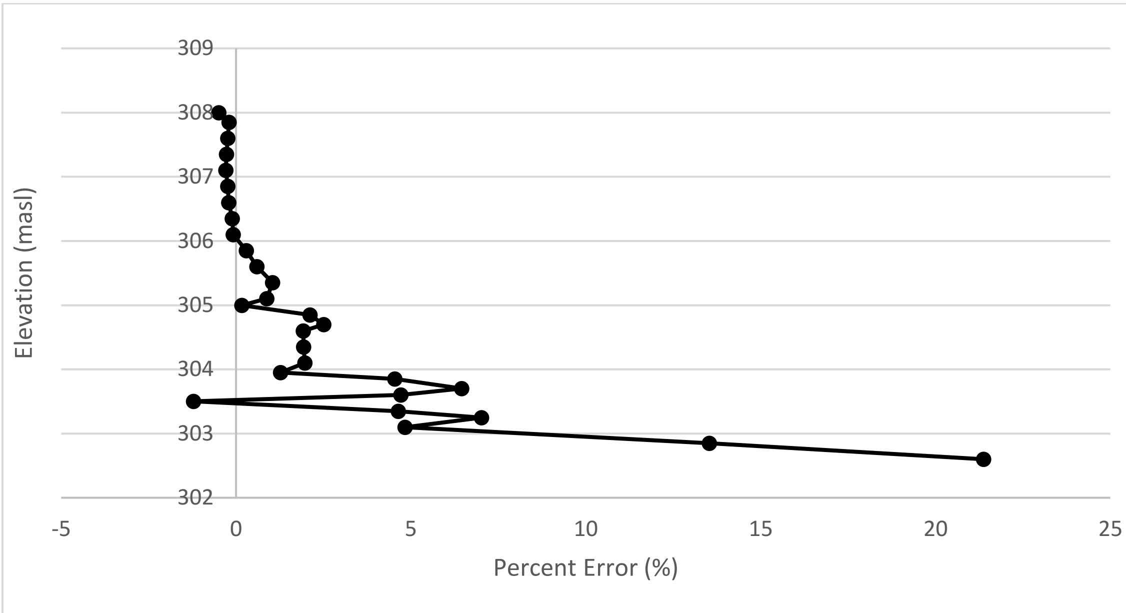

Figure 4.2: Percent error of CE-QUAL W2 bathymetric grid, compared to the Surfer 16 bathymetric map of Lower Unnamed Lake

4.1.2 Water Balance

Field-determined water level elevation was recorded using an ONSET HOBO pressure logger within Lower Unnamed Lake (Figure 4.3). It was evident that a drainage point in the lake was not being accounted for, as the uncalibrated modelled water level was 1.9 m higher than the field recorded elevation at the end of the modelled year. After adding an additional outflow to calibrate the water level, the model water level had an absolute mean error (AME) of 0.03 ± 0.03 m and a root-mean-square error (RMSE) of 0.046 m (n = 8160).

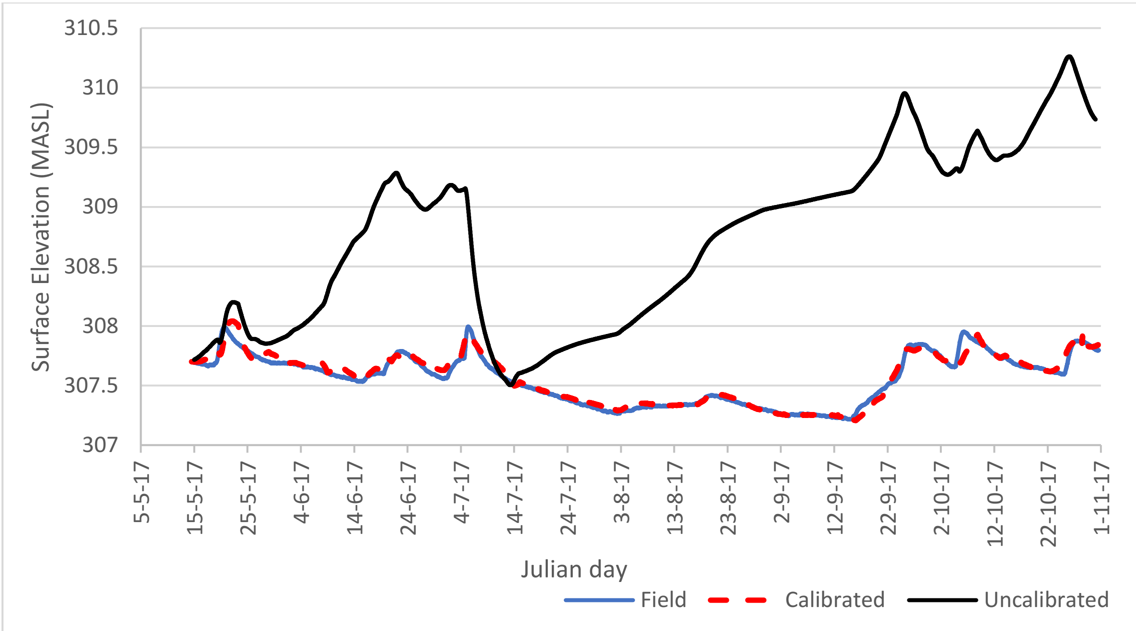

Figure 4.3: Water level elevation of Lower Unnamed Lake and model

In order to calibrate the water level, the outflow rate was modified (Figure 4.4). The total withdrawal volume after calibration was 7% greater than the uncalibrated withdrawal volume.

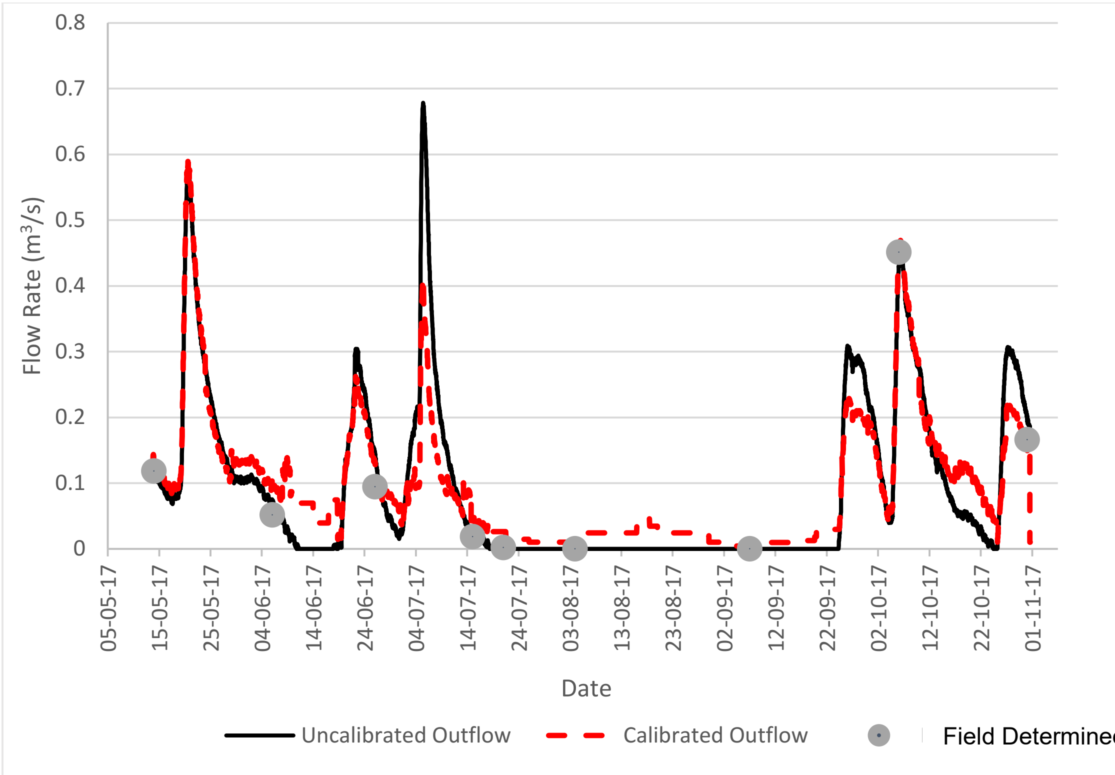

Figure 4.4: Flow rate of outflow from Lower Unnamed Lake

Water level deviation of the calibrated model and field data was plotted (Figure 4.5). The discrepancies in water level on May 19th, May 22nd, June 22th, July 3rd, September 23rd, October 4th and October 24th are a result of the water level in the model lagging water level in the lake during high flow periods (Figure 4.4). The model normalized the water level shortly after high flow periods.

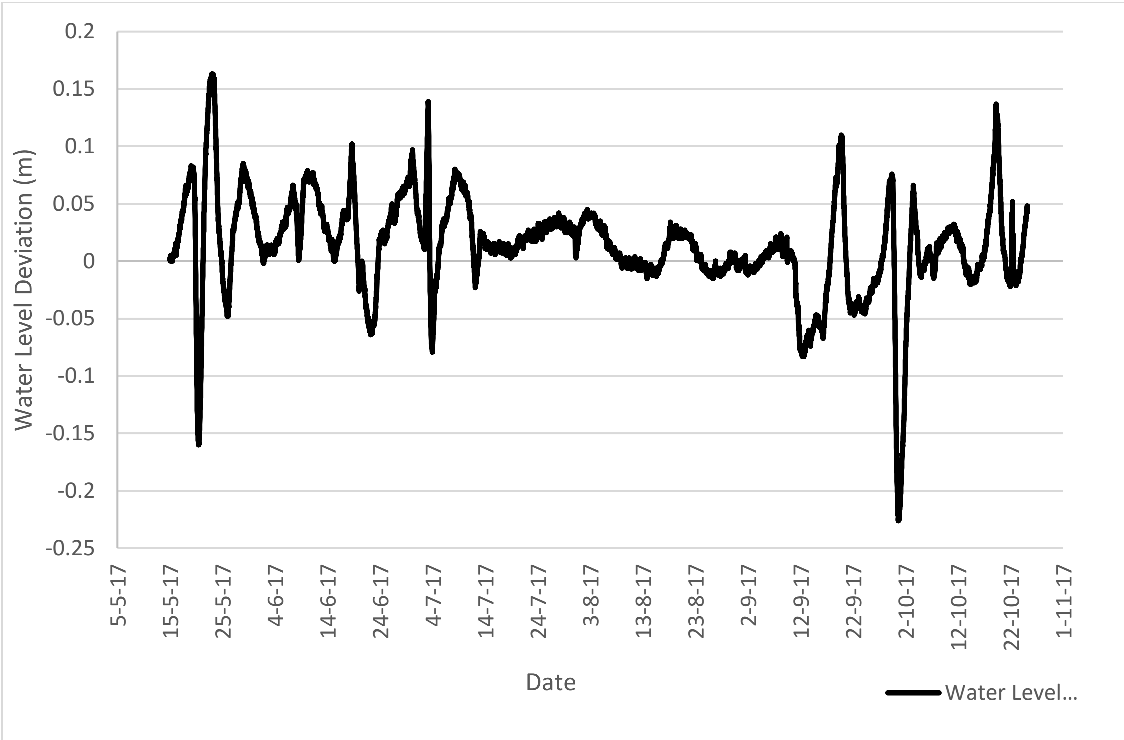

Figure 4.5: Water level deviation of the calibrated model and Lower Unnamed Lake

4.2 Calibrated Model Accuracy

The model was calibrated against Lower Unnamed Lake profiles for temperature, TDS and dissolved oxygen. All profiles were taken at the deepest section of the lake, on the west end, at sample location “A” (16 U 577674 E 5393620; Figure 3.6).

4.2.1 Temperature Calibration Profiles

Temperature profiles from the model were compared to field data with a calibration tolerance of 48 hours. The mean AME for temperature between the model and field data was 0.72 ± .42 °C. The RMSE was 1.20 °C (n = 86), suggesting the model was sufficiently calibrated, with regards to temperature, as an AME <1 °C is recommended (Cole & Wells, 2017). The AME is greater than 1 °C on June 8th and July 15th (Figure 4.6).

The model had the greatest temperature discrepancy on June 8th, with an AME of 1.72°C, in which the epilimnion temperature in the model is underpredicted by 2 °C, while epilimnion depth extends 0.5 m deeper within the model. The hypolimnion temperature is overpredicted by 2.2 °C. July 15th had an AME of 1.05 °C, in which the model underpredicted metalimnion thermocline depth by 0.25 m, resulting in a deeper modelled hypolimnion.

Hypolimnion temperature was overestimated by the model on June 8th, June 26th, July 15th and August 5th by 2.3 °C, 1 °C, 1.2 °C and 1.7 °C, respectively. The model was however highly accurate at predicting lake temperature during the fall and throughout turnover (September 7th - October 30st), with an AME of 0.20 °C, 0.16 8°C and 0.36 °C, respectively.

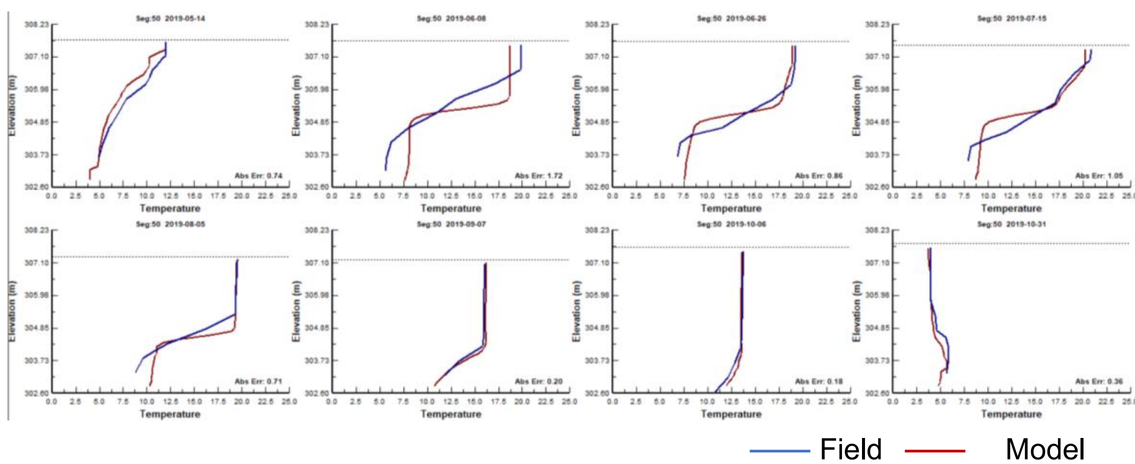

Figure 4.6: Modelled and field observed temperature profiles for Lower Unnamed Lake.

4.2.2 Lake Outflow Temperature Calibration

The temperature at the outflow location of Lower Unnamed Lake was monitored with a temperature logger and compared to modelled outflow temperature (Figure 4.7). The AME of the model run year was 1.08 ± 0.19 °C, with RSME of 1.41 °C, r^2 of 0.87 and n = 8164. One notable discrepancy is on September 9th to 15th, where the field observed temperature drops lower by a maximum of 5 °C. The model is sufficiently calibrated with regards to outflow temperature.

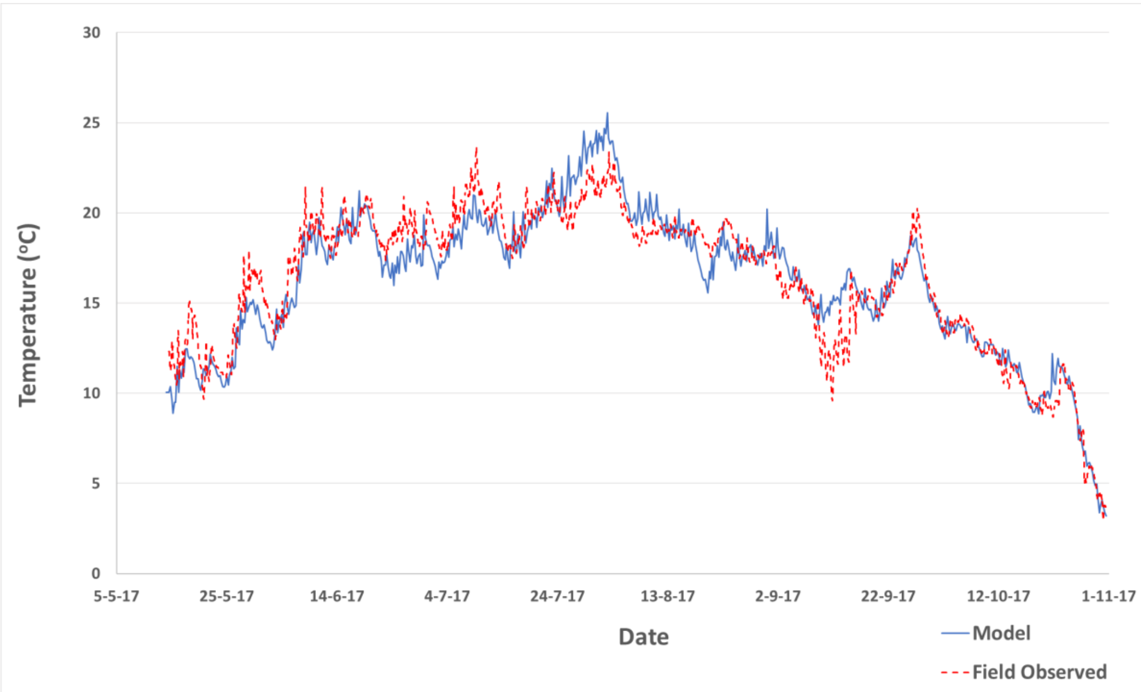

Figure 4.7: Modelled and field observed outflow temperatures

4.2.2 Total Dissolved Solids Calibration Profiles

The concentration of total dissolved solids (mg/L) profiles from the model were compared to field data with a calibration tolerance of 168 hours in order to account for the impact of Pond 102 discharge rates and allow the model to stabilize. The mean AME for TDS, comparing the model to field data was 98 mg/L ± 60 mg/L, with a mean percentage deviation of 17.4% ± 10.5%, and a RMSE of 128.78 mg/L (n=108) for all calibration dates (Figure 4.8). The greatest deviation of TDS concentration between the model and field data occurs on July 15th and August 5th, in which the concentration of TDS throughout the water column in the model was greater than what was determined in the field, with an absolute mean error of 193 mg/L (32%) and 191 mg/L (30%), respectively. Hypolimnion TDS increases within the model below 303.75 MASL, in the deepest 1 m of the lake on July 15th and beyond, rather than the TDS isocline evident in the field data.

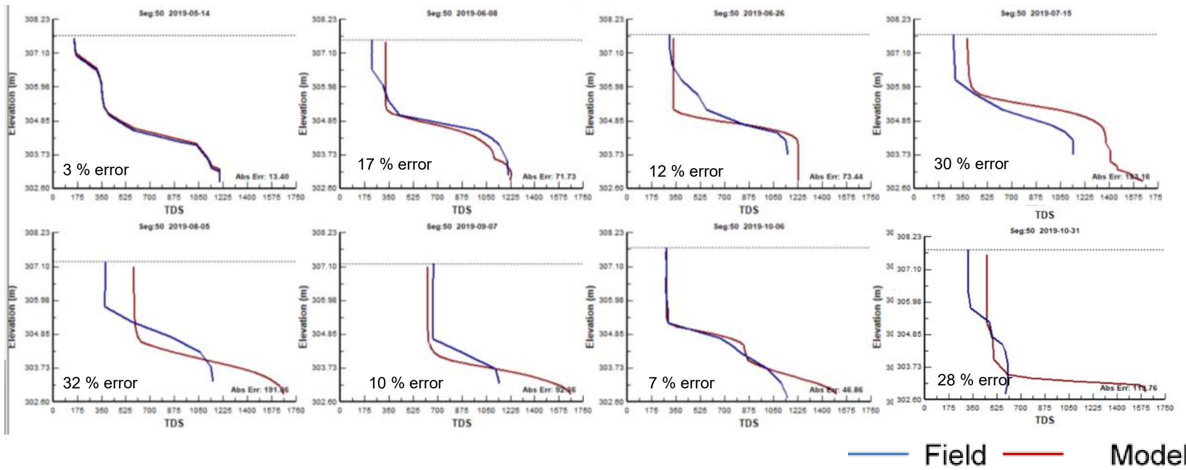

Figure 4.8: Modelled and field observed TDS profiles for Lower Unnamed Lake.

The modelled concentration of TDS in lower hypolimnion of the final calibration date (October 30th) was greater than observed from 303.25 MASL (0.4 m above sediment), indicating that the model did not turnover in the deepest 0.4 m, as was observed in the lake. The concentration of total dissolved solids was well represented within the model, with exception of July 15th and August 5th. Due to the increase TDS throughout the lake, it is evident that the high discharge rate of low-TDS inflow from UUL was accurately accounted for on July 5th.

4.2.3 Lake Outflow Total Dissolved Solids Calibration

The concentration of TDS at the outflow location was monitored using a conductivity meter and was compared to the model TDS outflow (Figure 4.9). The model outflow TDS had an AME 70 ± 45 mg/L (29 ± 23%, RSME = 83 mg/L, N = 2443), throughout May 13th - July 7th. The error then increased to an AME of 202 ± 60 mg/L (59

± 33%, RSME = 211 mg/L, n = 3037) throughout July 7th - September 5th. From September 5th to the end of the run year, the modeled TDS had an AME of 29 ± 46 mg/L (6 ± 10%, RMSE = 55 mg/L, n = 2616). The overprediction in TDS from July 7th to September 5th indicates that the high flow event from UUL, on July 4th was being underpredicted in the model. Both the modelled and observed increase with similar slopes (7.1 & 6.9 mg/L/day) after the high flow event. Aside from the increased concentration of TDS as a result of underpredicting the high flow event, the concentration of TDS is well represented by the model. The average AME throughout the model period was 106 ± 60 mg/L (33 ± 33%) and the RMSE was 129 mg/L (n = 8164).

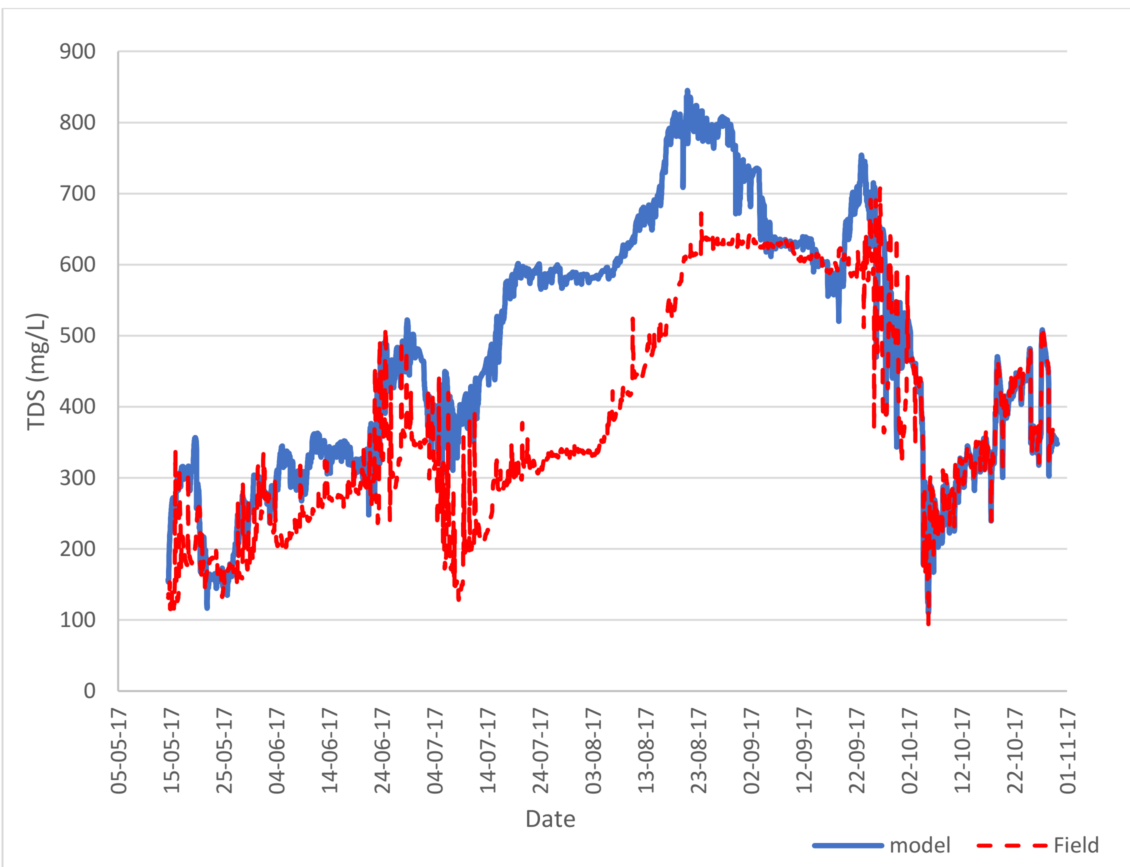

Figure 4.9: Modelled and Field TDS concentration (mg/L) of lake outflow

4.2.4 Dissolved Oxygen Profiles

Dissolved oxygen concentration (mg/L) profiles from the model were compared to field data with a calibration tolerance of 48 hours. The mean AME for all profiles was 0.68 mg/L ± 0.14 mg/L, with a RMSE of 0.96 mg/L (n = 71) (Figure 4.10). On the June 8th the model overpredicts the depth of oxygen saturation from the surface to the heterograde curve by ≈ 1 m. On June 26th, the modelled dissolved oxygen profile is an isocline, while the field profile is reduced from 7.5 mg/L in the epilimnion to 6 mg/L in the hypolimnion. The modelled dissolved oxygen profile remains an isocline after turnover, as opposed to the field, in which hypolimnion dissolved oxygen is reduced 3.25 m below the water surface (ELASL 304.6 m). The heterograde curve in the oxygen profile on July 15th and August 5th was expressed by the model. The AME of all modelled dissolved oxygen profiles were lower than 1 °C, and thus dissolved oxygen was deemed to be sufficiently modelled.

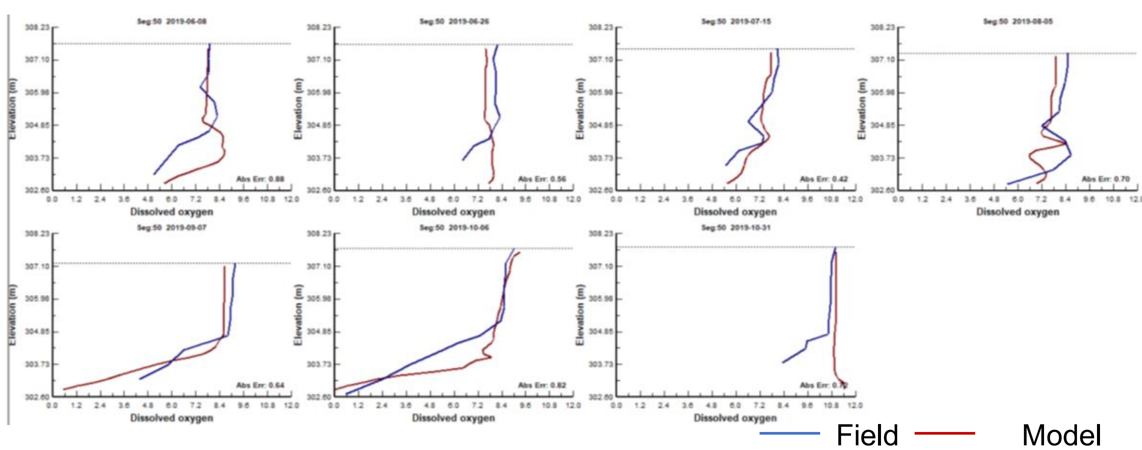

Figure 4.10: Modelled and field profiles of the concentration of dissolved oxygen

4.3 Proposed Pond 102 Discharge Location Model

A model of Lower Unnamed Lake was developed with the dischagre locaiton of Pond 102 modified (Figure 3.4-3.5).

4.3.1 Proposed 102 Discharge Location Temperature Profiles

Modelled temperature profiles from the current discharge location were plotted against the proposed discharge location every ten days and during turnover October 29th (Figure 4.11). Modifying the discharge location increased epilimnion temperature from June 13th to July 23rd, by a Mean Absolute deviation (MAD) of 1.33 ± 0.52 °C and root-mean-square deviation (RMSD) of 2.49 °C.

The variation in epilimnion temperature increased from the initiation of the model run until June 23rd, where the proposed discharge location epilimnion was 2 °C greater than the current location. After June 23rd the variation in epilimnion temperature decreased until August 2nd, where the epilimnion temperature varied by a MAD of 0.80 ± 0.01 °C (RSMD of 0.08 °C, n = 22). For the remainder of the model run year (August 2nd - October 3st), epilimnetic temperatures were similar, varying by a MAD of 0.31 ± 0.21 °C, with a RSMD of 0.38 °C (n = 255).

Epilimnion depth was increased in the proposed location model from May 24th to August 22nd, apart from August 2nd, where epilimnion depth was equal (2.87 m below water surface, 304.7 MASL). Epilimnion depth was increased by an average of a MAD 0.60 ± 0.26 m, with a RMSD of 0.66 m (n = 732) during that time period.

Hypolimnetic temperature was increased in the proposed location model from initiation of the model run to August 22nd by a MAD of 3.27 ± 2.67 °C, with a RSMD of 2.37 °C (n = 237). By September 1st the variation in temperature was reduced to 1.08 ± 0.57 °C (RMSE = 1.21 °C, n = 11) (J-day 244). From September 1st to turnover (October 29th) hypolimnion temperature in the proposed location model was lower than the current location model by a MAD of 1.62 ± 0.73 °C (RSMD = 1.78 °C, n = 40).

The model for the proposed location lacks the prominent isothermal hypolimnion, apparent in the current location model from May 24th to August 22nd. The hypolimnion temperature profile is near linear in the proposed model from the epilimnion to the sediment water interface (Figure 4.11).

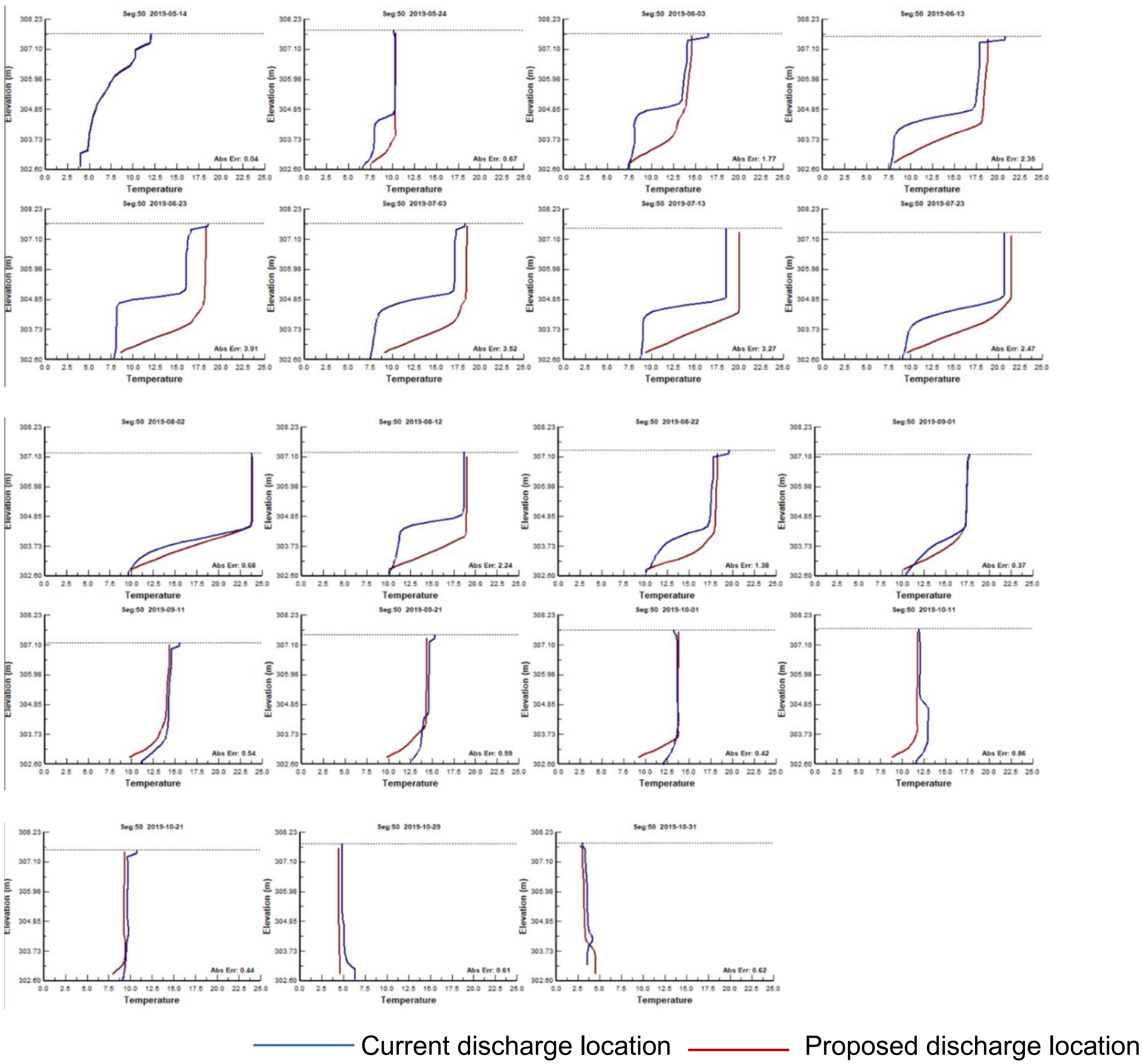

Figure 4.11: Modelled temperature (°C) profiles of the current and proposed discharge location models.

4.3.2 Temperature at the Sediment-Water Interface

The temperature at the sediment-water interface of the at the deepest section of the model (lulw2 0.18 km) in branch 2, column 50, layer 45 (302.85 MASL), coresponding with sample location “A” (16 U 577674 E 5393620) was plotted for the current and proposed discharge location model (Figure 4.12). The proposed and current location model had similar temperatures from the initiation of the model run year (May 12th) until August 1st, varying by a MAD of 0.41 ± 0.42 (RSMD = 0.59, n = 161). From August 1st to October 17th, the proposed location model temperature was lower than the current location model by a MAD of 1.79 ± 0.97 °C (RSMD = 2.03 °C, n = 339). From October 23rd to the end of the remainder of the model run year (October 30th) the sediment temperature was similar, varying by a MAD by of 0.55 ± 0.30 °C (RSMD = 0.63 °C, n = 339). The sediment temperature for the whole model run year varied by a MAD of 1.05 ± 0.99 °C (RSMD = 1.44, n = 339).

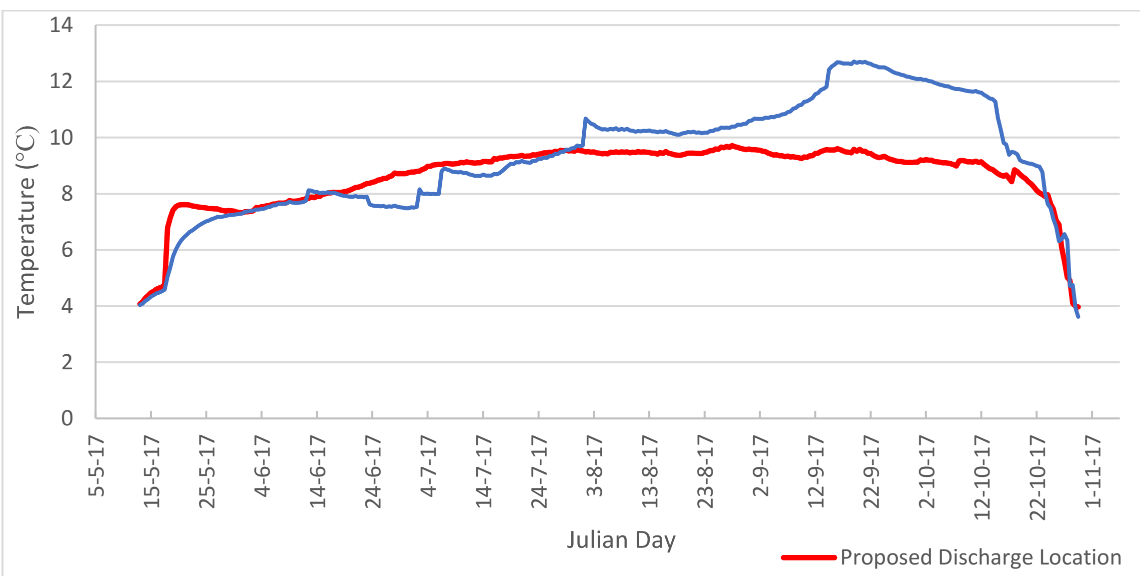

Figure 4.12: Temperature at the sediment-water interface of the current and proposed discharge location models.

4.3.3 Proposed 102 Discharge Location Total Dissolved Solids Profiles

Profiles of the proposed discharge location were plotted against the current discharge location model. By May 24th the TDS gradient was eliminated in the proposed location.The TDS concentration profile remained near isoclines thoughout most of the remainder of the year. (Figure 4.13).

After June 3rd, the concentration of TDS is greater the hypolimnion, relative to the epiliminion in the proposed model is increased on July 3rd & 13th and October 1st & 11th. The concentration of TDS in the hypolimnion is lower than the epilimion in the proposed model on June 23rd, July 23rd, and August 8th.

The epilimnion of the proposed location model has a similar TDS concentration as the respective depth as the current location model, with a MAD of 40 ± 39 mg/L (RMSD = 56 mg/L (n = 406). Relocating the discharge to the proposed location eliminates chemical stratification for almost all of the model run year.

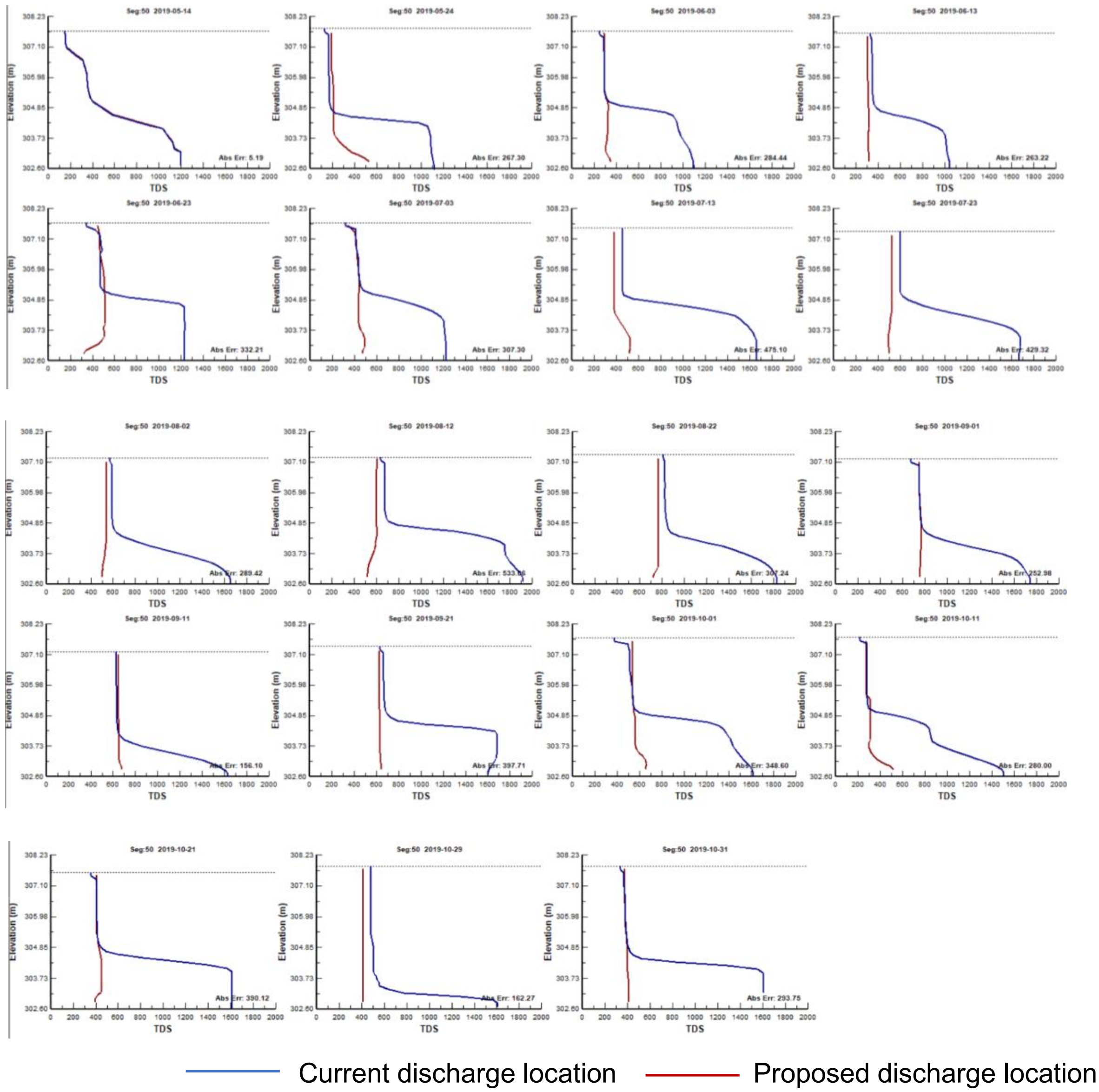

Figure 4.13: Modelled TDS (mg/L) profiles for the current and proposed discharge location model.

4.3.4 Hypolimnion - Epilimnion TDS Ratio

The ratio of the concentration of TDS in the hypolimnion (303.7 MASL) and TDS in the epilimnion, at a depth of 0.5 m below the water surface, and was plotted in Figure 4.14. A depth of 303.7 MASL (1.12 m above sediment) was selected to represent the hypolimnion to avoid the tendency of the model to over-estimate TDS below 303.7 MASL (Figure 4.6). A ratio of 1 indicates that there is no chemocline. A hypolimnion /

epilinmion TDS ratio greater than 1 indicates greater chemical stratificaiton. The current discharge location has isoclines on May 19th, October 2nd and October 28th. The ratio in the proposed discharge location model has the same initial TDS concentration profile within the lake. The ratio is diminished on May 19th. A ratio of < 1.1 persists throughout the year, with the exception of May 19th - May 27th, June 20th - July 14th and October 3rd - October 13th.

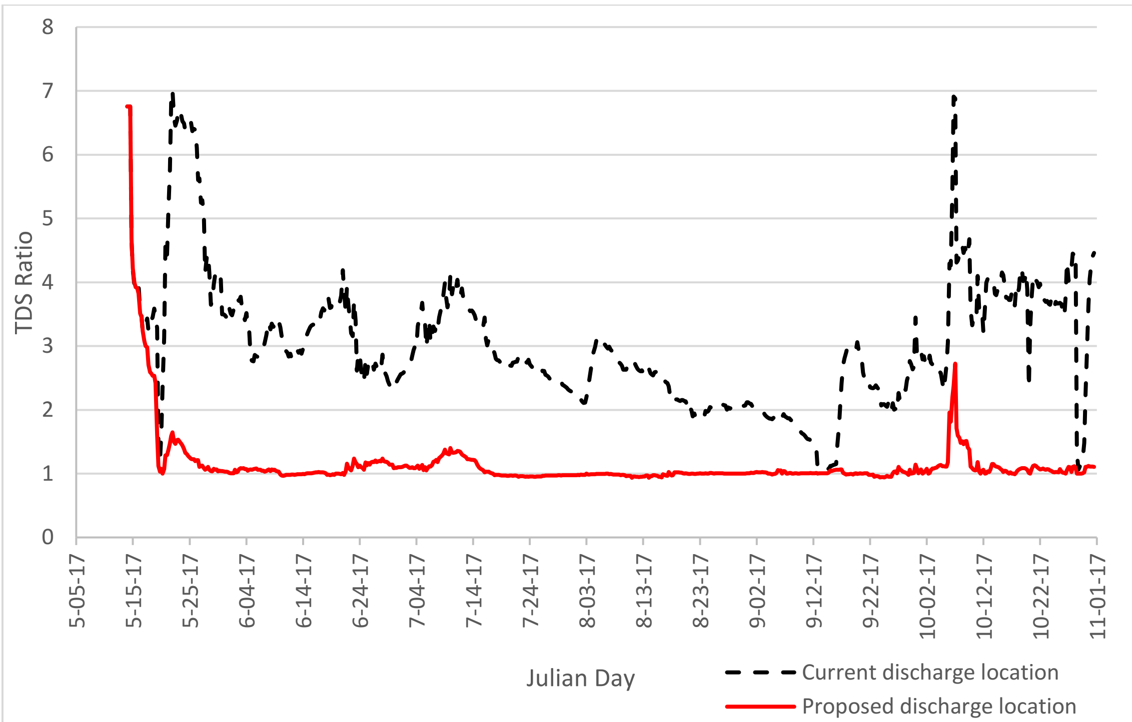

Figure 4.14: Hypolimnion - epilimnion TDS ratio for the proposed and current discharge location model.

4.3.5 Total Dissolved Solids in West Basin

The concentration of TDS at sample location “A”, at the deepest section of the lake, within the west basin (16U 577674 E 5393620) was plotted over the model run year for the current and proposed discharge location model in (Figure 4.15). The greatest concentration of TDS in the proposed location 770 mg/l, while the greatest concentration of TDS in the current location is 1760 mg/l. The proposed discharge location reduced hypolimnion TDS in the west end of Lower Unnamed Lake model.

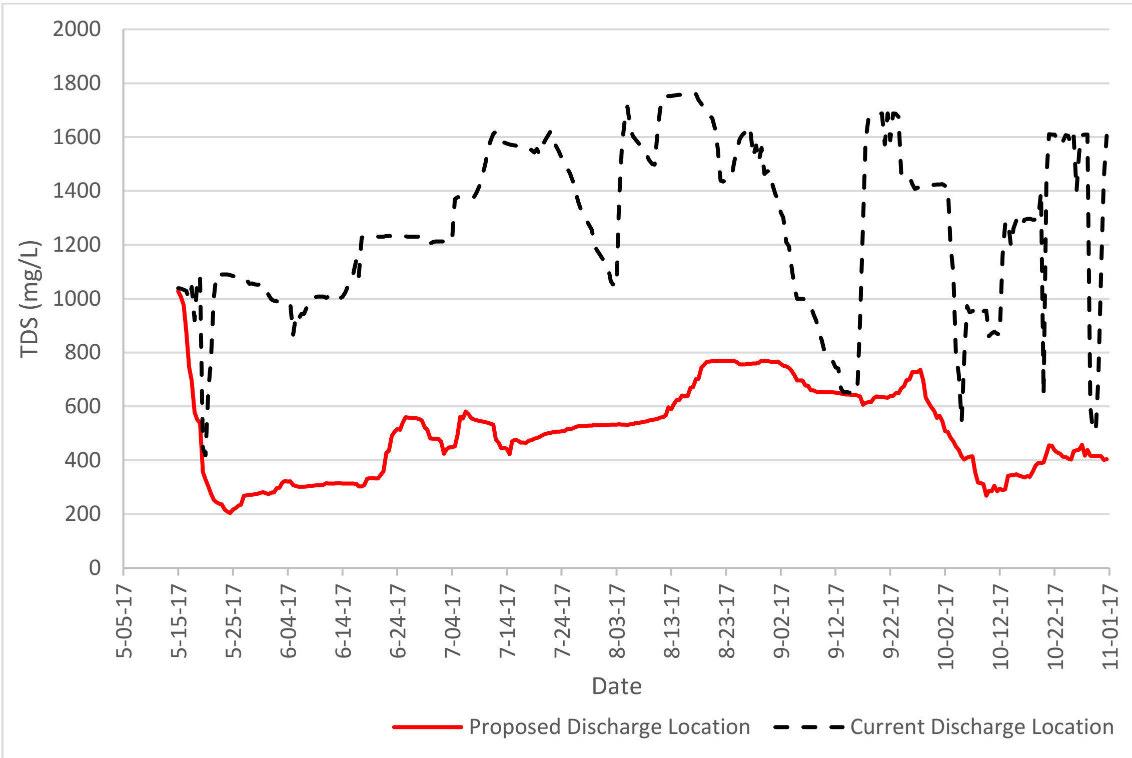

Figure 4.15: Modelled TDS (mg/L) concentration for the current and proposed discharge location in the west end of the lake model.

4.3.6 Total Dissolved Solids in East Basin of Lower Unnamed Lake

The concentration of TDS at the east end of Lower Unnamed lake (16U 578777, E 5393548), at sample location "B", the portion upstream of both the current and proposed discharge location was modelled. Figure 4.16 illustrates that the proposed discharge location increases the concentration of TDS on the east end of the lake, 0.5 m above the bottom of the lake (306.35 MASL). The concentration of TDS is greater in the proposed discharge location model throughout the entire the model run year.

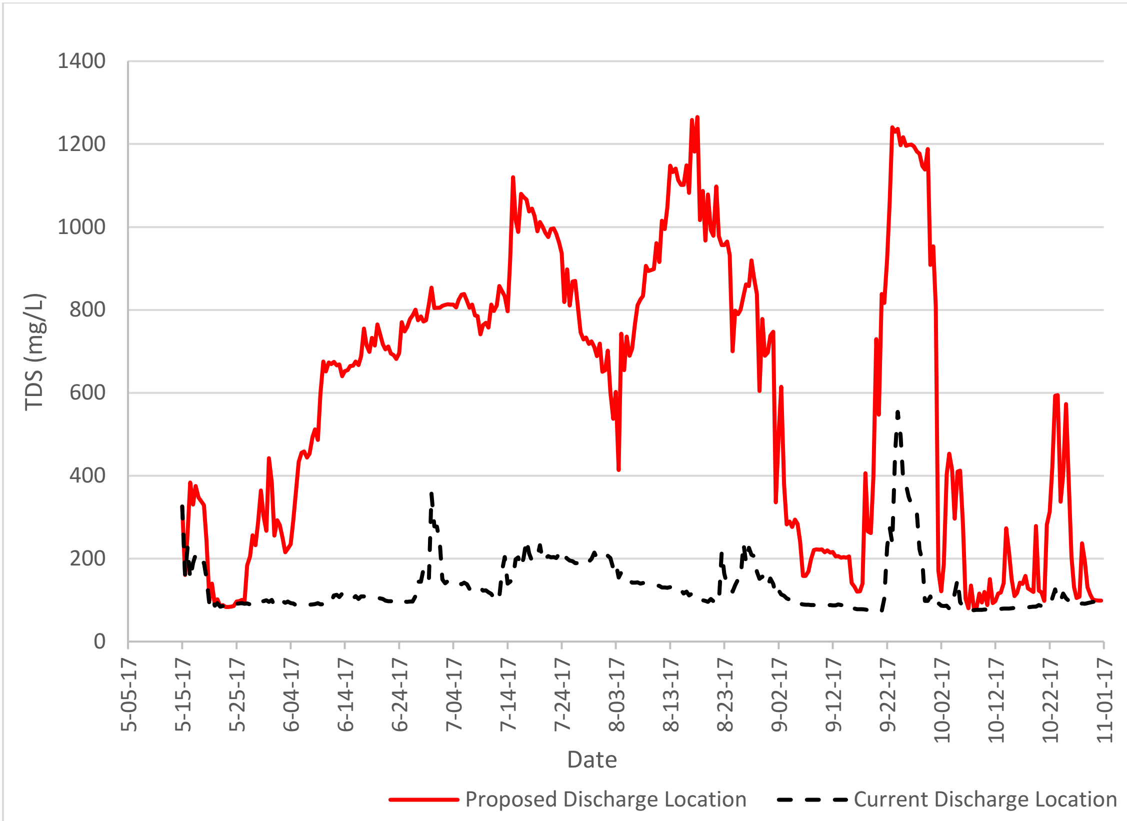

Figure 4.16: Modelled concentration of TDS at the east end of Lower Unnamed Lake under the current discharge location and proposed discharge location.

4.3.7 Proposed Outflow Total Dissolved Solids

The modelled current location and proposed location concentration of TDS of the outflow of the lake were plotted (4.17). The AME of the outflow concentration of TDS was 33 ± 23 mg/L. The absolute percentage variation was 7.2 ± 5.1% and the RMSE was 0.49 mg/L. The concentration of TDS discharged into the watershed was similar for both the current and proposed discharge locations.

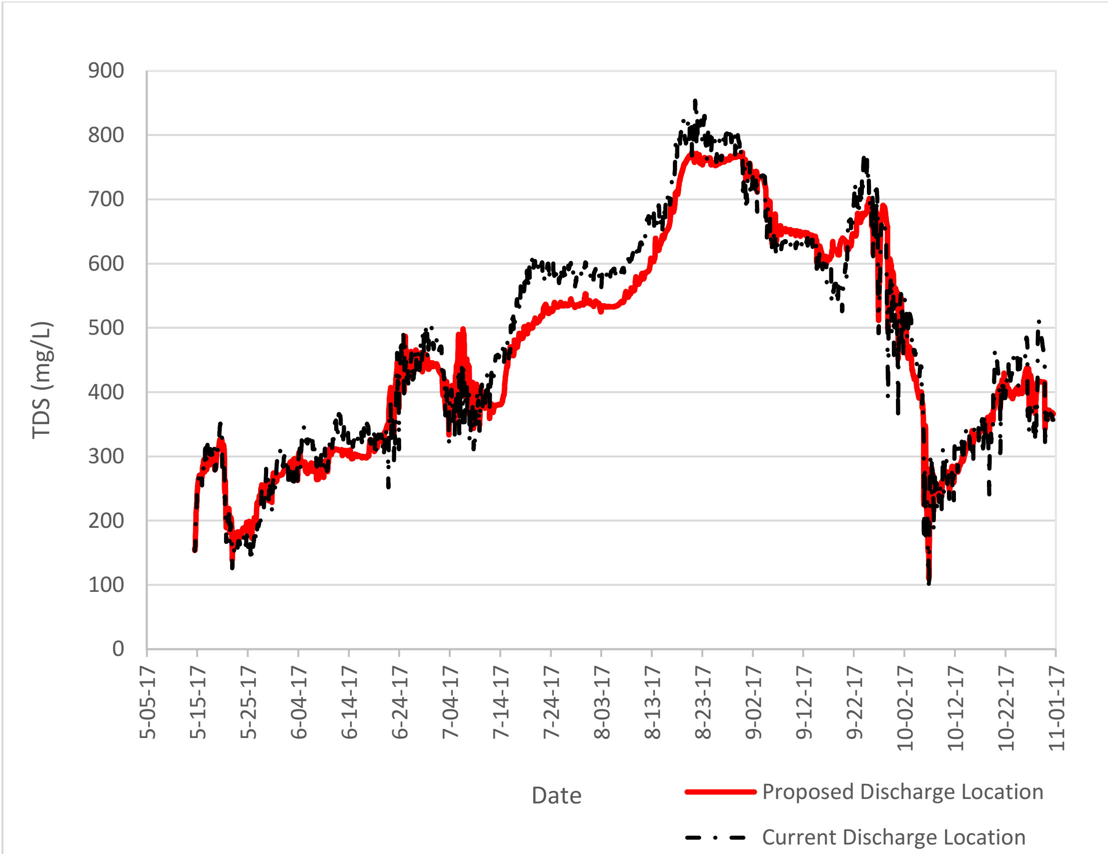

Figure 4.17: Concentration of TDS of lake outflow for the current and proposed discharge location.

4.3.8 Distriabution of Total Dissolved Solids

Figure 4.19 & 4.20 are screenshots of the animation of the TDS concentration across the lake model on July 15th. July 15th were chosen as a representitave date, as discharge from Pond 102 was high and the inflow from Upper Unnamed lake was moderate, resulting in strong gradients in TDS and momentum and prominent mixing patterns. The main basin (IulW2) of the current discharge location exhibits a strong gradient of the concentration of TDS. The shallow section on the east end of the lake (IulW1) had a lower concentration of TDS, compared to the epilimnion of the main basin (Figure 4.18).

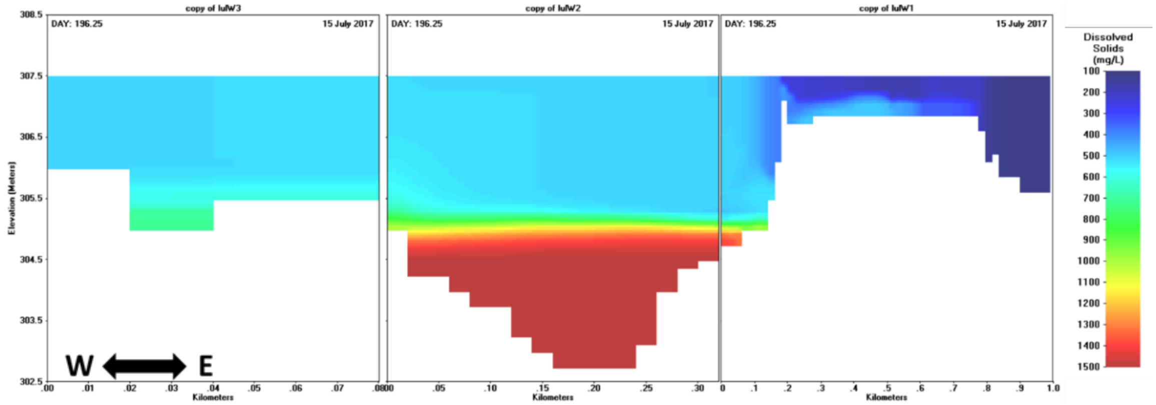

Figure 4.18: Lake profile of the concentration of TDS in the current discharge locaiton model

Figure 4.19 illuistrates the lake profile of the proposed discharge model. The main basin (lulW2) did not exhibit a TDS gradient. The shallow section on the east end of the lake (lulW1) has a greater concentration of TDS, compared to the epilimnion of the main basin (Figure 4.19). The greatest concentration of TDS is at the bottom of the lake in the shallow section, at the location of the proposed discharge (lulw1 0.4 km).

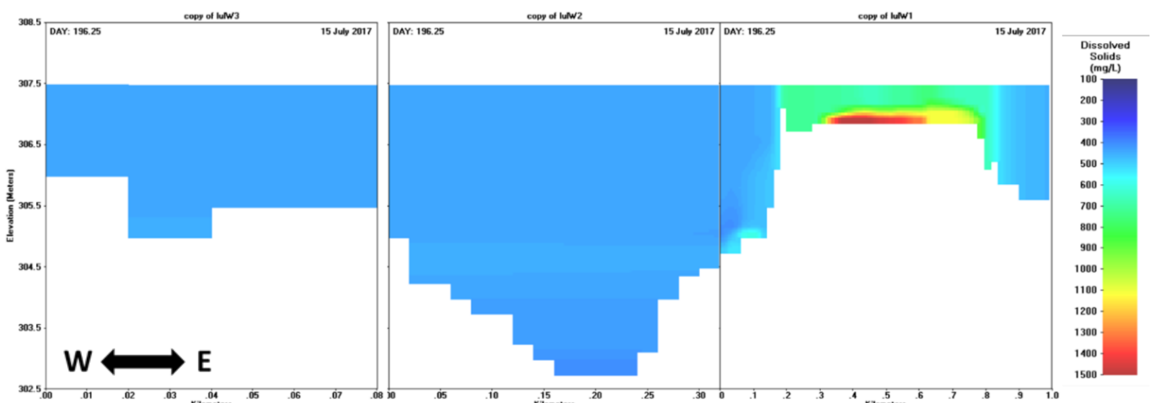

Figure 4.19: Lake profile of the concentration of TDS in the current discharge locaiton model.

4.3.9 Dispersion of Total Dissolved Solids & Water Mixing Patterns

Figures 4.20 - 4.21 illistrate the concentration of total dissolved solids and vectors for water momentum within the main basin (lulW2) of the lake model. The water circulation patterns in both models were similar. The surface to 0.25 m (307.25 MASL) below the water surface flows east to west. Beneath that, the upper epilimnion convection is from west to east (307.25 - 306.25 MASL). The water momentum within the lower region of the eplimnion flows east to west (306.25 - 305.25 MASL). The epilimnion is slightly deeper in the proposed discharge location model (307.5 – 305.0 MASL), compared to the current locaiton model (307.5 – 305.25 MASL). The increased velocity is the result of convection in the littoral zone. There is little momentum in the hypolimnion of both models.

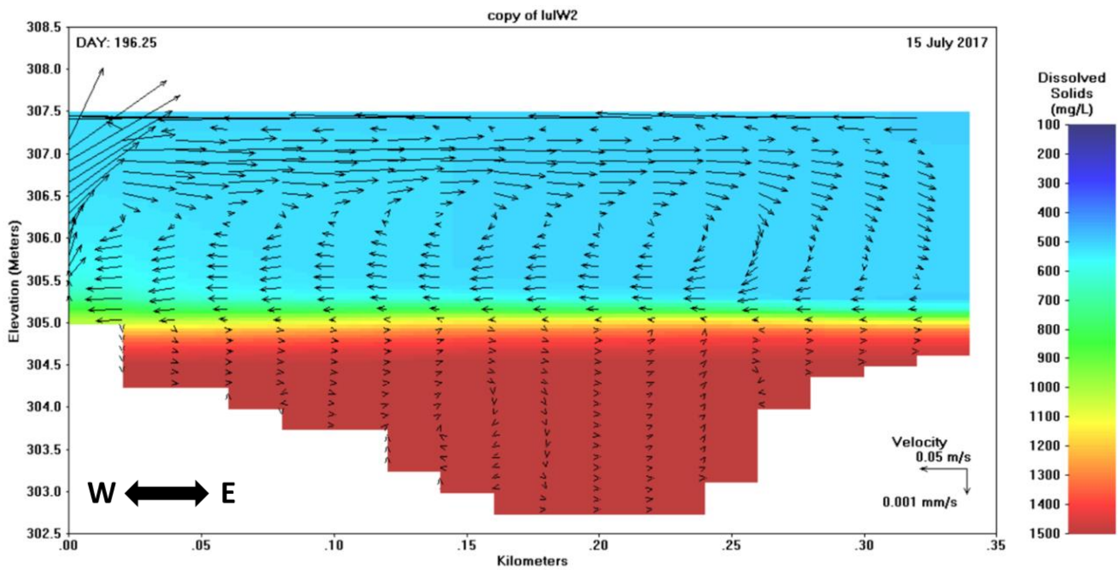

Figure 4.20: Concentration of TDS and water momentum in the main basin of the lake model under the current discharge location.

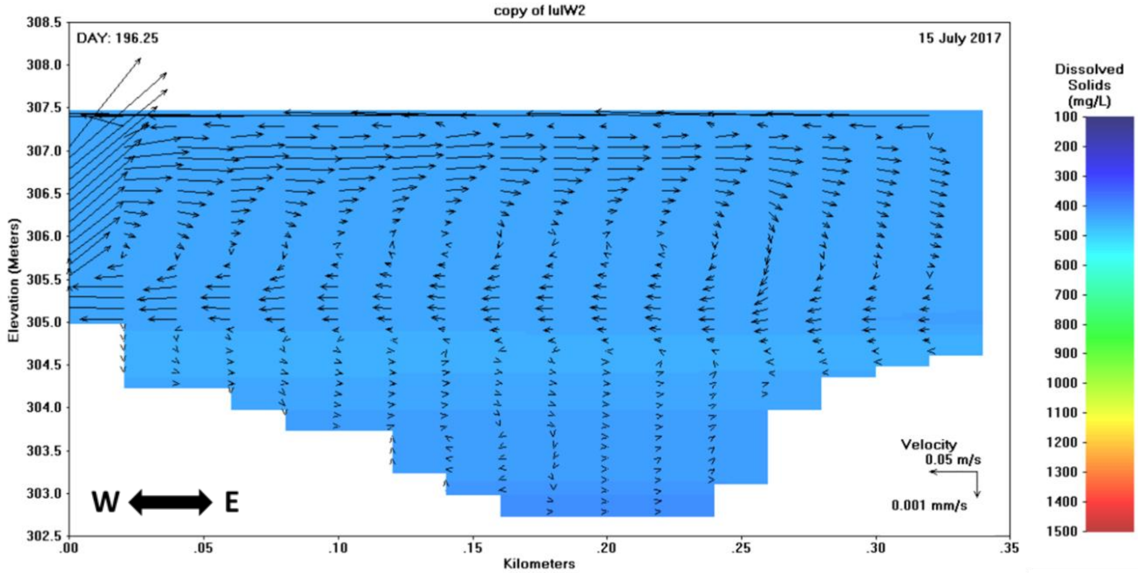

Figure 4.21: Concentration of TDS and water momentum in the main basin of the lake model under the current discharge location.

Figures 4.22 - 4.23 illistrate the concentration of total dissolved solids and vectors for water momentum within the east end (lulW1) of both models. Both the current location model (Figure 4.22) and the proposed location model (Figure 4.23) had similar water circulation patterns. The furthermost east basin (0.8 - 1.0 km), where the Upper Unnamed Lake flowed into lower was fully turning over in both models. The shallow section (0.2 – 0.8 km) of both models exhibit stratification in the concentration of TDS and water momentum.

In the east end (lulW1) of the current locaiton model, discharge water with a greater concentration of TDS flowed from the main basin (0 - 0.2 km), over the shallow section, to the east end, where the discahrge water interfaced with the lower TDS water from Upper Unnamed Lake and became diluted until the water reached the east basin (0.8 - 1 km). Water from the two sources was then fully mixed. The fully mixed water then flowed east to west, into the main basin (Figure 4.22).

Discharge water from the proposed discharge location (0.4km lulw1) flowed east, along the bottom of the channel to the east basin, where the discharge water was fully mixed with inflow from Upper Unnamed Lake. The modelled fully mixed water then flows east to west, passing over the high TDS discharge water of the proposed discharge location and mixed along the interface, thus diluting the TDS in the discharge water (Figure 4.23.). There was a prominent lateral gradient of TDS where the main basin reaches the shallow channel (0.2 km) of 450 mg/L and 800 mg/L, respectivaly.

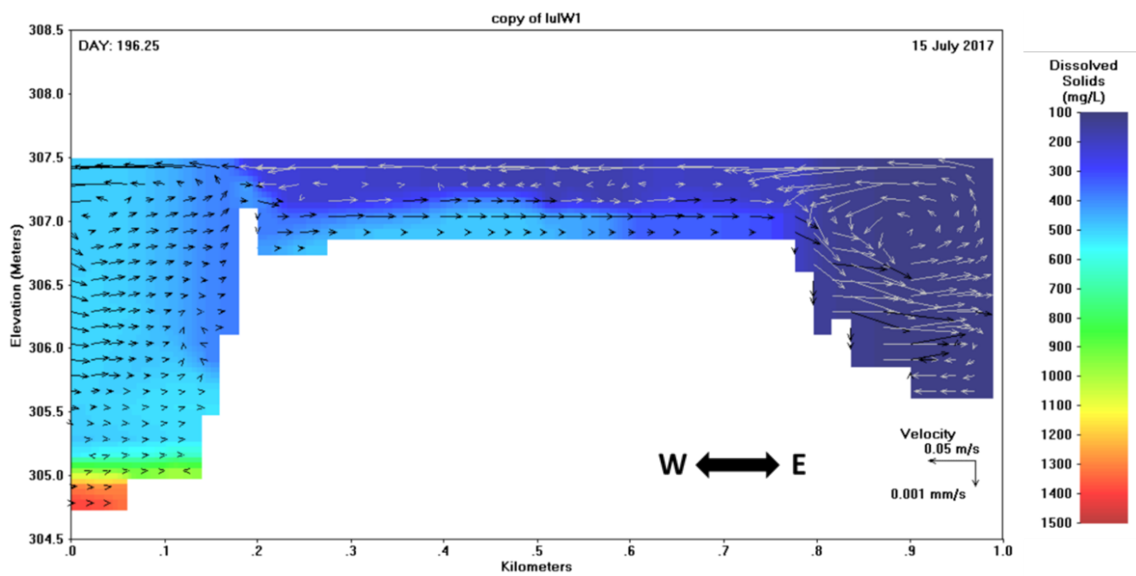

Figure 4.22: Concentration of TDS and water momentum in the east end of the lake model under the current discharge location.

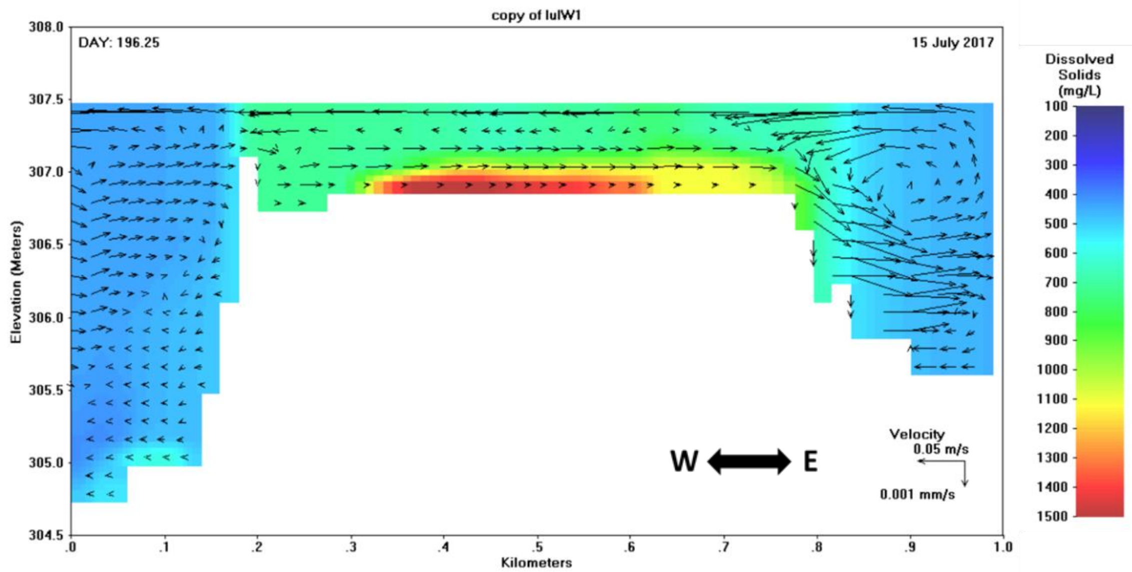

Figure 4.23: Concentration of TDS and water momentum in the east end of the lake model under the current discharge location.

4.3.10 Proposed 102 Discharge Location Dissolved Oxygen Profiles

Dissolved oxygen profiles in the current and proposed discharge location modes were plotted in Figure 4.24. The disolved oxygen profile in the current discharge location model had a prominent heterograde curve, inicating an increase in dissolved oxygen. The heterograde curve was initiated at approximatly 304.85 MASL, 2.25 m above the sediment in the deepest section of the lake. The proposed model did not contain a heterograde curve at any time. The epilimion concentration of dissolved oxygen was largely uneffected by moving the discharge location, varying by a MAD of 0.19 ± 0.14 mg/L (RSMD = .023, n = 249).

By May 24th, hypolimnietic dissolved oxygen in the proposed discharge model was lower from 7.2 mg/L in the current location model to 5.5 mg/L. The lower hypoliminion of the proposed discharge model became hypoxic, - with the concentration of dissolved oxygen < 2 mg/L - on June 23rd and continued to be until September 21st. Hypoliminion dissolved oxygen was reduced by a mean of 3.22 ± 2.02 mg/L (RSMD = 3.80 mg/L, n = 105) from May 24th to August 12th. Both models had a similar concentration of hypoliminetic dissolved oxygen from Auguest 22nd to October 11, with a MAD of 0.96 ± 0.80 mg/L (RSMD = 1.25 mg/L, n = 64). Both models were fully saturated in dissolved oxygen during and after turnover (October 28th & 30th).

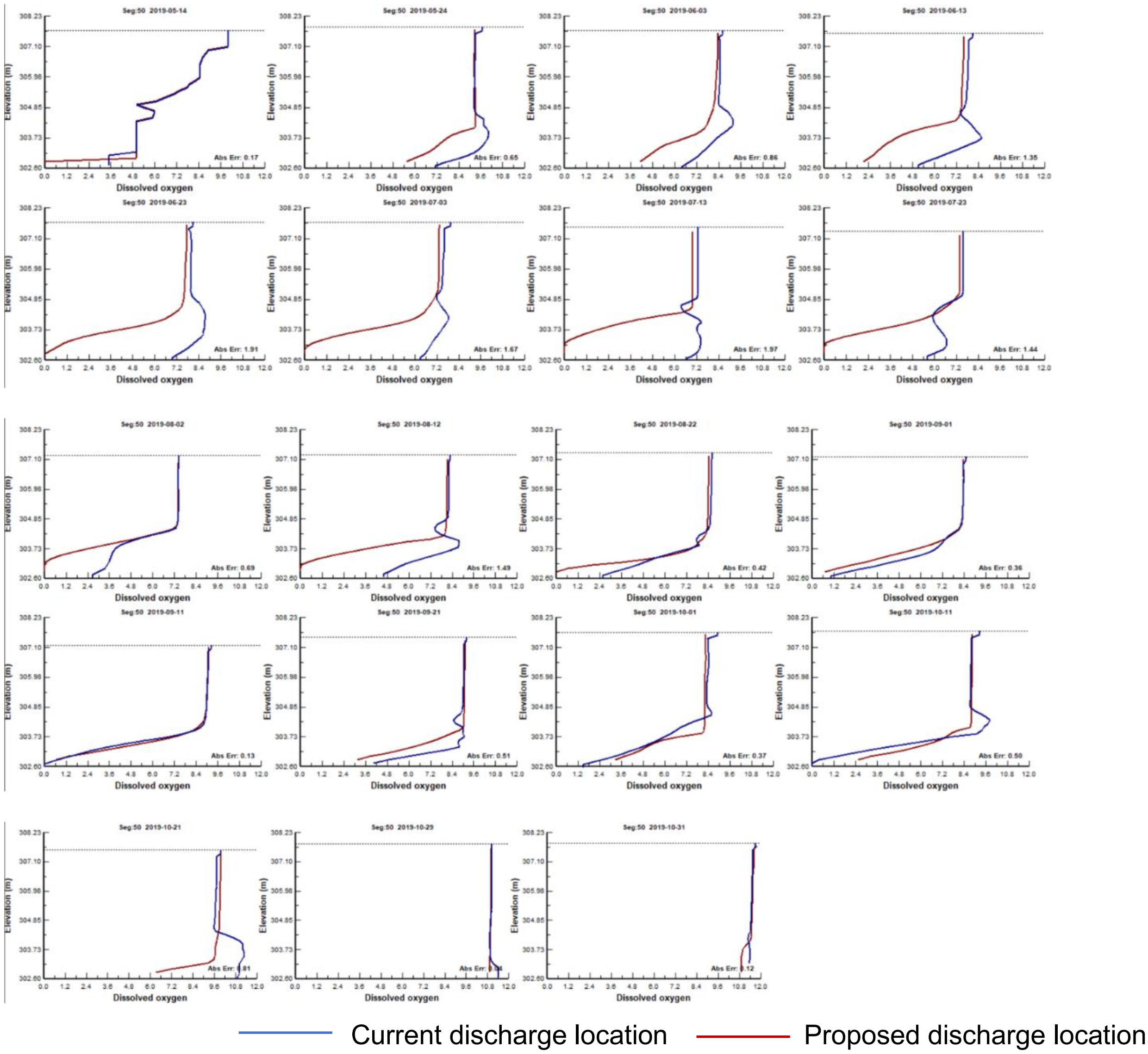

Figure 4.24: Modelled dissolved oxygen (mg/L) profiles for the current and proposed discharge location model.

4.3.11 Hypolimnion - Epilimnion Density Ratio

The current discharge location model hypolimnion / epilimnion density ratio approched 1 on May 19th, September 12th and October 28th (Figure 4.25). The density ratio trended to increase from May 19th to a maximum of 1.003 on July 28th. Afterwards, the density ratio decreased until it approaches 1 on September 12th. The density ratio then increased and remains moderate (1.0005 – 1.0015 until turnover, on October 28th. After turnover the density difference is resetablished.

The proposed discahrege model has a lower hypolimnion / epilimnion density ratio than the current model for the entireety of the run year. The density ratio approached 1 on May 20th, August 8th & 20th, September 9th, 13th, 17th & 19th, October 2nd, 12th, 17th, 20th, 26th & 29th. Due to the lower ratio of hypolimnion / epilimnion density difference, the proposed dischagre location results in the lake being more sususeptiable to turnover. Relocating Pond 102 to the proposed discharge location greatly reduces density-induced stability.

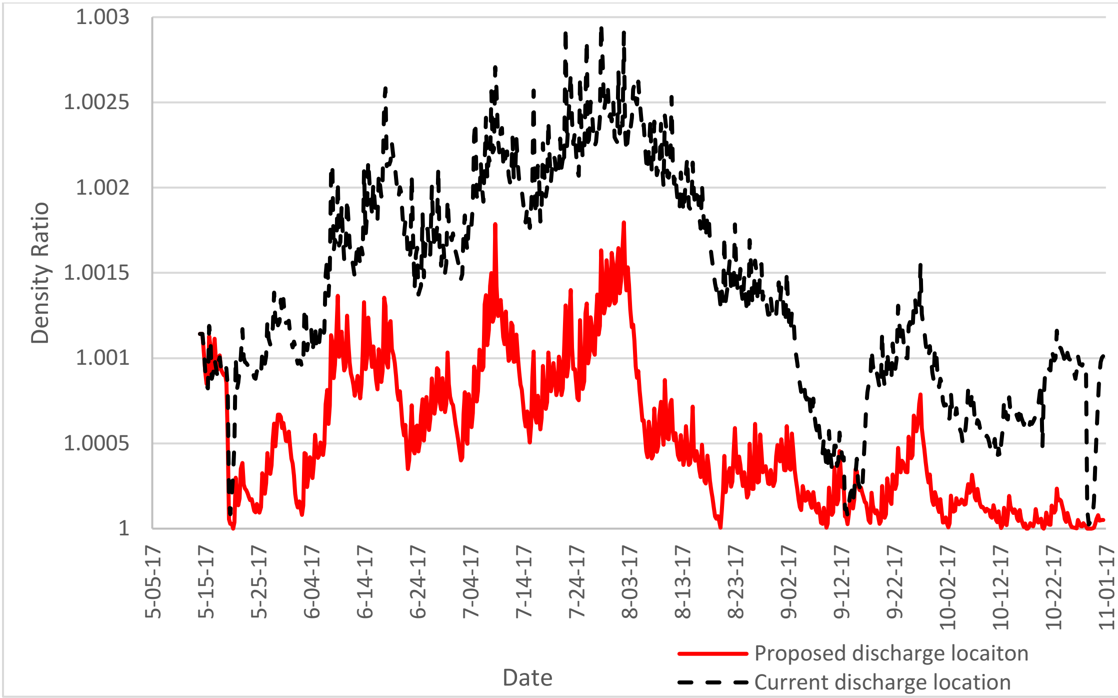

Figure 4.25: Hypolimnion - epiliminion density ratio in the current and proposed discharge location models.

4.4 Lake Model with Pond 102 Discharge Eliminated

The discharge from Pond 102 was removed from the model and compared with the temperature, TDS and dissolved oxygen within the proposed location model.

4.4.1 Pond 102 Discharge Eliminated and Proposed Discharge Location Temperature Profiles

Temperature profiles in the unimpacted and proposed discharge location models were plotted every ten days, and during turnover (October 29th) (Figure 26). Temperature profiles in both models were similar, with a MAD of 0.46 ± 0.44 °C throughout the model run year (RSMD = 0.64, n = 731). During turnover, the unimpacted model was 0.70 °C warmer. Modifying the discharge location resulted in similar temperatures, as if the lake did not receive discharge from Pond 102.

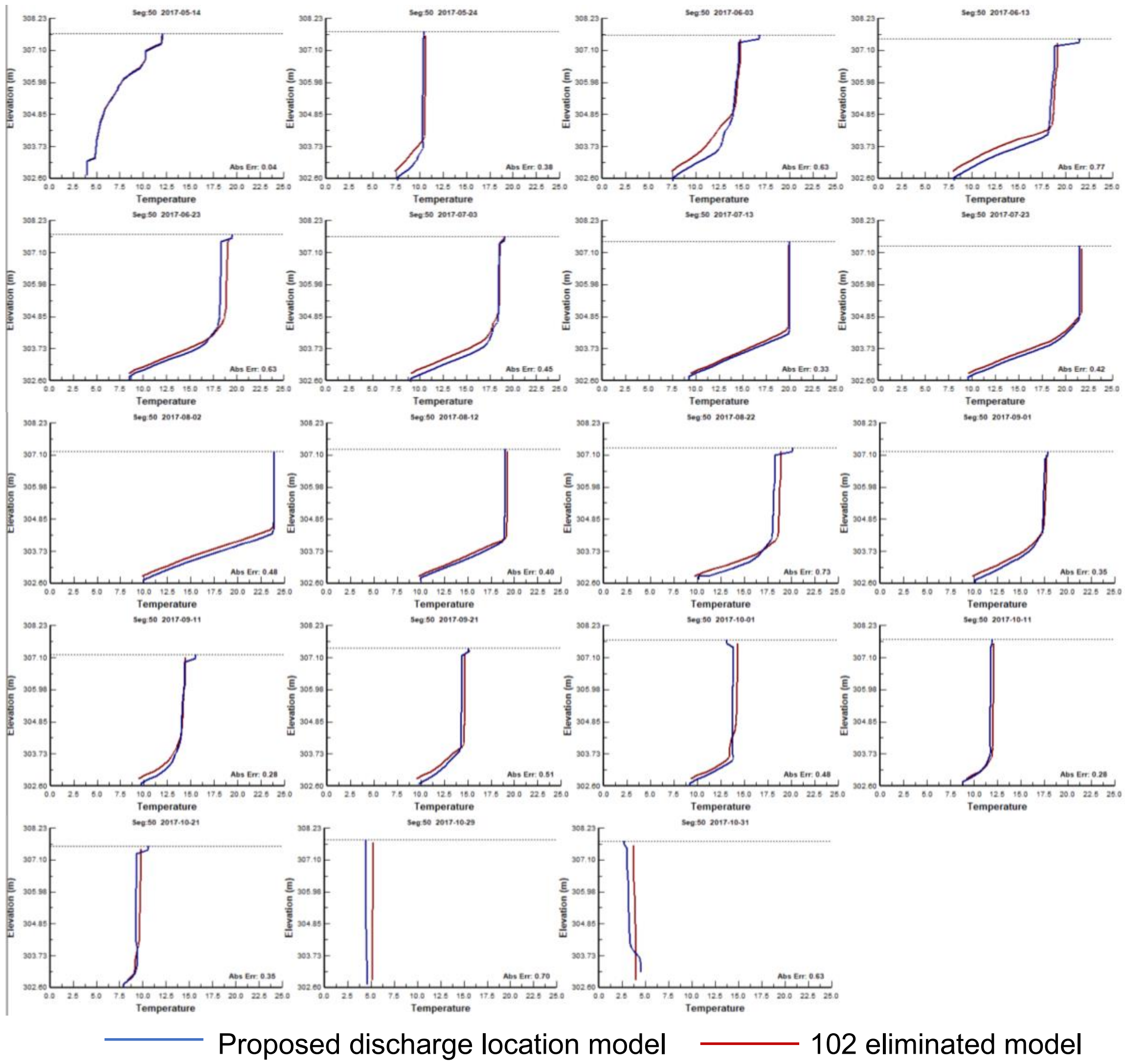

Figure 4.26: Modelled dissolved oxygen (mg/L) profiles for the Pond 102 discharge eliminated and proposed discharge location models.

4.4.2 Pond 102 Discharge Eliminated and Proposed Discharge Location

Total Dissolved Solids Profiles

TDS profiles in the unimpacted and proposed discharge location models were plotted every ten days, and during turnover (October 29th) (Figure 27). Both models diminish the TDS gradient in a similar manner in the initial 30 days. By July 13th the chemical stratification is eliminated and continues to be so throughout the remainder of the model run year. From July 13 throughout the run year the concentration of TDS was

83.78 ± 7.70 mg/L (n = 533). The average concentration in the proposed discharge location model was 512.98 ± 149.42 mg/L (n = 533).

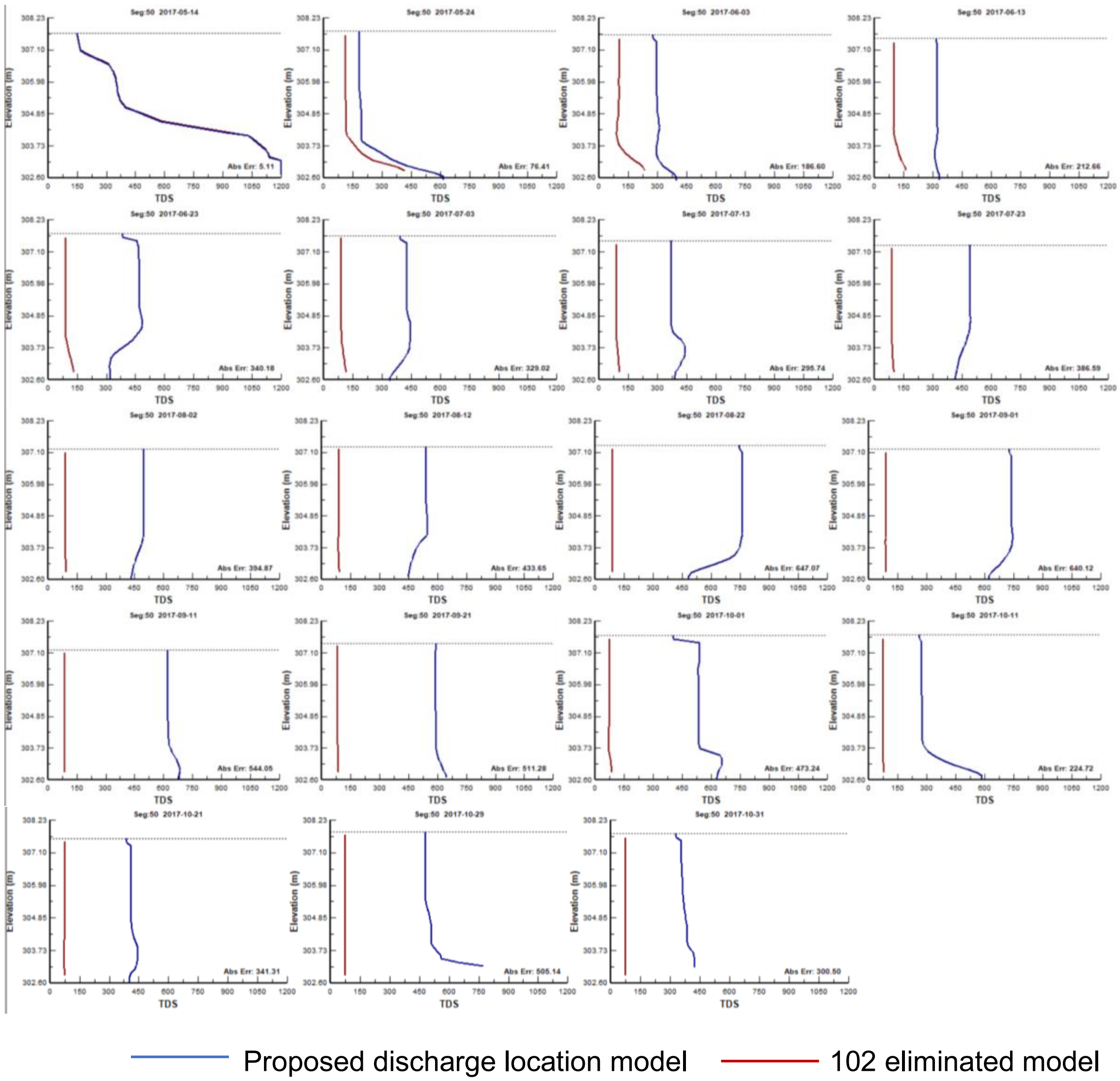

Figure 4.27: Modelled TDS (mg/L) profiles for the Pond 102 discharge eliminated and proposed discharge location models.

4.4.3 Unimpacted and Proposed Discharge Location Dissolved Oxygen Profiles

Dissolved oxygen profiles were plotted every ten days, and during turnover (October 29th) for the unimpacted and proposed location models (Figure 4.28). The dissolved oxygen was similar in the proposed location model and unimpacted model, with a MAD of 0.41 ± 0.46 mg/L (RSMD = 0.62 mg/L, n = 731). The unimpacted model has a heterograde curve on June 2nd, September 30th, October 10th and October 20th. During turnover, the unimpacted model is 0.63 mg/L lower than the proposed discharge model.

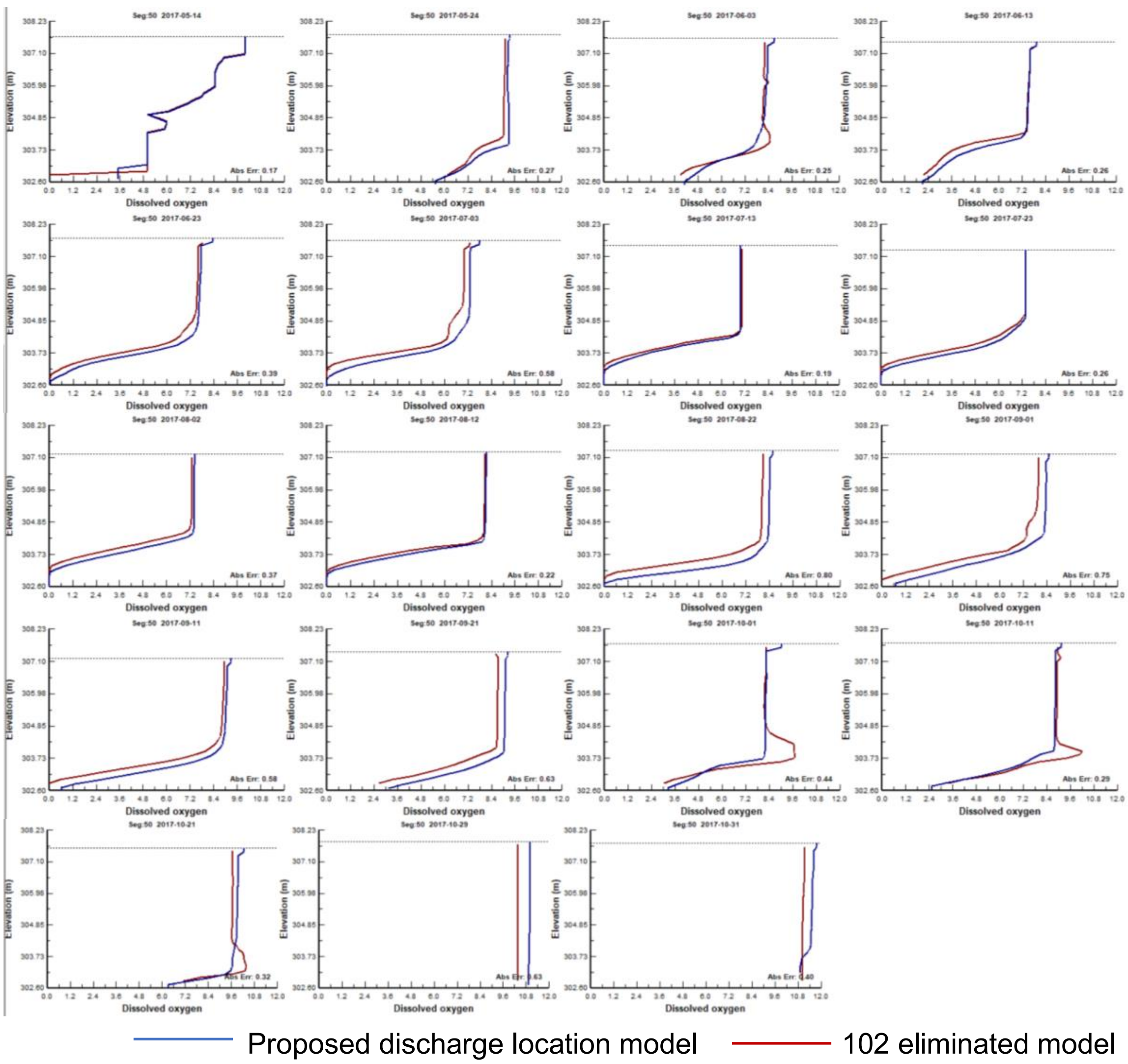

Figure 4.28: Modelled dissolved oxygen (mg/L) profiles for the Pond 102 discharge eliminated and proposed discharge location models.

4.5 Meromictic Potential Under the Current and Proposed Discharge Location Models

The flow rate, Pond 102 discharge TDS and wind sheltering coefficient for the current and proposed discharge location models were modified to assess the potential for a meromictic condition to develop.

4.5.1 Hypolimnion - Epilimnion TDS Ratio of Meromictic potential in both Current and Proposed Discharge location models

The ratio of hypolimnion / epilimnion TDS in the current and proposed location meromictic potential models were plotted in Figure 4.29. The TDS ratio in the current discharge location was greater than 2.9 throughout the model run year, indicating that a substantial TDS gradient persisted throughout the model run year. The TDS ratio in the current discharge location model indicated that turnover did not occur.

The TDS ratio in the proposed discharge location is approximately 1 from May 22nd, throughout the remainder of the model run year, indicating that there was no TDS gradient present. The proposed discharge location largely eliminated chemical stratification.

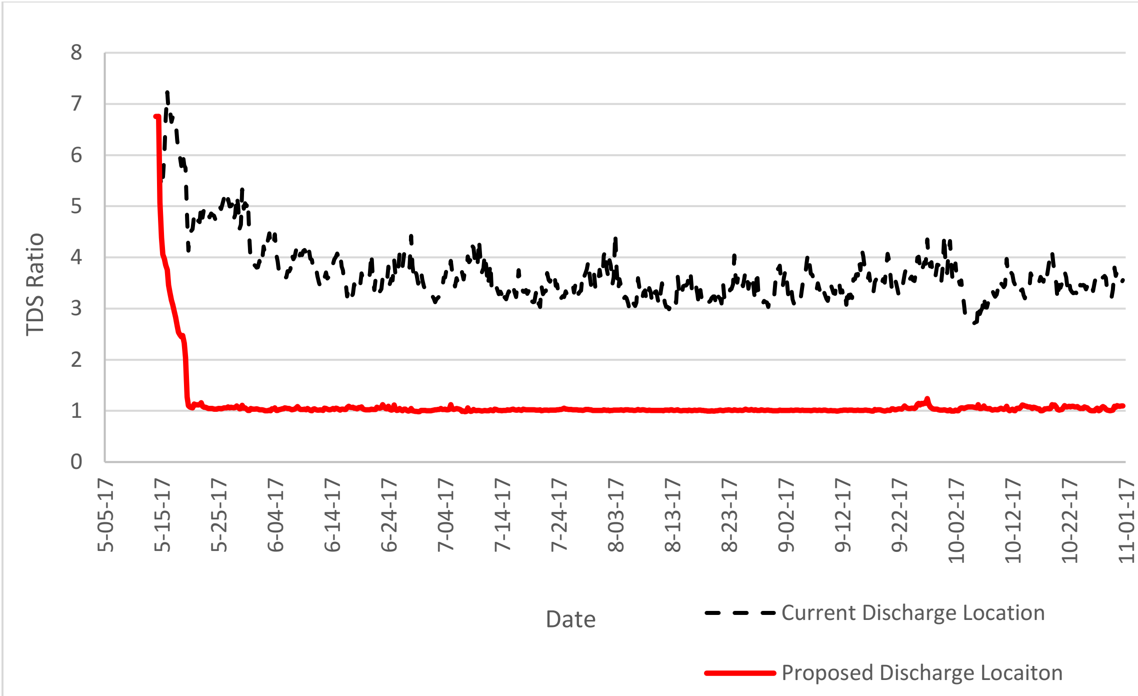

4.29: Total Dissolved Solids Ratio for the current and proposed discharge location in the meromictic potential models

4.5.2 Hypolimnion - Epilimnion Density Ratio of Meromictic Potential in both Current and Proposed Discharge Location Models

The ratio of hypolimnion / epilimnion density in the current and proposed location meromictic potential models were plotted in Figure 4.30. The current discharge location model density ratio is greater than 1.001 throughout the model run year, indicating that turnover did not occur. The density ratio in the proposed location model was 1 on May 20th, September 9th, and intermediately from October 12th throughout the remainder of the model run year, indicating turnover occurred in the proposed location model.

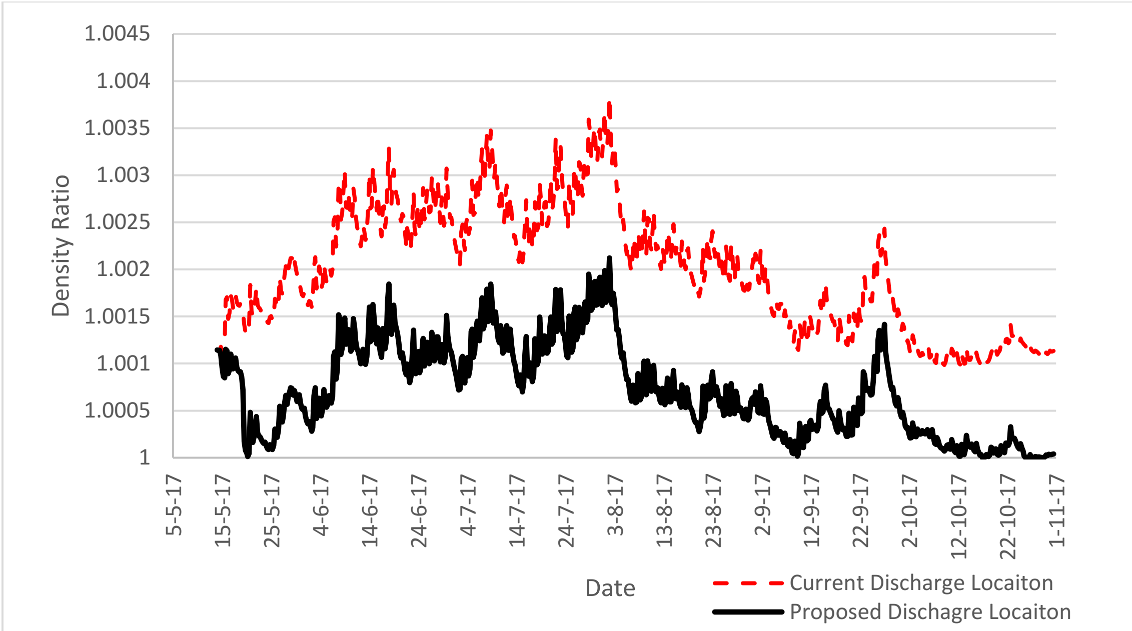

4.30: Density Ratio for the current and proposed discharge location in the meromictic potential models

5 Discussion

5.1 Model Accuracy

A CE-QUAL W2 model of Lower Unnamed Lake was developed and calibrated. A detailed explanation of all calibration parameters was discussed in Appendix C 1.

Temperature

Notable deviations of modelled values compared to observed values were discussed below. Temperature profiles and outflow temperatures were well-calibrated, with an AME of 0.72 °C and 1.08 °C, respectively (Figure 4.6; Figure 4.7). The CE-QUAL W2 manual recommends temperature be within an AME of less than 1 °C, therefor the model was effectively calibrated, with regards to temperature (Cole & Wells, 2013). The temperature profiles and outflow temperatures were progressively more accurate as the model year progressed. Deviation in temperature accuracy was attributed to a limitation in CE-QUAL W2. Sediment temperature and the coefficient for bottom heat exchange are constant throughout the year in the model. Constant sediment temperature may work in large, deep lakes, where hypolimnion and sediment temperature is largely unchanged, but shallow lakes, such as LUL experience a variation in sediment temperature throughout the year (Fang & Stefan, 1996; Birge *et al.* 1927). The addition of a dynamic sediment temperature function within the model would eliminate this predicament.

Total Dissolved Solids

Total dissolved solids were well represented within the model, with the exception of July and August (Figure 4.8; Figure 4.9). This corresponded with a high flow period from UUL (Figure A.12). The field determined outflow TDS was reduced to 131 mg/L, while the modelled TDS was only reduced to 309 mg/L, although the model and observed exhibited the same concentration on July 6th. It is likely that the inflow was under-predicted during the high flow period on July 7th, as a result in variable stage height, resulting in less low-TDS water diluting the high-TDS lake water within the model (USGS, 2013). The concentration of TDS was overpredicted by the model in the deepest 0.5 m of the lake. The cause of the error was likely due to errors in the bathymetric grid artificially increased frictional forces and inhibited eddy development (Lu & Wang, 2009; Limerinos, 1970; Jarrett 1984). Stream gauging during high flow events would increase the accuracy of modelled TDS.

Dissolved Oxygen

The CE-QUAL W2 manual suggested that dissolved oxygen profiles should have an AME less than 1 mg/L (Cole & Wells, 2013. Although the model did not include algae, all calibration dates were under 1 mg/L. The mean AME for all dates was 0.68 mg/L (Figure 4.10). After turnover, on October 30th, the model dissolved oxygen remains as an isocline, fully saturated throughout the water column. However, within the Lower Unnamed Lake, the concentration of hypolimnion dissolved oxygen was reduced. The model did not account for an increased rate in oxygen consumption as a result of turnover (Galvez & Niell, 1992). The sediment in Lower Unnamed Lake consisted of a high proportion of organic matter, averaging 30% w/w, and low bulk density, averaging 0.14 g/cm^3. There were a large population of macrophytes, including *Equisetum sp*. and *Typha sp.* within the lake (Appendix A, Figure A.21). Macrophytes contribute autochthonous organic matter, which settles to the sediment and is then re-suspended during turnover, releasing nutrients and organic matter into the water column (Andersen & Olsen, 1994), resultin in increased biological oxygen demand (Human *et al.* 2015). Sediment resuspension was one of, but not the only limitation in the CE-QUAL W2 model dissolved oxygen model of Lower Unnamed Lake. Future studies should include a detailed survey of the algal community to effectively include algae within the model. Another source of error, which contributed to the discrepancies in hypolimnion dissolved oxygen was the distribution of inflows in CE-QAUL W2. Pond 102 discharge was assumed to be fully saturated. In the Lower Unnamed Lake, the discharge water flowed over the littoral zone, and over the sediment-water-interface, as the discharge water was more dense than the epilimnion. It is likely that at this time dissolved oxygen was consumed by the sediment. As a result, the discharge water would likely of have had a lower concentration of dissolved oxygen when it reached the hypolimnion (Matisoff & Gerald, 2005). The aforementioned process does not occur in CE-QUAL W2, as the model is laterally averaged. The model instantaneously input the discharge evenly, across the cell with corresponding density (Cole & Wells, 2013). Consequently, the concentration of dissolved oxygen in the model discharge water within the hypolimnion is greater than what was observed in the field. Including algae and macrophytes, as well as modifying the concentration of dissolved oxygen in the Pond 102 discharge would improve dissolved oxygen accuracy.

A CE-QUAL W2 model of Lower Unnamed Lake was successfully developed. Inputs from future years or scenarios may be input and reasonably accurate results can be expected.

5.2 Determination of Lower Unnamed Lake Mictic State

Quantifying the propensity for turnover was a key objective for this study. It was hypothesised that LUL would turnover once during the fall and remain stable for the remainder of the model run year. Although LUL did exhibit strong chemical stratification, complete turnover occurred in the fall. Additionally, two other major mixing events occurred during the model run year. LUL was not observed to be meromictic, conversely, evidence suggests that LUL was, in fact, polymictic, turning over multiple times a year. Turnover occurrence was also supported by field observations.

The modelled epilimnion - hypolimnion TDS and density gradient is eroded three times over the model run year, on May 19th, September 13th, on October 28th (Figure 4.14; Figure 4.25; Appendix B, Figure B.1). The model mixed to a depth of 0.5 m above the sediment, at the deepest section of the lake on each of the mixing events (301.1 MASL). Lake mixing occurs as the result of two separate processes: direct wind stirring and shear-generated turbulence (Etimead-Shadhidi & Imberger, 2001; Lorrai *et al.* 2011).

The mixing on May 19 was the result of the high flow rate from UUL displacing the water in LUL (Appendix A, Figure. A.12). This was evident by the water momentum velocity vectors in Appendix B (Figure B.21). The high flow rate resulted in the turbulent flow between the boundary of the epilimnion and hypolimnion. IncreasinFg velocity increases shear stress and thus, laminar flow becomes turbulent (Streeter, 1996). The high flow event from UUL caused the epilimnion water velocity to increase, this increasing shear stress between the epilimnion and hypolimnion.

The increased shear stress created eddies and cross-currents perpendicular to the flow, resulted in increased diffusivity and mixing within the metalimnion (Geankoplis, 2003). The depth at which the hypolimnion stratification is eroded is a factor of shear stress and time. The longer the duration of high-flow, the deeper the mixing will occur, as the surfaces of the layers interact and are eroded by turbulent eddies over time. The depth of flow-induced mixing is also influenced by the bathymetry. Bathymetry determines through the ratio of surface area to volume. The increased surface area will result in an increased Richardson number, governing the production of eddies and seiches (Falconer *et al. 1991*; Lu & Wang, 2009; Tansley *et al.,* 2001). The deepest 1 m makes up only 1.8% of the volume of the west basin of LUL and is characterized by a steep sediment - elevation gradient. Eddy momentum and seiching is reduced in waterbodies with multiple deep basins, disconnected, by shallow sections (Pickett & Hood 2008). This was observed in LUL. The greatest velocity of water momentum is at 305.75 MASL, the centerline of depth for most of the lake, which is typical of small to medium-sized basins (Spiegel & Imberger, 1980). The water flowed from the east end the west end before the eddy flowed into the deep section of the lake. The water flowing over the deep section has less velocity, therefore is less likely to form turbulent eddies and erode hypolimnion stratification.

The high flow event was caused by the blow out of a beaver dam that governs the flow into LUL. The dam blew out periodically, releasing a high-quantity of low-TDS water from UUL, into LUL (Appendix A, Figure A.13-A.15). It is likely that the stream-flow rating curve did not accurately estimate the flow rate at that time, as the depth was greater than what was measured in the field sampling, an extrapolation had to be made. The dam failed at about the same time in both 2016 and 2017, suggesting that it may be a regular occurrence and cause for future mixing within the lake.

The mixing event on September 13th was due to a combination of Pond 102 not being discharged into the lake for the 16 prior days from and a moderate wind of 30 km/h (Figure A.12). When Pond 102 was not being discharged, the chemocline eroded as a result of direct wind stirring and an increase in inflow from the added inflow. The erosion of the chemocline eroded more rapidly than expected. Some lakes mine influenced lakes, such as Cleaver and Lim Lake had similar variations in TDS as LUL, but maintained stability, in a meromictic condition for years after active discharge was terminated (Denhom et al 1995; Haapaaho 2003; Uchtenhagan & Lee, 2016). The rapid erosion of the chemocline can be attributed to the bathymetry of LUL. There is a long, smooth transitional zone between the lacustrine zone and littoral zone allows for the development of large-scale eddy development. Upon ceasing discharge the chemical gradient is eroded and the lake is released from chemical stratification

Complete turnover of the water column occurred on October 27th. The turnover was effectively stimulated by the model, with the exception of the deepest 0.5 m (Figure 4.8). Turnover on October 27th was also observed in the field temperature, TDS and dissolved oxygen profiles (Figure 4.6; 4.8; 4.10).

Prior to this study, there was concern that LUL may be, or may become meromictic. This study determined that LUL was not meromictic. It is likely that LUL was polymictic in 2017.

5.3 Modified Pond 102 Discharge Location

The Pond 102 discharge location was modified to a section upstream of the current location in order to prevent chemical stratification. It was hypothesised that modifying the discharge location would eliminate chemical stratification and reduce water column stability. Modifying the discharge location did eliminate the chemical stratification, but also resulted in a lower concentration of hypolimnion dissolved oxygen and increased hypolimnion temperature for a portion of the model year.

The variation in water quality and hydrodynamics of the current Pond 102 discharge location model (CLM) and proposed Pond 102 discharge location model (PLM) was analysed by assessing the temperature, concentration and distribution of TDS, concentration of dissolved oxygen, hypolimnion-epilimnion density, water momentum velocity vectors and the concentration of TDS at the outflow.

The epilimnion temperature in the PLM was greater than the CLM from June 3rd to July 23rd, reaching a maximum variation of 2°C (Figure 4.11). The discharge rate of Pond 102 was relatively high during this time (Figure A.12). Discharge water from the PLM cycled through the littoral zone before flowing into the main basin. When in the littoral zone, the water absorbs solar radiation and becomes heated. While both models had the same water temperature in the littoral zone, there is a greater volume flowing through it in the PLM (Figure B.33). The water is heated to a greater degree in the shallow region because there was more surface area at the water surface, relative to volume, allowing the water to be exposed to a greater amount of long-wave solar radiation (Williams *et al.,* 1980). Additionally, shortwave solar radiation absorbed by the sediment is re-radiated back into the water column (de la Fuente, 2014). For the remainder of the year, epilimnion temperature varied by only <0.5^{o}C (Figure 4.11). The differential in epilimnion temperatures was due to the solar inclination at that time of year (Gonzalez *et al.,* 2015). The greater variation in epilimnion temperature was in the three weeks before and four weeks after the greatest solar angle of inclination, on June 21st. The increase in solar energy at that time of year results in a proportionately greater variation in temperature between the surface water in the main basin and the surface water in the shallow channel. Because of the relatively high light extinction (λ =0.94 m^{-1}) of the water in LUL, little solar radiation reaches the sediment to be re-radiated and heat the water in the main basin. For the remainder of the year, the solar radiation was less intense, resulting in a lesser variation in heating.

Epilimnion depth was increased from the initiation of the model run to the end of August, by an average of 0.6 m in the PLM (Figure 4.11). Increased epilimnion depth was due to the elimination of chemical stratification, as the density contrast between the epilimnion and hypolimnion impacts thermocline depth (Gorham & Boyce, 1989). The density gradient, caused by chemical stratification of the epilimnion and hypolimnion, resulted in the two layers more resistant to shear stress at the interface. When there is less resistance to shear stress, the laminar flow between the two layers becomes turbulent, and mixing occurs. The mixed water then cycles through the epilimnion from the surface, where it warms, to the metalimnion. This process results in the epilimnion temperature to be relatively unchanged, but epilimnion depth to increase.

It was notable that rather than having a pronounced metalimnion and hypolimnion, the thermocline of the PLM extends from the epilimnion to the sediment, which is common in shallow lakes that are prone to turnover from wind-mixing and lakes with low residence time, LUL being both (Lewis & Cam, 1993). Rather than a true metalimnion forming, the temperature gradient persists from the sediment to the epilimnion (Zauje *et al,* 1995). Without a stable hypolimnion, large enough to allow for the formation of internal seiching currents and mix the water within the hypolimnion, an isocline in temperature does not occur (Williams *et al,* 1980; Wain and Rehmann, 2010). Hypolimnietic temperature was greater in the PLM in the summer months, from June to the end of August, by an average of 3.2 ^{o}C, as a result of decreased residence time within the hypolimnion there was less time for the water to lose heat to the sediment.

The chemocline in the PLM was eroded twenty days into the run year. An isocline persisted throughout most of the remainder of the model run year. A slight increase in the hypolimnion concentration of TDS was observed on May 22nd, June 26th – July 27th, periods of high flow from the Pond 102 discharge (Figure A.12). The increase in hypolimnion TDS on October 7th was the result of discharge from Pond 102 (Figure 4.13). The concentration of TDS in the epilimnion was not changed within the two models, with a MAD of 40 ± 39 mg/L. The similar epilimnion concentration of TDS resulted in a similar concentration of TDS flowing out of LUL, as the two models varied by 33 ± 23 mg/L (Figure 4.17). The discharge and epilimnion concentration of TDS was relatively unchanged as both models and what was observed in the field, was that UUL inflow becomes fully mixed with Pond 102 discharge before flowing out of the lake. What varies was the distribution of the elevated concentration of TDS/ In the CLM, the concentration of TDS was elevated in the west basin, as opposed to the PLM, where the concentration of TDS was elevated in the east end of the lake (Figure 4.16). Modifying the discharge location increases the dimension of the surface of the interface between where Pond 102 discharge and LUL lake water, as the distance between the interface and the deep point in the main basin was increased. Increasing the dimension of the surface interface increases the Reynolds number, which causes turbulent flow and results in the two fluids mixing.

Modifying the discharge location had no significant impact on the concentration of dissolved oxygen in the epilimnion, varying by a MAD of only 0.19 ± 0.14 mg/l throughout the model run year. The concentration of dissolved oxygen in the hypolimnion, however, was immediately reduced in the PLM, after the initiation of the model and continued to be so until August 12th (Figure 4.26). Pond 102 was fully saturated with dissolved oxygen. In the CLM, the saturated discharge water flows directly into the hypolimnion, increasing the concentration of dissolved oxygen within the lake. This was evident by the prominent heterograde curve in the dissolved oxygen profile, wherein the concentration of dissolved oxygen increases within the hypolimnion. In the PLM, Pond 102 was discharged in the shallow channel. The discharge water then mixes with water from the inflow from UUL, diluting the concentration of TDS and reducing the density and exchanges oxygen with both the sediment and atmosphere and the before it reaches the main basin. As a result, dissolved oxygen was being delivered to the hypolimnion in the CLM, but not the PLM. This caused the hypolimnion in the PLM to become hypoxic, with a concentration of dissolved oxygen < 2^{o}C. The hypoxic condition would reduce available fish habitat and may result in the production the potentially toxic compounds, such as hydrogen sulphide (Zhang *et al.,* 2017, Boehrer & Schultz, 2008, Wang *et al.,* 2015). The hypoxic condition will alter the redox potential of the water, creating a reducing environment, as oxygen is no longer present to act as an electron acceptor (Borch *et al.,* 2008). When oxygen is not available for an electron acceptor, sulphur reducing bacteria in the sediment reduce sulphur to sulphide in the form of hydrogen sulphide (Kondo, 2006). Hydrogen sulphide is toxic, as it affects auxin transport in plants (Zang *et al.,* 2017). In animals, hydrogen sulphide impacts the central nervous system, as it binds with iron in the mitochondrial cytochrome enzymes, inhibiting cellular respiration (Lindenmann *et al.,* 2010). Due to the high concentration of organic matter in the sediment, it is likely that a hypoxic condition will cause methanogenesis, an anaerobic process in which methane is produced, as opposed to carbon dioxide (Holowenko, 2000). Methane is a potent greenhouse gas that contributes to climate change (Rodhe, 1990).

The ability for a stratified lake to resist mixing is governed by the variation in density between the epilimnion and hypolimnion (Hutchinson, 1957). A density ratio of 1 indicated that there was no density gradient stabilizing the lake. The density ratio in the CLM approached 1 on all three mixing events, while the PLM density ratio approached 1 eight additional times, towards the end of the model run year (Figure 4.25). The density ratio was greater midsummer in the CLM, indicating a greater degree of stratification. Modifying the discharge to the proposed location reduces density-induced stability within the lake, making it more prone to turnover in the PLM.

5.4 Elimination of Pond 102 Discharge into the Lower Unnamed Lake Model

The CE-QUAL W2 model of LUL was modified by removing the discharge from Pond 102, in order to evaluate the hydrodynamics and water quality of LUL if it was not influenced by Pond 102. The model that eliminated Pond 102 discharge (EDM) was compared to the PLM. It was hypothesised that the elimination of Pond 102 discharge will largely eliminate chemically induced stability, causing LUL to be polymictic. The thermocline depth and concentration of dissolved oxygen were expected to increase.

There was no substantial variation in temperature (MAD = 0.46 °C) or dissolved oxygen (MAD = 0.41 mg/L) between the PLM and (Figure 4.26; Figure 4.28). The PLM had slight increases in hypolimnion TDS and dissolved oxygen during high flow rates, towards the end of the year, as a result of some discharge water not fully mixing before reaching the hypolimnion, but both models exhibited isoclines for most of the model run year. As the EDM was not impacted by the high-TDS discharge, the concentration of TDS within the lake profile remained < 100 mg/L throughout the year (4.27).

The EDM had nearly identical temperature and dissolved oxygen profiles as the PLM, meaning that elimination of Pond 102 discharge would result in a deeper thermocline, increased hypolimnetic temperature and decreased hypolimnetic dissolved oxygen, compared to the current conditions. The deeper epilimnion was due to the diminished density gradient allowing for deeper wind-induced mixing of the epilimnion (Gorham & Boyce, 1989). Increased hypolimnetic temperature was the result of decreased stratification, which allowed parcels of warm water to interface with the hypolimnion (Williams et al, 1980; Wain and Rehmann, 2010). Decreased hypolimnetic dissolved oxygen for a portion of the model run year was due to the elimination of Pond 102, which injected high concentrations of dissolved oxygen into the hypolimnion. Without a steady source of dissolved oxygen, the hypolimnion became hypoxic (Figure 4.28).

5.5 Meromictic Potential of the Current and Proposed Discharge Location Models

The wind sheltering coefficient, discharge and inflow rates and Pond 102 discharge concentration of TDS were modified to assess the potential of the current Pond 102 discharge location model and proposed Pond 102 discharge location model to become meromictic. It was hypothesised that the CLM has the potential to become meromictic and the PLM does not have the potential to become meromictic.

The meromictic potential CLM maintained a TDS and a density gradient for the entirety of the model run year, indicating that turnover did not occur (Figure 4.28-4.29). Under the conditions of the meromictic potential model, the current discharge location was meromictic. The constant discharge rate from all inflows and Pond 102 discharge eliminated the high flow events that provided shear stress to the epilimnion-hypolimnion boundary layer and provided the hypolimnion with a constant source of high-TDS water to recharge what was lost to boundary-mixing (Geankoplis, 2003). Lowering the wind sheltering coefficient and storm intensity resulted in less shear stress and wind-induced mixing and chemocline erosion (Etimead-Shadhidi & Imberger, 2001). Setting the Pond 102 discharge TDS concentration to the maximum observed concentration resulted in increased buoyant stability, as the hypolimnion was not being periodically diluted (Howard, 1963). The combination of steady flow, reduced wind and increased, constant concentration of TDS resulted in the CLM to be meromictic, as it did not turn over.

The proposed 102 discharge location model did turnover under the potential meromictic conditions. Because the PLM was discharged into the shallow channel (Figure 3.5), the distance between the least dense and most dense parcels of water was lesser, resulting in lesser buoyancy, therefore, less shear stress is required to mix the Pond 102 discharge water with the natural lake water (Lorrai *et al,.* 2011; Figure 4.23). The discharge and natural lake water were fully mixed before the discharge was allowed to segregate within the hypolimnion of the west basin.

The current discharge location model has the potential to become meromictic under the conditions provided, while the proposed discharge location model does not. The models suggested that modifying the discharge location to the proposed location, upstream will promote mixing and inhibit future meromixis from forming.

5.6 Conclusions

A CE-QUAL W2 model that effectively simulated the water quality and hydrodynamics of Lower Unnamed Lake was successfully developed and calibrated. Although the mictic state of LUL was previously of concern, two major mixing events and full turnover was observed within the model and in the field demonstrating that during 2017 LUL was not meromictic, a was likely polymictic. Modifying the discharge location of Pond 102 upstream, in the shallow channel largely eliminated chemical stratification and resulted in a lesser degree of density-induced stability, compared to the current location. Although the proposed discharge location caused the LUL model to become more susceptible to turnover, hypolimnetic temperature and thermocline depth increased and hypolimnetic dissolved oxygen decreased in the west basin. The modified discharge location resulted in a lesser concentration of dissolved solids in the west basin, but a greater concentration of dissolved solids in the east basin. When discharge from Pond 102 was eliminated from the model, the hydrodynamics, dissolved oxygen and temperature were all similar to those produced in the proposed discharge location model, suggesting that modifying the discharge location resulted in the aforementioned constituents more closely aligning with the natural conditions. By modifying model input parameters, it was demonstrated that LUL had the potential to become meromictic when Pond 102 was discharged into the current location, but not when Pond 102 was discharged into the proposed location.

This model can be applied in years to come, to assess the impact of various discharge regimes to evaluate the propensity for LUL to become meromictic. If conditions arise where LUL may become meromictic, the Pond 102 discharge location can be modified to the prosed location to promote mixing and inhibit chemical stratification.

Literature Cited

Balistrieri, L. S., Box, S. E., Bookstrom, A. A., & Ikramuddin, M. (1999). Assessing the influence of reacting pyrite and carbonate minerals on the geochemistry of drainage in the Coeur d'Alene mining district. *Environmental Science & Technology*, *33*(19), 3347-3353.

Balistrieri, L. S., Murray, J. W., & Paul, B. (1994). The geochemical cycling of trace elements in a biogenic meromictic lake. Geochimica et Cosmochimica Acta, 58(19), 3993-4008.

Barry, R.G. & Chorley, R.J., 1992. *Atmosphere, Weather & Climate*, 6th edn. Routledge, London. 392pp.

Bertram, P. E. (1993). Total phosphorus and dissolved oxygen trends in the central basin of Lake Erie, 1970–1991. *Journal of Great Lakes Research*, *19*(2), 224-236.

Birge, E. A. (1915). "On the evidence of temperature seiches." Trans. Wisconsin Acad. Sci., 16, 1005-1016.

Boehrer, Bertram, and Martin Schultze (2008). "Stratification of lakes." Reviews of Geophysics 46.2

Borch, T., Kretzschmar, R., Kappler, A., Cappellen, P. V., Ginder-Vogel, M., Voegelin, A., & Campbell, K. (2009). Biogeochemical redox processes and their impact on contaminant dynamics. *Environmental science & technology*, *44*(1), 15-23.

Bouffard, D., & Wüest, A. (2019). Convection in lakes. *Annual Review of Fluid Mechanics*, *51*, 189-215.

Bouffard, D., Boegman, L., Ackerman, J. D., Valipour, R., & Rao, Y. R. (2014). Near-inertial wave driven dissolved oxygen transfer through the thermocline of a large lake. *Journal of Great Lakes Research*, *40*(2), 300-307.

Bowell, R. J., & Bruce, I. (1995). Geochemistry of iron ochres and mine waters from Levant Mine, Cornwall. *Applied Geochemistry*, *10*(2), 237-250.

Brown, G. E., Henrich, V. E., & Casey, W. H. (1999). Metal oxide surfaces and their interactions with aqueous solutions and microbial organisms. Chemical Reviews, 99, 77–174.

Burns, N. M., Rockwell, D. C., Bertram, P. E., Dolan, D. M., & Ciborowski, J. J. (2005). Trends in temperature, Secchi depth, and dissolved oxygen depletion rates in the central basin of Lake Erie, 1983–2002. *Journal of Great Lakes Research*, *31*, 35-49.

Capanema, L. X. D. L., & Ciminelli, V. S. T. (2003). An investigation of acid rock drainage (ARD) occurrence in a gold mine located in a Southeastern Brazil region. Rem: Revista Escola de Minas, 56(3), 201-206.

Carpenter, S. R., Cole, J. J., Pace, M. L., & Wilkinson, G. M. (2016). Response of plankton to nutrients, planktivory and terrestrial organic matter: a model analysis of whole‐lake experiments. *Ecology letters*, *19*(3), 230-239.

Clemente, C. A., Submitted, A. T., Partial, I. N., Of, F., Requirements, T. H. E., The, F. O. R., … Science, A. (2010). Assessment of Waste Rock Weathering Characteristicts of at the Antamina Mine Based on field cells experiment. Mining Engenering

Cloern, J. E., Cole, B. E., & Oremland, R. S. (1983). Autotrophic processes in meromictic Big Soda Lake, Nevada. *Limnology and Oceanography*, *28*(6), 1049-1061.

Cox, J. J., Valliant, W. W. & Ann Altman, K., (2017) Technical report on the Hemlo Mine, Marathon, Ontatio, Canada. NI 43-101 Report.

Davis, D.W., (1998). Geochronology of Rocks from the Hemlo Area: Canadian Mining Industry Research Organization, Hemlo Re- search Project Final Report, vol. 5, 17 pp.

de la Fuente, A. (2014). Heat and dissolved oxygen exchanges between the sediment and water column in a shallow salty lagoon. *Journal of Geophysical Research: Biogeosciences*, *119*(4), 596-613.

Denholm E, Dickson TA, Halbert BE (1995) Meromictic Lake Conditions Downstream of the Winston Lake Mine. Paper Presented at the 1995 Conference on Mining and the Environment in Sudbury, ON. May 28th – June 5th. pp 1-10

Duthie HC, Carter JCH (1970) The meromixis of Sunfish Lake, Southern Ontario. Journal of Fisheries Research Board of Canada 27: 847-856.

Duthie, H. C., & Carter, J. C. (1970). The meromixis of Sunfish Lake, Southern Ontario. Journal of the Fisheries Board of Canada, 27(5), 847-856.

Elberling, B., & Nicholson, R. V. (1996). Field determination of sulphide oxidation rates in mine tailings. *Water Resources Research*, *32*(6), 1773-1784.

Esfahani, M. R., Stretz, H. A., & Wells, M. J. (2015). Abiotic reversible self-assembly of fulvic and humic acid aggregates in low electrolytic conductivity solutions by dynamic light

EPA. (2012, March). Channel Processes: Suspended Sediment Transport. In Water: Science & Technology. Retrieved from scattering and zeta potential investigation. *Science of the Total Environment*, *537*, 81-92.4

Espana, J. S., Pamo, E. L., Diez, M., & Santofimia, E. (2009). Physico-chemical gradients and meromictic stratification in Cueva de la Mora and other acidic pit lakes of the Iberian Pyrite Belt. Mine Water and the Environment, 28(1), 15-29.

Espana, J. S., Pamo, E. L., Diez, M., & Santofimia, E. (2009). Physico-chemical gradients and meromictic stratification in Cueva de la Mora and other acidic pit lakes of the Iberian Pyrite Belt. *Mine Water and the Environment*, *28*(1), 15-29.

Etemad-Shahidi, A., & Imberger, J. (2001). Anatomy of turbulence in thermally stratified lakes. *Limnology and Oceanography*, *46*(5), 1158-1170.

Falconer, R. A., George, D. G., & Hall, P. (1991). Three-dimensional numerical modelling of wind-driven circulation in a shallow homogeneous lake. *Journal of hydrology*, *124*(1-2), 59-79.

Fang, X., & Stefan, H. G. (1996). Dynamics of heat exchange between sediment and water in a lake. *Water Resources Research*, *32*(6), 1719-1727.

Fang, X., & Stefan, H. G. (1996). Dynamics of heat exchange between sediment and water in a lake. *Water Resources Research*, *32*(6), 1719-1727.

Fang, X., & Stefan, H. G. (1996). Long-term lake water temperature and ice cover simulations/measurements. *Cold Regions Science and Technology*, *24*(3), 289-304.

Fendorf, S. E. (1995). Surface reactions of chromium in soils and waters. Geoderman, 67, 55–71.

Ficker, H., Gassner, H., Achleitner, D., & Schabetsberger, R. (2011). Ectogenic meromixis of Lake Hallstättersee, Austria induced by waste water intrusions from salt mining. Water, Air, & Soil Pollution, 218(1-4), 109-120.

Fisher, T. S. R. (2002). M.Sc. Thesis. Limnology of the Meromictic Island Copper Mine pit lake. University of British Columbia.

Fisher, T. S., & Lawrence, G. A. (2006). Treatment of acid rock drainage in a meromictic mine pit lake. Journal of Environmental Engineering, 132(4), 515-526.

Forsberg, C. (1989). Importance of sediments in understanding nutrient cyclings in lakes. *Hydrobiologia*, *176*(1), 263-277.

Fraser, W. W., & Robertson, J. D. (1994). Subaqueous disposal of reactive mine waste: an overview and update of case studies-MEND/Canada. *Bureau of Mines Special Publication, SP*, *6*, 250-259.

Gahan, C. S., Cunha, M. L., & Sandström, Å. (2009). Comparative study on different steel slags as neutralising agent in bioleaching. *Hydrometallurgy*, *95*(3-4), 190-197.

Galperin, B., Sukoriansky, S., & Anderson, P. S. (2007). On the critical Richardson number in stably stratified turbulence. *Atmospheric Science Letters*, *8*(3), 65-69.

Gálvez, J. A., & Niell, F. X. (1992). Sediment resuspension in a monomictic eutrophic reservoir. *Hydrobiologia*, *235*(1), 133-141.

Gambrell, R. P. (1994). Trace and toxic metals in wetlands—a review. *Journal of environmental Quality*, *23*(5), 883-891.

GARD Guide. (2013). Global Acid Rock Drainage Guide , INAP: The International Network for Acid Prevention. Retrieved from http://www.gardguide.com

Geankoplis, Christie John (2003). Transport Processes and Separation Process Principles. Prentice Hall Professional Technical Reference. ISBN 978-0-13-101367-4. Archived from the original on 2015-05-01.

González Abad, G., Liu, X., Chance, K., Wang, H., Kurosu, T. P., & Suleiman, R. (2015). Updated Smithsonian Astrophysical Observatory Ozone Monitoring Instrument (SAO OMI) formaldehyde retrieval. *Atmospheric Measurement Techniques*, *8*(1), 19-32.

Gorham, E., & Boyce, F. M. (1989). Influence of lake surface area and depth upon thermal stratification and the depth of the summer thermocline. *Journal of Great Lakes Research*, *15*(2), 233-245.

Guerrero, R., Montesinos, E., Esteve, I., & Abella, C. (1980). Physiological adaptation and growth of purple and green sulfur bacteria in a meromictic lake (Vila) as compared to a holomictic lake (Siso). In *Shallow Lakes Contributions to their Limnology* (pp. 161-171). Springer, Dordrecht.

Haapa – aho K (2004) M.Sc. Thesis. The Effectiveness of Self-Restoration for Two Small Mine Impacted Shield Lakes, Lakehead University, Department of Biology, Thunder Bay

Hakala A (2004) Meromixis as a part of lake evolution – observations and a revised classification of true meromictic lakes in Finland. Boreal Environmental Research. 9: 37-53

Harris, D.C., (1989). The mineralogy and geochemistry of the Hemlo gold deposit, Ontario. Geol. Surv. Can., Econ. Geol. Rep., 38, 88 pp

Hausmann, J., and B. Boehrer (2006), Hypolimniontemperaturen unter 4°C in einem Salzsee-das Solbad Leopoldshall bei Stassfurt in Sachsen-Anhalt, in Tagungsbericht 2005 (Karlsruhe), pp. 87–90, Dtsch. Ges. für Limnol., Berlin, Germany.

Heikkinen, P. M., Räisänen, M. L., & Johnson, R. H. (2009). *Mine Water and the Environment*, *28*(1), 30-49. Geochemical characterisation of seepage and drainage water quality from two sulphide mine tailings impoundments: acid mine drainage versus neutral mine drainage.

Heikkinen, P. M., Räisänen, M. L., & Johnson, R. H. (2009). *Mine Water and the Environment*, *28*(1), 30-49. Geochemical characterisation of seepage and drainage water quality from two sulphide mine tailings impoundments: acid mine drainage versus neutral mine drainage.

Henry, W. (1803). "Experiments on the quantity of gases absorbed by water, at different temperatures, and under different pressures". *Phil. Trans. R. Soc. Lond*. **93**: 29–274.

Hollibaugh, J. T., Carini, S., Gürleyük, H., Jellison, R., Joye, S. B., LeCleir, G., ... & Wallschläger, D. (2005). Arsenic speciation in Mono Lake, California: Response to seasonal stratification and anoxia. *Geochimica et Cosmochimica Acta*, *69*(8), 1925-1937.

Holowenko, F. M., MacKinnon, M. D., & Fedorak, P. M. (2000). Methanogens and sulfate-reducing bacteria in oil sands fine tailings waste. *Canadian Journal of Microbiology*, *46*(10), 927-937.

Hondzo, M., & Stefan, H. G. (1991). Three case studies of lake temperature and stratification response to warmer climate. *Water Resources Research*, *27*(8), 1837-1846.

Howard, L. N. 1963 Neutral curves and stability boundaries in stratified flow. J. Fluid Mech. 16, 333-42.

Human, L. R., Snow, G. C., Adams, J. B., Bate, G. C., & Yang, S. C. (2015). The role of submerged macrophytes and macroalgae in nutrient cycling: A budget approach. *Estuarine, Coastal and Shelf Science*, *154*, 169-178.

Huppert, H. E. (1973). On Howard's technique for perturbing neutral solutions of the Taylor-Goldstein equation. *Journal of Fluid Mechanics*, *57*(2), 361-368.

Hutchinson G.E. (1957) Treatise on limnilogy Vol. III. Limnological Botany, IV

Hutchinson, 1957 G.E. HutchinsonA treatise on Limnology – vol. 1 John Wiley & Sons, New York (1957)

Hutchinson, G. Evelyn (1937). "A contribution to the limnology of arid regions". *Transactions of the Connecticut Academy of Arts and Sciences*. **33**: 47–132. As cited by Hakala (2004).

Hypolimnion oxygen consumption in lakes: discussion of productivity and morphometry effects

Idso, S. B., Jackson, R. D., Reginato, R. J., Kimball, B. A., & Nakayama, F. S. (1975). The dependence of bare soil albedo on soil water content. *Journal of applied meteorology*, *14*(1), 109-113.

Imboden, D. M., and A. Wüest (1995), Mixing mechanisms in lakes, in Physics and Chemistry of Lakes, edited by A. Lerman et al., pp. 83–138, Springer, Berlin, Germany.

Ishigaki, T., Nakanishi, A., Tateda, M., Ike, M., & Fujita, M. (2005). Bioleaching of metal from municipal waste incineration fly ash using a mixed culture of sulfur-oxidizing and iron-oxidizing bacteria. *Chemosphere*, *60*(8), 1087-1094.

Jabbari, A., Boegman, L., MacKay, M., & Nakhaei, N. (2016, September). Modeling the oxygen depletion within stratified bottom boundary layers of lakes. In *International Symposium on Stratified Flows* (Vol. 1, No. 1).

Jacobson, Mark Z. (2005). *Fundamentals of Atmospheric Modeling* (2nd ed.). Cambridge University Press. p. 317. ISBN 0521548659.

Jorgensen, S. E. (Ed.). (2016). *Handbook of ecological models used in ecosystem and environmental management* (Vol. 3). CRC press.

Katsev, S., Verburg, P., Llirós, M., Minor, E. C., Kruger, B. R., & Li, J. (2017). Tropical Meromictic Lakes: Specifics of Meromixis and Case Studies of Lakes Tanganyika, Malawi, and Matano. In *Ecology of Meromictic Lakes* (pp. 277-323). Springer, Cham.

Khalil, A., Hanich, L., Bannari, A., Zouhri, L., Pourret, O., & Hakkou, R. (2013). Assessment of soil contamination around an abandoned mine in a semi-arid environment using geochemistry and geostatistics: Pre-work of geochemical process modeling with numerical models. Journal of Geochemical Exploration, 125, 117–129

Kirk, J.T.O. Light and Photosynthesis in Aquatic Ecosystems, 3rd ed.; Cambridge University Press: Cambridge, UK, 2011.

Kittrell, F. W., Jones, S. L., & Ingols, R. S. (1959). Effects of impoundments on dissolved oxygen resources [with Discussion]. *Sewage and Industrial Wastes*, *31*(9), 1065-1081.

Kõiv, T., Nõges, T., & Laas, A. (2011). Phosphorus retention as a function of external loading, hydraulic turnover time, area and relative depth in 54 lakes and reservoirs. *Hydrobiologia*, *660*(1), 105-115.

Kondo, R., Osawa, K., Mochizuki, L., Fujioka, Y., and Butani, J. 2006. "Abundance and diversity of sulphate-reducing bacterioplankton in Lake Suigetsu, a meromictic lake in Fukui, Japan". Plankton Benthos Res. 4:165-177.

Kraemer, B. M., Anneville, O., Chandra, S., Dix, M., Kuusisto, E., Livingstone, D. M., ... & Tamatamah, R. (2015). Morphometry and average temperature affect lake stratification responses to climate change. *Geophysical Research Letters*, *42*(12), 4981-4988.

Kraus, E. B., and Turner, J. S. 1967. A onedimensional model of the seasonal thermocline, Part II. Tel/us 19:98-105.

Küsel, K. (2003). Microbial cycling of iron and sulfur in acidic coal mining lake sediments. *Water, Air and Soil Pollution: Focus*, *3*(1), 67-90.

Lee, T. M. (1996). Hydrogeologic controls on the groundwater interactions with an acidic lake in karst terrain, Lake Barco, Florida. *Water Resources Research*, *32*(4), 831-844

Lee, Z.; Weidemann, A.; Kindle, J.; Arnone, R.; Carder, K.L.; Davis, C. Euphotic zone depth: Its derivation and implication to ocean-color remote sensing. J. Geophys. Res. 2007, 112, C03009:1–C03009:11.

Lehman, J. T., & Branstrator, D. K. (1994). Nutrient dynamics and turnover rates of phosphate and sulfate in Lake Victoria, East Africa. *Limnology and Oceanography*, *39*(2), 227-233.

Li, L. Y., Chen, M., Grace, J. R., Tazaki, K., Shiraki, K., Asada, R., & Watanabe, H. (2007). Remediation of acid rock drainage by regenerable natural clinoptilolite. *Water, air, and soil pollution*, *180*(1-4), 11-27.

Li, W., Li, S., Yin, Y., Ji, J., & Pu, P. (2001). Meromixis in Zige Tangco, central Tibetan Plateau. *Science in China Series D: Earth Sciences*, *44*(1), 338-342.

Lindenmann, J.; Matzi, V.; Neuboeck, N.; Ratzenhofer-Komenda, B.; Maier, A; Smolle-Juettner, F. M. (December 2010). "Severe hydrogen sulphide poisoning treated with 4-dimethylaminophenol and hyperbaric oxygen". Diving and Hyperbaric Medicine. 40 (4): 213–217. PMID 23111938. Retrieved 2013-06-0

Lindsay, M. B., Moncur, M. C., Bain, J. G., Jambor, J. L., Ptacek, C. J., & Blowes, D. W. (2015). Geochemical and mineralogical aspects of sulfide mine tailings. *Applied Geochemistry*, *57*, 157-177.

Lindsay, M. B., Moncur, M. C., Bain, J. G., Jambor, J. L., Ptacek, C. J., & Blowes, D. W. (2015). Geochemical and mineralogical aspects of sulfide mine tailings. *Applied Geochemistry*, *57*, 157-177.

Liu, C., Yu, H. Y., Liu, C., Li, F., Xu, X., & Wang, Q. (2015). Arsenic availability in rice from a mining area: is amorphous iron oxide-bound arsenic a source or sink?. *Environmental pollution*, *199*, 95-101.

Lorrai, C., Umlauf, L., Becherer, J. K., Lorke, A., & Wüest, A. (2011). Boundary mixing in lakes: 2. Combined effects of shear-and convectively induced turbulence on basin-scale mixing. *Journal of Geophysical Research: Oceans*, *116*(C10).

Lu, J., & Wang, L. (2009). Numerical study of large eddy structures—separated flows Passing sills. In *Advances in Water Resources and Hydraulic Engineering* (pp. 1795-1799). Springer, Berlin, Heidelberg.

Lukianova, R. Y., Uvarov, V. M., & Coisson, P. (2017). High-latitude F region large-scale ionospheric irregularities under different solar wind and zenith angle conditions. *Advances in Space Research*, *59*(2), 557-570.

Lyons, W. A. (1982). Turbulent diffusion and pollutant transport in shoreline environments. In *Lectures on Air Pollution and Environmental Impact Analyses* (pp. 136-208). American Meteorological Society, Boston, MA.

Lienemann, C. P., Gaillard, J. F., & Perret, D. (2000). Speciation, reactivity, and cycling of Fe and Pb in a meromictic lake. *Geochimica et Cosmochimica Acta*, *64*(2), 169-183.

Manasrah, R., Raheed, M., & Badran, M. I. (2006). Relationships between water temperature, nutrients and dissolved oxygen in the northern Gulf of Aqaba, Red Sea. *Oceanologia*, *48*(2).

Maranger, R. P. M. J., & Pullin, M. J. (2003). Elemental complexation by dissolved organic matter in lakes: Implications for Fe speciation and the speciation and the bioavailability of Fe and P. In *Aquatic Ecosystems* (pp. 185-214). Academic Press.

Markfort CD, Perez ALS, Thill JW, Jaster DA, Porté-Agel F, Stefan HG (2010) Wind sheltering of a lake by a tree canopy or bluff topography. Water Resour. Res. 46: 1-13 W03530, doi:10.1029/2009WR007759

Markvart & CastaŁżer (2003). *Practical Handbook of Photovoltaics: Fundamentals and Applications*. Elsevier. ISBN 978-1-85617-390-2.

Marsalek, P. M., Watt, W. E., Marsalek, J., & Anderson, B. C. (2000). Winter flow dynamics of an on-stream stormwater management pond. *Water Quality Research Journal*, *35*(3), 505-524.

Matisoff, G., & Neeson, T. M. (2005). Oxygen concentration and demand in Lake Erie sediments. *Journal of Great Lakes Research*, *31*, 284-295.

McNaughton, K. A., & Lee, P. F. (2010). Water quality effects from an aquaculture operation in a meromictic Iron Pit Lake in Northwestern Ontario, Canada. Water Quality Research Journal, 45(1), 13-24.

MEND (Canada), 2000. MEND Manual Report 5.4.2 - 2000, Mine Environment Neutral Drainage, Ottawa, Canada

Mend. (2004) Review of Water Quality Issues in Neutral pH Drainage : Examples and Emerging Priorities for the Mining Industry in Canada.

Mercer JW, Faust CR (1980b) Ground-Water Modeling: Numerical Models. Ground Water 18: 108-115

Meriläinen, J. (1970, January). On the limnology of the meromictic Lake Valkiajärvi, in the Finnish Lake District. In *Annales Botanici Fennici* (pp. 29-51). SOCIETAS BIOLOGICA FENNICA VANAMO.

Merriam, E. R., Petty, J. T., Merovich Jr, G. T., Fulton, J. B., & Strager, M. P. (2011). Additive effects of mining and residential development on stream conditions in a central Appalachian watershed. Journal of the North American Benthological Society, 30(2), 399-418.

Metal Mining Effluent Regulations (SOR/2002-222) http://lawslois.justice.gc.ca/eng/regulations/sor-2002-222/index.html

Miles J. 1961. On the stability of heterogeneous shear flows. Journal of Fluid Mechanics 10: 496–508.

Minnow (Minnow Environmental Inc.) 2013. Williams Mine Storm Water Monitoring Interpretive Report. Report prepared for Williams Operating Corporation.

Molenda, T. (2014). Impact of saline mine water: development of a meromictic reservoir in Poland. *Mine Water and the Environment*, *33*(4), 327-334.

Molenda, T. (2018). Impact of a Saline Mine Water Discharge on the Development of a Meromictic Pond, the Rontok Wielki Reservoir, Poland. Mine Water and the Environment, 37(4), 807-814.

Molenda, T. (2018). Impact of a Saline Mine Water Discharge on the Development of a Meromictic Pond, the Rontok Wielki Reservoir, Poland. *Mine Water and the Environment*, *37*(4), 807-814.

Moore, J. N., & Luoma, S. N. (1990). Hazardous wastes from large-scale metal extraction. A case study. *Environmental Science & Technology*, *24*(9), 1278-1285.

Morley, D. W., Leng, M. J., Mackay, A. W., Sloane, H. J., Rioual, P., & Battarbee, R. W. (2004). Cleaning of lake sediment samples for diatom oxygen isotope analysis. *Journal of Paleolimnology*, *31*(3), 391-401.

Muir, T. L. (2002). The Hemlo gold deposit, Ontario, Canada: Principal deposit characteristics and constraints on mineralization. Ore Geology Reviews, 21(1–2), 1–66.

Njuguna, S. G. (1988). Nutrient-phytoplankton relationships in a tropical meromictic soda lake. In *Saline Lakes* (pp. 15-28). Springer, Dordrecht.

Nordstrom, D. K. (1982). *Aqueous pyrite oxidation and the consequent formation of secondary iron minerals* (No. acidsulfateweat, pp. 37-56). Soil Science Society of America.

Öhlander, B., Chatwin, T., & Alakangas, L. (2012). Management of sulfide-bearing waste, a challenge for the mining industry. Minerals, 2(1), 1-10.

Overmann, J., Beatty, J. T., & Hall, K. J. (1996). Purple sulfur bacteria control the growth of aerobic heterotrophic bacterioplankton in a meromictic salt lake. *Appl. Environ. Microbiol.*, *62*(9), 3251-3258.

Oxyanions in waste: occurrence, leaching, stabilisation, relation to wastewater treatment c. vandecasteele * , g. cornelis. (n.d.), 149–159.

Pace, M. L., & Prairie, Y. T. (2005). Respiration in lakes. *Respiration in aquatic ecosystems*, *1*, 103-122.

Pan, Y., & Fleet, M. E. (1995). The late Archean Hemlo gold deposit, Ontario, Canada: a review and synthesis. *Ore Geology Reviews*, *9*(6), 455-488.

Pasche, N., Dinkel, C., Mu# x00FC; ller, B., Schmid, M., est, A. W. X., & Wehrlia, B. (2009). Physical and biogeochemical limits to internal nutrient loading of meromictic Lake Kivu. *Limnology and Oceanography*, *54*(6), 1863-1873.

Patterson JC, PF Hamblin, J Imberger (1984) Classification and simulation of the vertical density structure in lakes. Limnology and Oceanography 29: 845-861

Pentecost, J. (2016). *How Does Manning's Roughness Coefficient Change with Varying Widths?* (Doctoral dissertation, The Ohio State University).

Peterson, H. E. (2014). *Unsaturated hydrology, evaporation, and geochemistry of neutral and acid rock drainage in highly heterogeneous mine waste rock at the Antamina mine, Peru*(Doctoral dissertation, University of British Columbia).

Pickett P, Hood S (2008) Lake Whatcom Watershed Total Phosphorus and Bacteria Total Maximum Daily Loads Volume 1. Water Quality Study Findings. Publication No 08-03-024. Prepared for Washington Department of Ecology. Olympia, WA. pp 1-145

Plante, B., Bussière, B., & Benzaazoua, M. (2014). Lab to field scale effects on contaminated neutral drainage prediction from the Tio mine waste rocks. *Journal of Geochemical Exploration*, *137*, 37-47.

Plante, B., Bussière, B., & Benzaazoua, M. (2014). Lab to field scale effects on contaminated neutral drainage prediction from the Tio mine waste rocks. *Journal of Geochemical Exploration*, *137*, 37-47.

Priscu, J. C., Axler, R. P., Carlton, R. G., Reuter, J. E., Arneson, P. A., & Goldman, C. R. (1982). Vertical profiles of primary productivity, biomass and physico-chemical properties in meromictic Big Soda Lake, Nevada, USA. *Hydrobiologia*, *96*(2), 113-120.

Read, J. S., Hamilton, D. P., Desai, A. R., Rose, K. C., MacIntyre, S., Lenters, J. D., ... & Rusak, J. A. (2012). Lake-size dependency of wind shear and convection as controls on gas exchange. *Geophysical Research Letters*, *39*(9).

Review of Water Quality Issues in Neutral pH Drainage : Examples and Emerging Priorities for the Mining Industry in Canada. (2004), (November). MEND

Rodhe, H. (1990). A comparison of the contribution of various gases to the greenhouse effect. *Science*, *248*(4960), 1217-1219.

Roland, F. A., Darchambeau, F., Morana, C., Bouillon, S., & Borges, A. V. (2017). Emission and oxidation of methane in a meromictic, eutrophic and temperate lake (Dendre, Belgium). *Chemosphere*, *168*, 756-764.

Rong, N., Shan, B., & Wang, C. (2016). Determination of sediment oxygen demand in the Ziya River watershed, China: Based on laboratory core incubation and microelectrode measurements. *International journal of environmental research and public health*, *13*(2), 232.

Rueda, F. J., & Schladow, S. G. (2003). Dynamics of large polymictic lake. II: Numerical simulations. *Journal of Hydraulic Engineering*, *129*(2), 92-101.

Sánchez-Andrea, Irene, et al., 2012. Quantification of Tinto River sediment microbial communities: importance of sulfate-reducing bacteria and their role in attenuating acid mine drainage. Applied and environmental microbiology**78.13**: 4638-4645.

Sander, R.: Compilation of Henry's law constants (version 4.0) for water as solvent, Atmos. Chem. Phys., 15, 4399-4981, https://doi.org/10.5194/acp-15-4399-2015, 2015.

Schindler DW (1971) Light, Temperature and Oxygen Regimes of Selected Lakes in the Experimental Lakes Area, Northwestern Ontario. Journal of Fisheries and Research Board of Canada 28: 157-169

Schmidt W (1915) Über den Energie-gehalt der Seen. Mit Beispielen vom Lunzer Untersee nach Messungen mit einem einfachen Temperaturlot. International Review of Hydrobiology Supplement, Leipig 6: 510

Schnieders, B.R., Scott, J.F., Smyk, M.C., O'Brien, M.S., (2000). Report of activities, 1999 Resident Geologists Program: Thunder Bay south district regional resident geologist report. Ontario Geological Survey, Open File Report 6005, 51 pp.

Schultze, M., Boehrer, B., Wendt-Potthoff, K., Katsev, S., & Brown, E. T. (2017). Chemical setting and biogeochemical reactions in meromictic lakes. In *Ecology of Meromictic lakes* (pp. 35-59). Springer, Cham.

Sherlock, E. J., Lawrence, R. W., & Poulin, R. (1995). On the neutralization of acid rock drainage by carbonate and silicate minerals. *Environmental Geology*, *25*(1), 43-54.

Shupe, M. D., & Intrieri, J. M. (2004). Cloud radiative forcing of the Arctic surface: The influence of cloud properties, surface albedo, and solar zenith angle. *Journal of Climate*, *17*(3), 616-628.

Sibert, R. J., Koretsky, C. M., & Wyman, D. A. (2015). Cultural meromixis: Effects of road salt on the chemical stratification of an urban kettle lake. *Chemical Geology*, *395*, 126-137.

Silberbauer, M. J. (1982). Phosphorus dynamics in the monimolimnion of Swartvlei. *Journal of the Limnological Society of southern Africa*, *8*(2), 54-60.

Silva, L. F., Izquierdo, M., Querol, X., Finkelman, R. B., Oliveira, M. L., Wollenschlager, M., ... & Macias, F. (2011). Leaching of potential hazardous elements of coal cleaning rejects. *Environmental monitoring and assessment*, *175*(1-4), 109-126.

Smith, L., Marcoline, J., Wagner, K., Nichol, C., & Beckie, R. (2004, May). Hydrologic and geochemical transport processes in mine waste rock. In *AGU Spring Meeting Abstracts*.

Sondergaard M. 2009. *Redox Potential. Vol. 2,* pp.852-859. In: G.E. Likens Encyclopedia of Inland Waters. Oxford: Elsevier

Spigel, R. H., and Imberger, J. 1980. The classification of mixed layer dynamics in lakes of small-to medium size. J. Phys. Ocean gr. 10: 1104-1121.

St. James, M.D.B and Lee, P. (2015). HBESc Thesis. uchtA Chemical Analysis and Bioassay of Soil Amendments using *Trifolium pretense* at a Former Iron Ore Mine (Steep Rock Mine) in Atikokan, On. Lakehead University, Department of Biology, Thunder Bay

Streeter, V.L. (1951-1966) Fluid Mechanics, Section 3.3 (4th edition). McGraw-Hill

Stumm, W. and Morgan, J. J. (1981): Aquatic chemistry, 2nd Ed.; John Wiley & Sons, New York

Sullivan, P. P., McWilliams, J. C., & Moeng, C. H. (2000). Simulation of turbulent flow over idealized water waves. *Journal of Fluid Mechanics*, *404*, 47-85.

Svensmark, H., & Friis-Christensen, E. (1997). Variation of cosmic ray flux and global cloud coverage—a missing link in solar-climate relationships. *Journal of atmospheric and solar-terrestrial physics*, *59*(11), 1225-1232.

Tansley, Claire E.; Marshall, David P. (2001). "Flow past a Cylinder on a Plane, with Application to Gulf Stream Separation and the Antarctic Circumpolar Current" (PDF). *Journal of Physical Oceanography*. **31** (11): 3274–3283.

Tennessee Valley Authority (TVA) 1972. Heat and Mass Transfer between a water surface and the atmosphere, Water Resources Report 0-6803, Lab Report #14, Norris, TN.

Tonolla, M., Peduzzi, R., & Hahn, D. (2005). Long-term population dynamics of phototrophic sulfur bacteria in the chemocline of Lake Cadagno, Switzerland. *Appl. Environ. Microbiol.*, *71*(7), 3544-3550.

Tsai, S. F., Lin, F. W., Chan, Y. F., & Chiang, K. P. (2016). Vertical distribution of pigmented and non-pigmented nanoflagellates in the East China Sea. *Continental Shelf Research*, *125*, 107-113.

Turnipseed, D. P., & Sauer, V. B. (2010). *Discharge measurements at gaging stations* (No. 3-A8). US Geological Survey.

Uchtenhagen, S & Lee, P. (2016). MSc. Thesis. Predicting Mixing Trends in Mine-Receiving Waters using Water Quality Modeling. Lakehead University, Department of Biology, Thunder Bay

Valerio, G., Cantelli, A., Monti, P., & Leuzzi, G. (2017). A modeling approach to identify the effective forcing exerted by wind on a prealpine lake surrounded by a complex topography. *Water Resources Research*, *53*(5), 4036-4052.

Valliant, R.I., Bradbrook, C.J., (1986). Relationship between stratig- raphy, faults and gold deposits, Page-Williams Mine, Hemlo, Ontario, Canada. In: Macdonald, J.A. (Ed.), Proceedings of Gold ’86, An International Symposium on the Geology of Gold Deposits.

van Niel, C. B. (1932). On the morphology and physiology of the purple and green sulphur bacteria. *Archiv für Mikrobiologie*, *3*(1), 1-112.

Van't Hoff, J. H. (1884). *Etudes de dynamique chimique* (Vol. 1). Muller.

Viollier, E., Jézéquel, D., Michard, G., Pèpe, M., Sarazin, G., & Alberic, P. (1995). Geochernical study of a crater lake (Pavin Lake, France): trace-element behaviour in the monimolimnion. *Chemical Geology*, *125*(1-2), 61-72.

W.L. Lewis, Jr. Can. J. Fish. Aquat. Sci. 40 (1993) 1779-1787. © Canadian Science Publishing

Wain, D. J., and C. R. Rehmann (2010), Transport by an intrusion generated by boundary mixing in a lake, Water Resour. Res., 46, W08517, doi:10.1029/2009WR008391.

Wang, L., Riseng, C. M., Mason, L. A., Wehrly, K. E., Rutherford, E. S., McKenna Jr, J. E., ... & Robertson, M. (2015). A spatial classification and database for management, research, and policy making: The Great Lakes aquatic habitat framework. *Journal of Great Lakes Research*, *41*(2), 584-596.

Weiss, R. F., Carmack, E. C., & Koropalov, V. M. (1991). Deep-water renewal and biological production in Lake Baikal. *Nature*, *349*(6311), 665.

Wetzel, R. G. (1990). Land-water interfaces: metabolic and limnological regulators. *Internationale Vereinigung für theoretische und angewandte Limnologie: Verhandlungen*, *24*(1), 6-24.

Williams, N. T. (2007). Modeling dissolved oxygen in Lake Powell using CE-QUAL-W2.

Winde, F., & van der Walt, I. J. (2004). The significance of groundwater–stream interactions and fluctuating stream chemistry on waterborne uranium contamination of streams—a case study from a gold mining site in South Africa. Journal of Hydrology, 287(1-4), 178-196.

Woolf, Harold M. (1968). "On the computation of solar elevation angles and the determination of sunrise and sunset times". *NASA technical memorandu, X-1646*. Washington, D.C.:

Zauke, G.-P., R. G. Niemeyer, and K.-P. Gilles (1995), Tropen, in Handbuch Angewandte Limnologie, edited by C. E. W. Steinberg et al., Chapter VIII-3.2, pp. 1–86, ecomed, Landsberg, Germany.

Zhang, P., Luo, Q., Wang, R., & Xu, J. (2017). Hydrogen sulfide toxicity inhibits primary root growth through the ROS-NO pathway. *Scientific reports*, *7*(1), 868.

Zhou, J., Qin, B., Casenave, C., Han, X., Yang, G., Wu, T., ... & Ma, J. (2015). Effects of wind wave turbulence on the phytoplankton community composition in large, shallow Lake Taihu. *Environmental Science and Pollution Research*, *22*(16), 12737-12746.

Appendix A: Model inputs

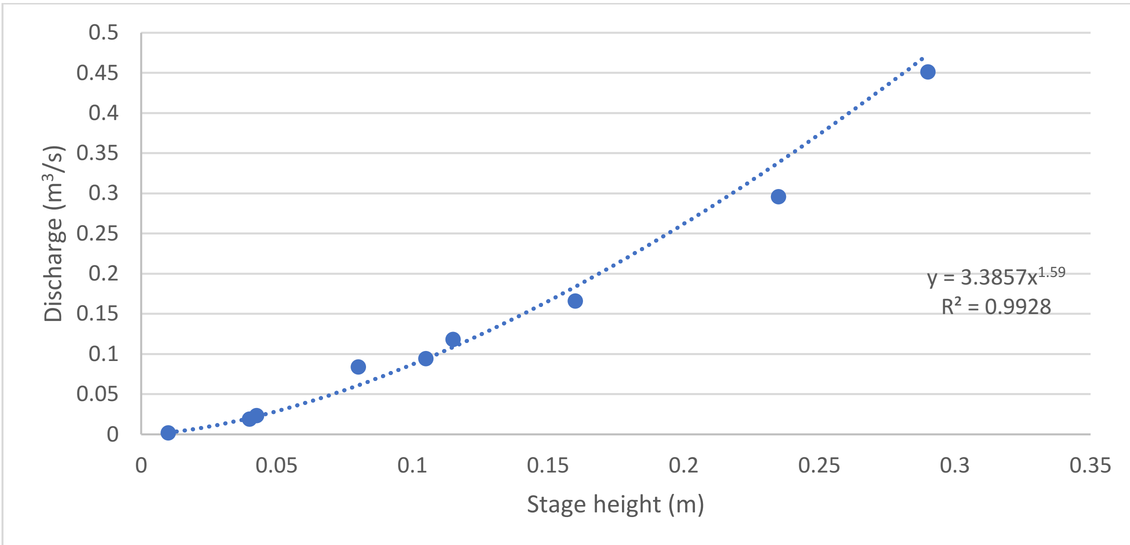

Figure A.1: Stream gauging rating curve for the outflow of LUL

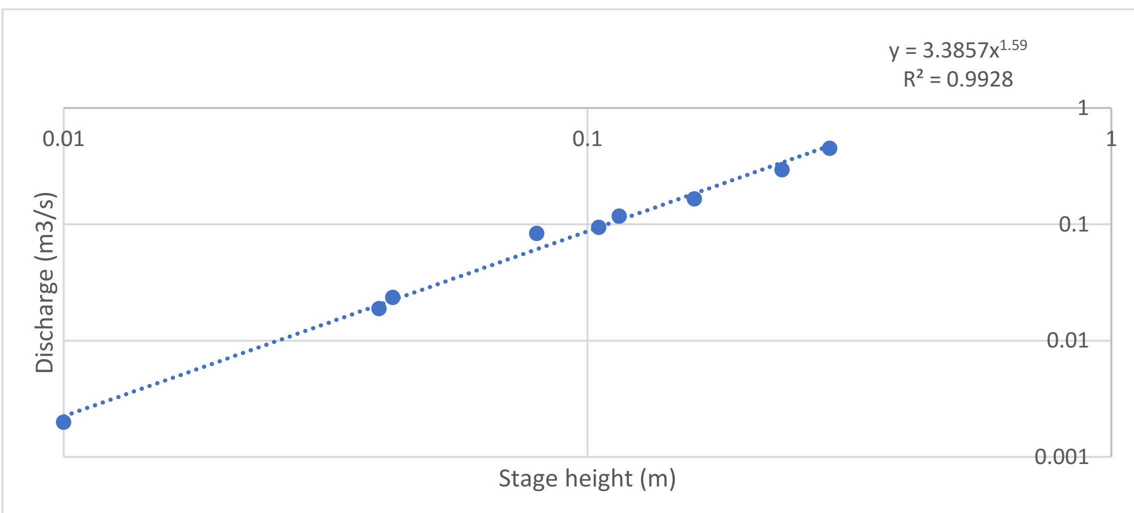

Figure A.2: Log-Log transformed stream gauging rating curve

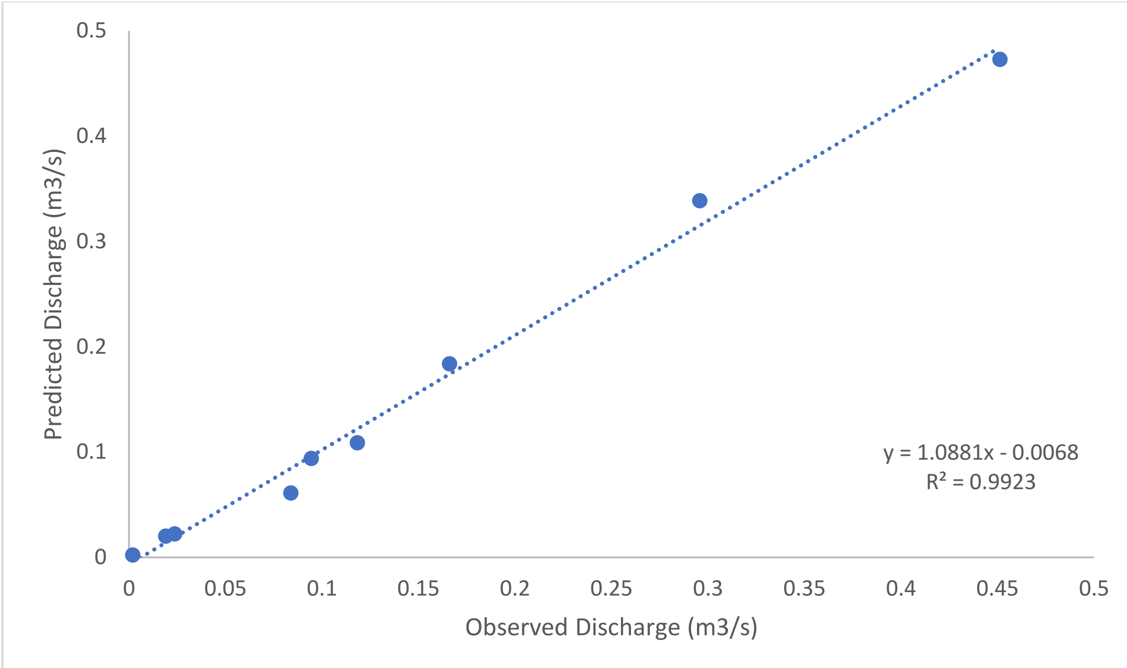

Figure A.3: Predicted and Overserved LUL outflow rate

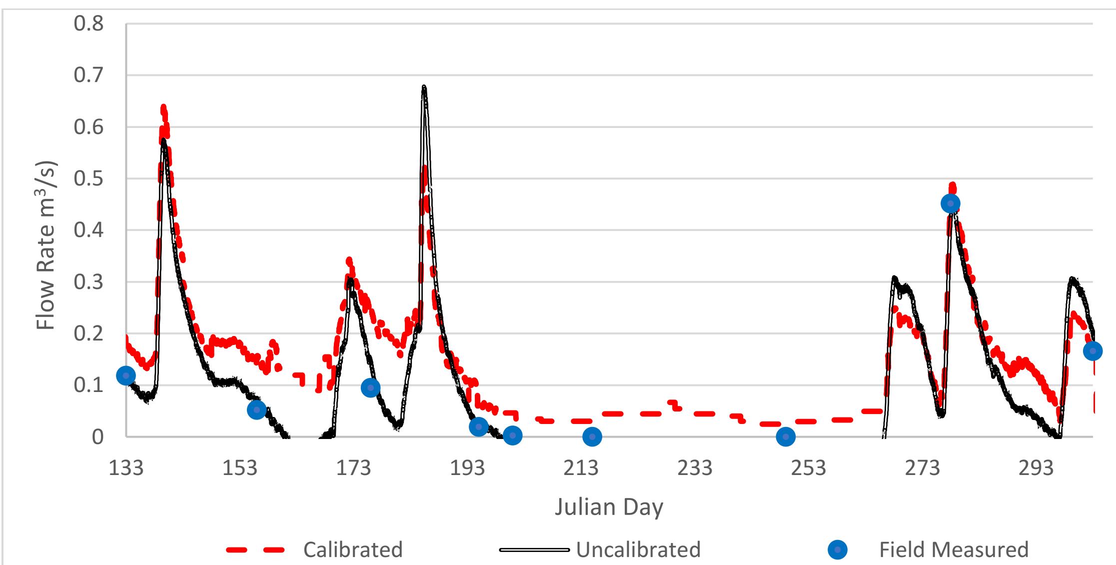

Figure A.4: Calibrated, Uncalibrated and Field determined outflow discharge rate

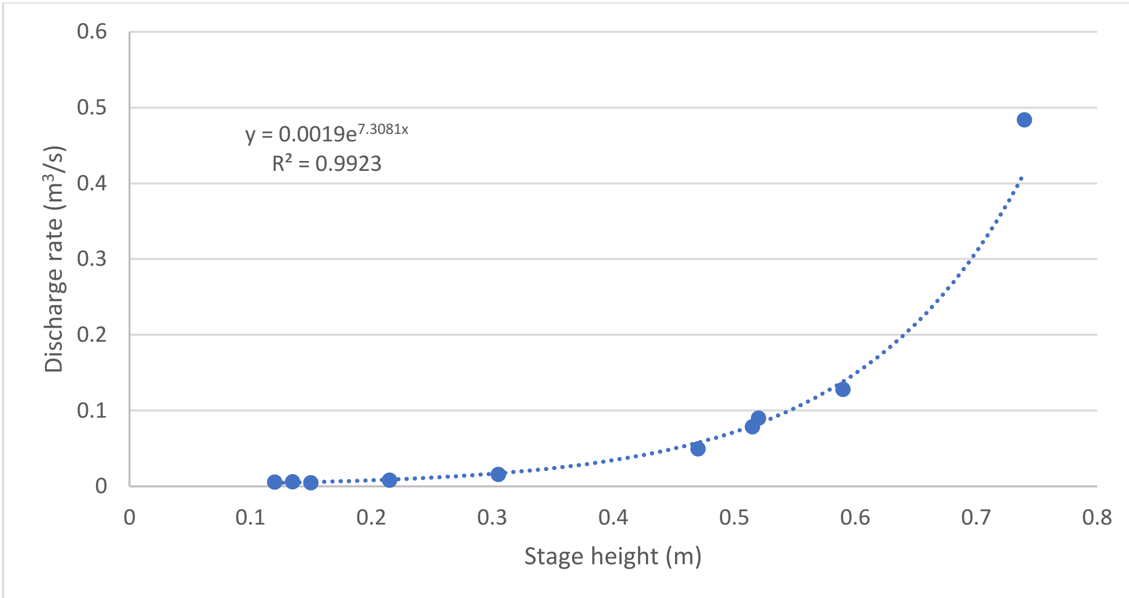

Figure: A.5: Stream gauging rating curve for all field determined inflow rates

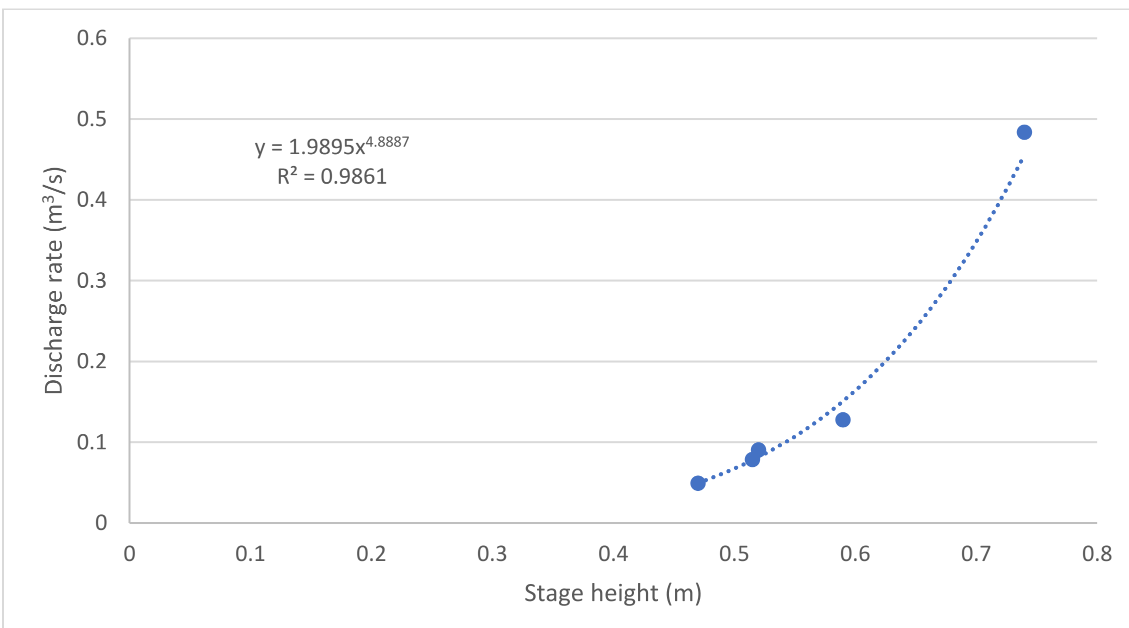

Figure: A.6: Stream gauging rating curve for the upper effective gauge, above 0.47 m

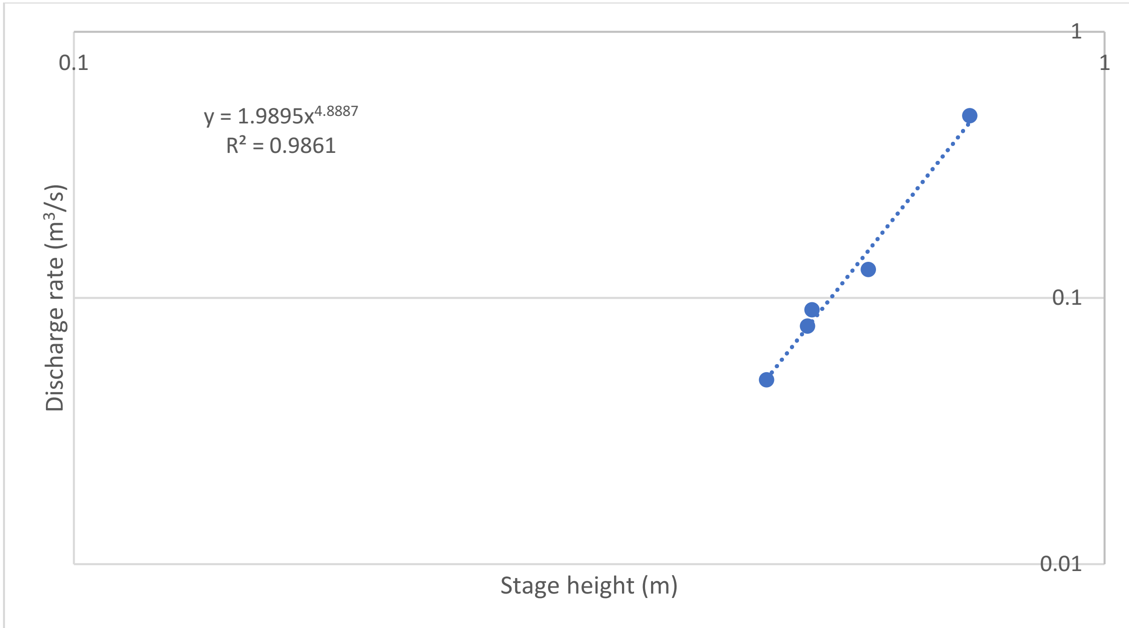

Figure: A.7: Log-log transformed stream gauging rating curve for the upper effective gauge of inflow from UUL

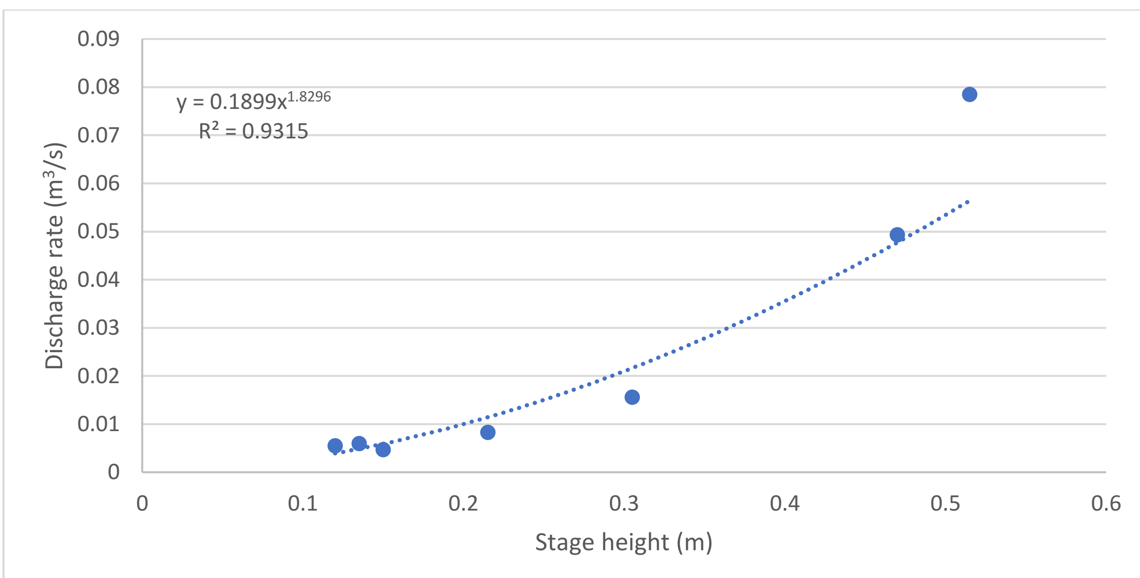

Figure: A.8: Stream gauging rating curve for the lower effective gauge of inflow from UUL

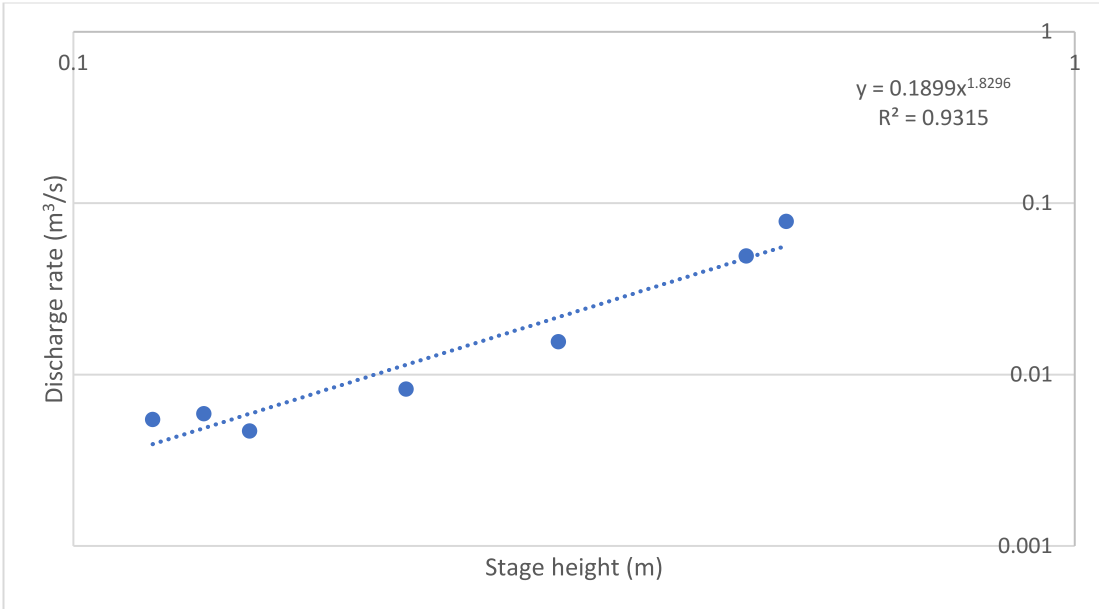

Figure: A.9: Log-log transformed stream gauging rating curve for the lower effective gauge of the inflow from UUL , below 0.47 m

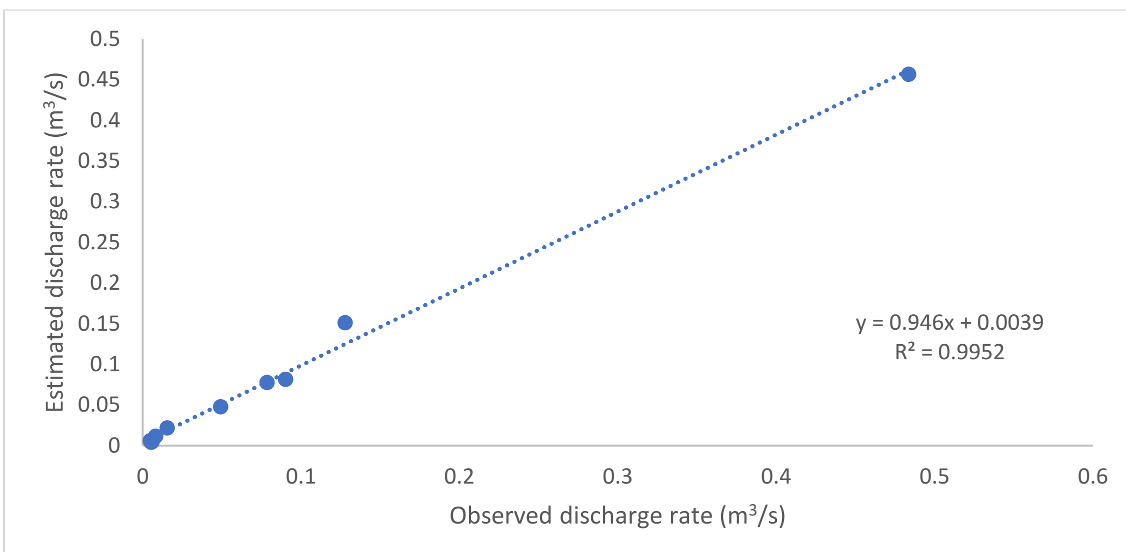

Figure: A.10: Estimated and Observed discharge rate from the inflow from UUL

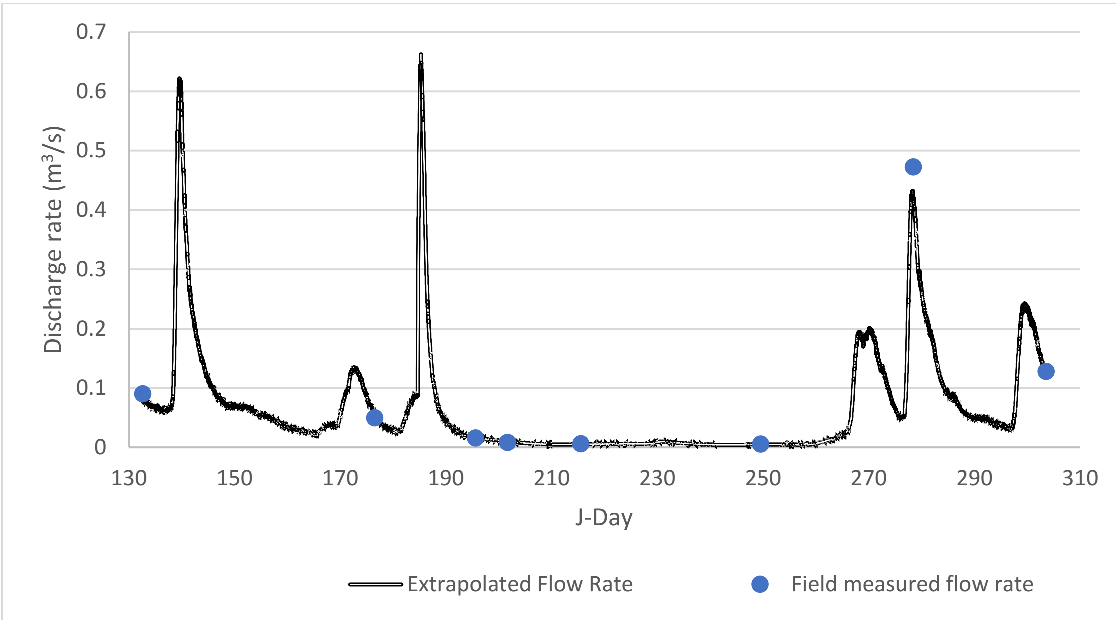

Figure: A.11: Extrapolated and field determined discharge rate from the inflow from UUL

The inflow from Upper Unnamed Lake, outflow, added inflow, Pond 102 and Pond 400 A were plotted in Figure 4.3. Pond 102 and 400 A discharge rates were provided by Barrick Hemlo. Inflow from Upper Unnamed Lake (UUL) and Lower Unnamed Lake (LUL) outflow stream gauging calculations, along with photos of unmonitored inflow and drainage points can be found in Appendix A.1-A.11. The added inflow is discharged into the east end of the lake model, near the model to account for an ungauged stream. The flow rate for the ungauged stream was set to 5 times the precipitation rate.

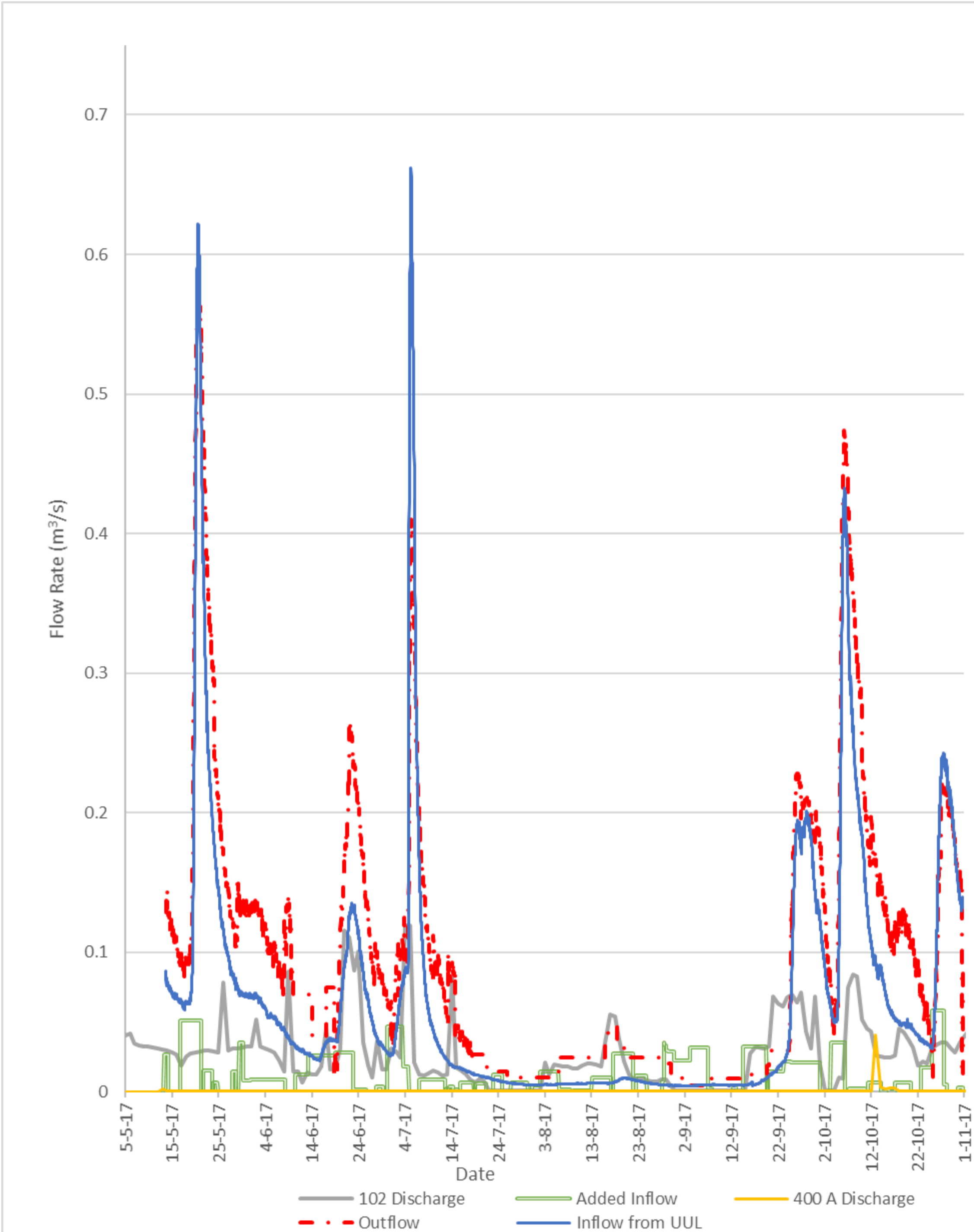

Figure A.12: Flow rates over the model year for lake model inflows and outflow

Figure: A.13: Photo of the Beaver dam blow out from 2016

Figure A.14: Photo of Beaver dam governing UUL discharge to LUL

Figure A.15: Photo of Upper Unnnamed Lake drainage as a result of 2016 beaver dam blowout

Figure A.16: Photos of Pond 102 Discharge into LUL

Figure A.17: Photos of ungauged inflow

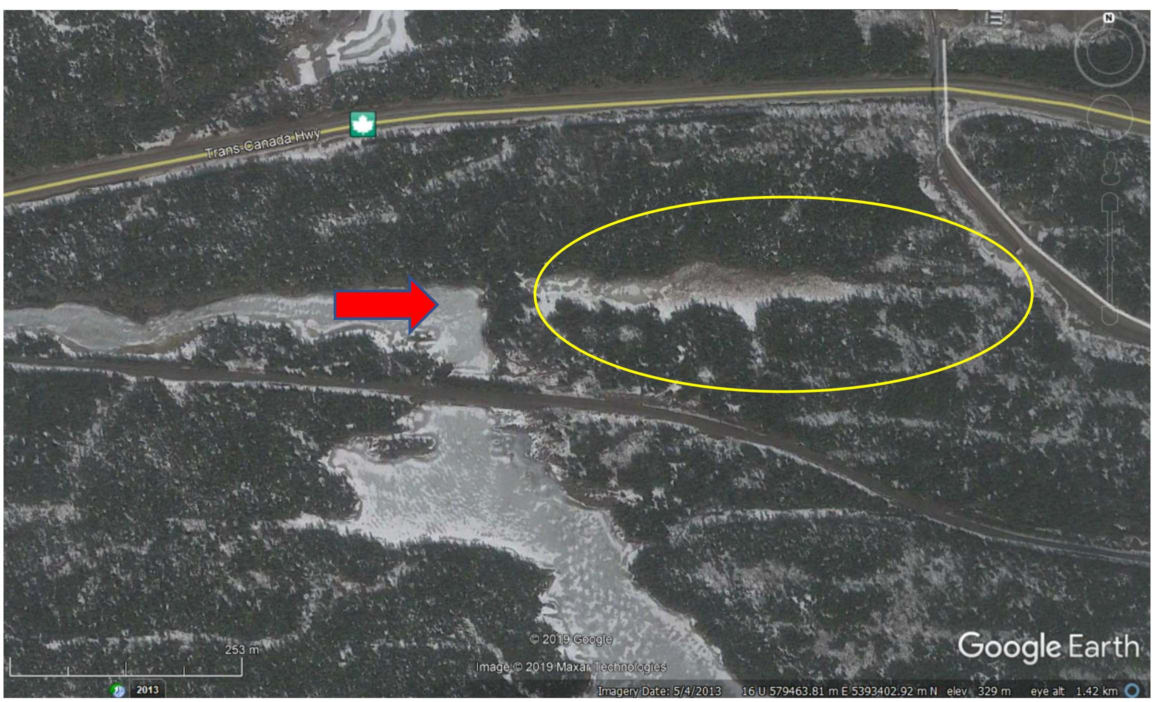

Figure A. 18: Location of ungauged inflow and wetland area

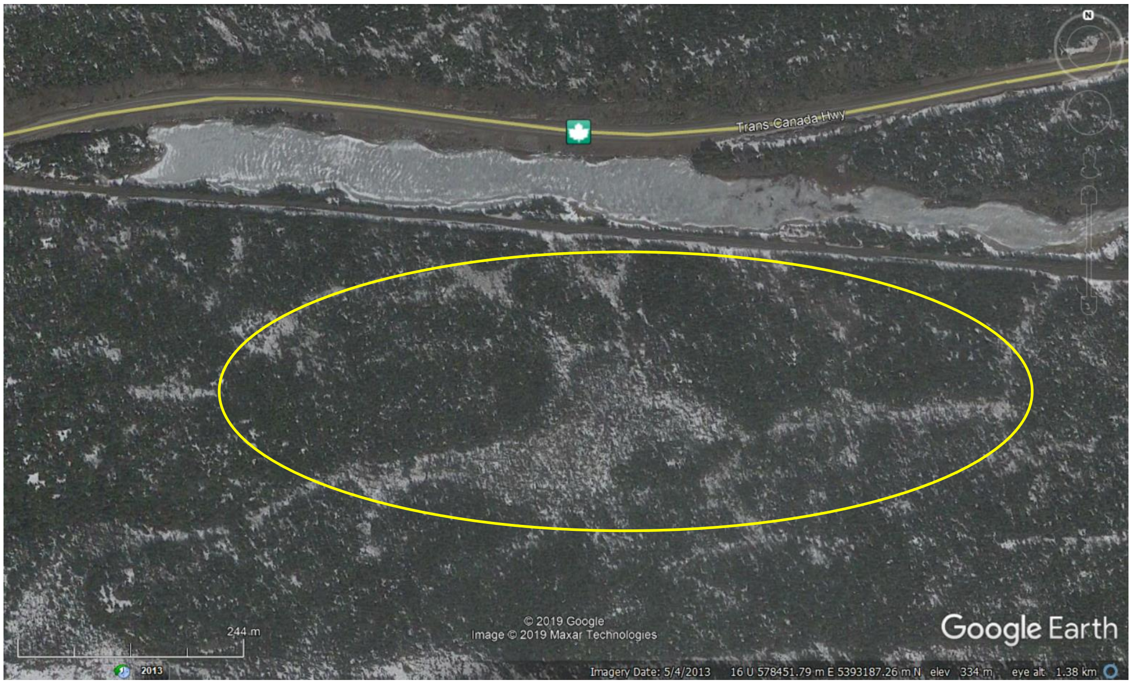

Figure A.19: Wetland area adjacent to the west end of Lower Unnamed Lake

Figure A.20: Photos of Ungauged outflow and standing water adjacent to LUL

Figure A.21: Photo of Ungauged outflow and standing water adjacent to LUL

Figure A. 22: Photo of the narrow channel of LUL

Figure A. 23: Photo of the outflow of LUL

Figure A. 24: Photo of LUL outflow during a period of no flow

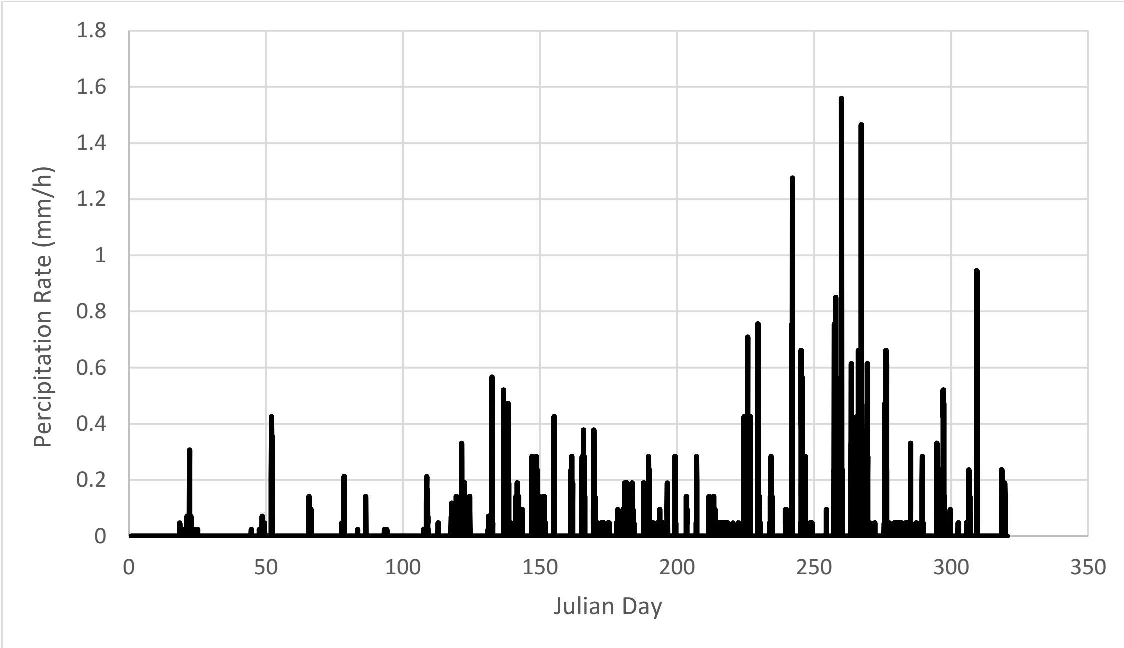

Figure A. 25: Precipitation rate

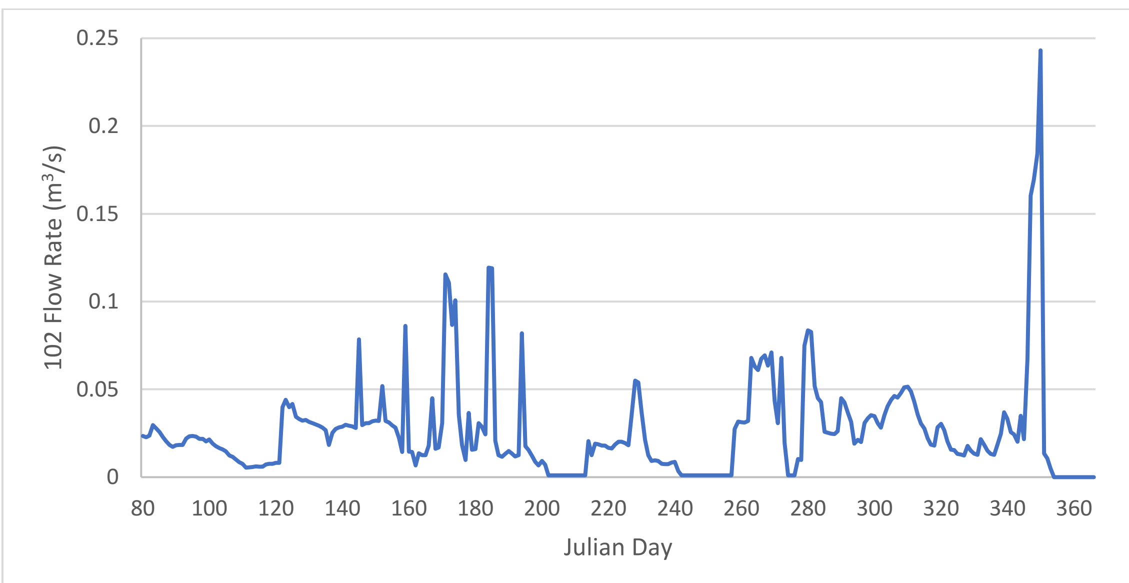

Figure A.26: Pond 102 discharge rate

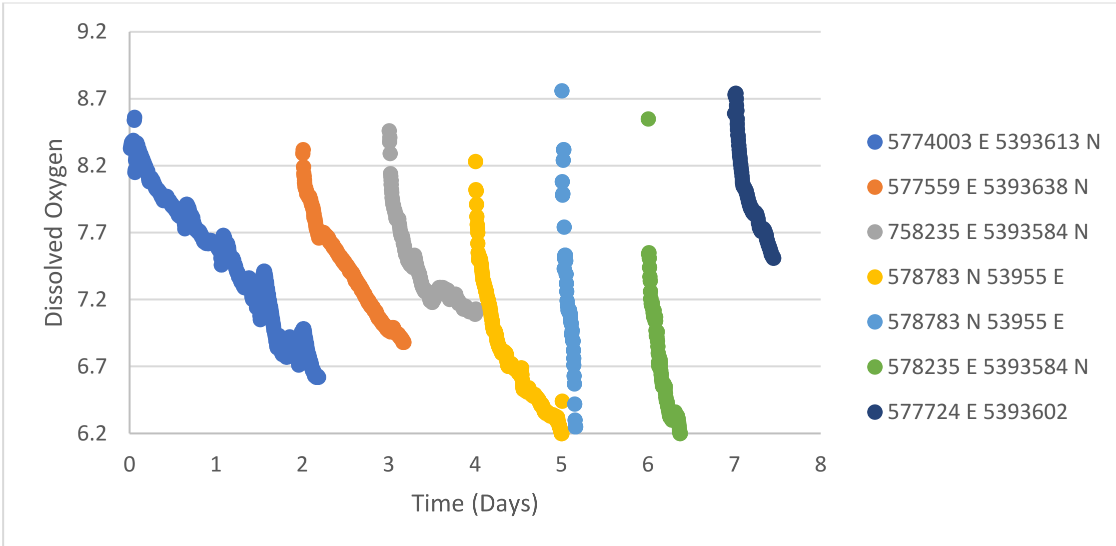

Figure A.27: Sediment oxygen demand of LUL sediment incubation

Appendix B: Model output data

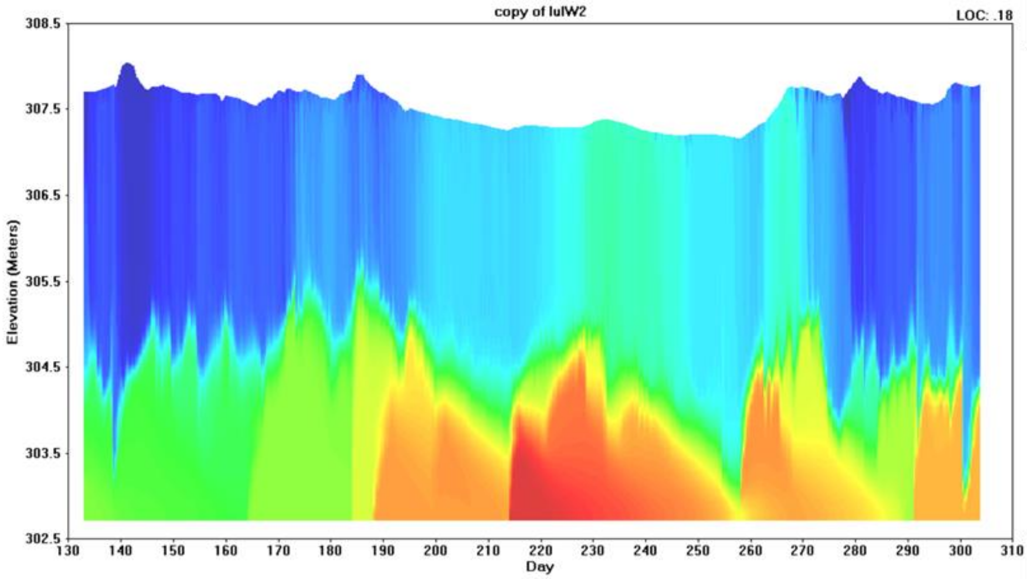

Figure B.1: Time-depth chart of the concentration of TDS in the west basin of the CLM

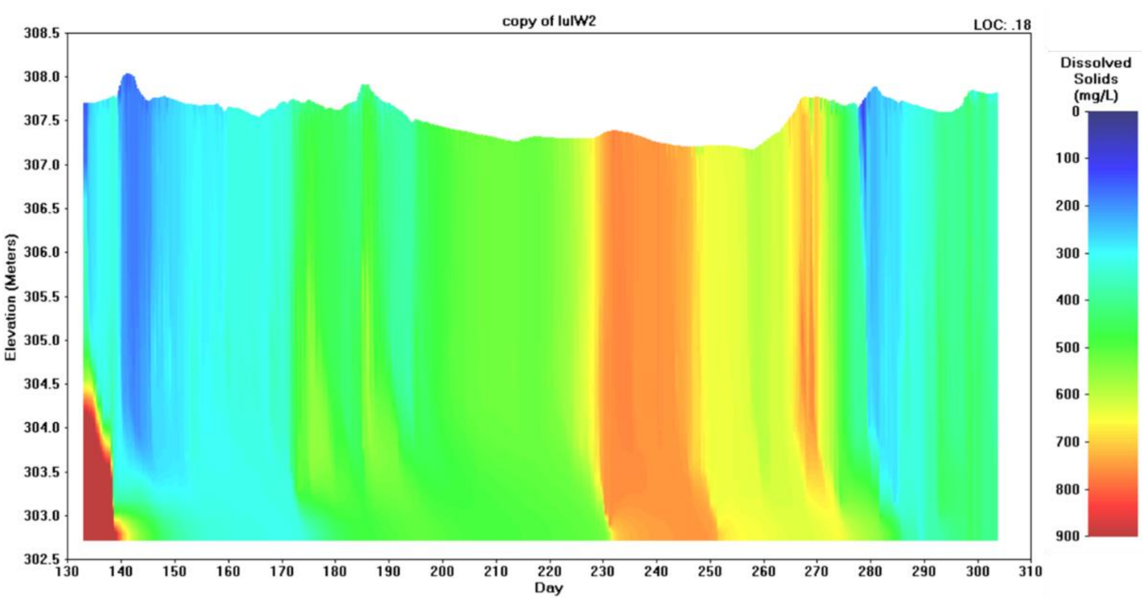

Figure B.2: Time-depth chart of the concentration of TDS in the west basin in the PLM

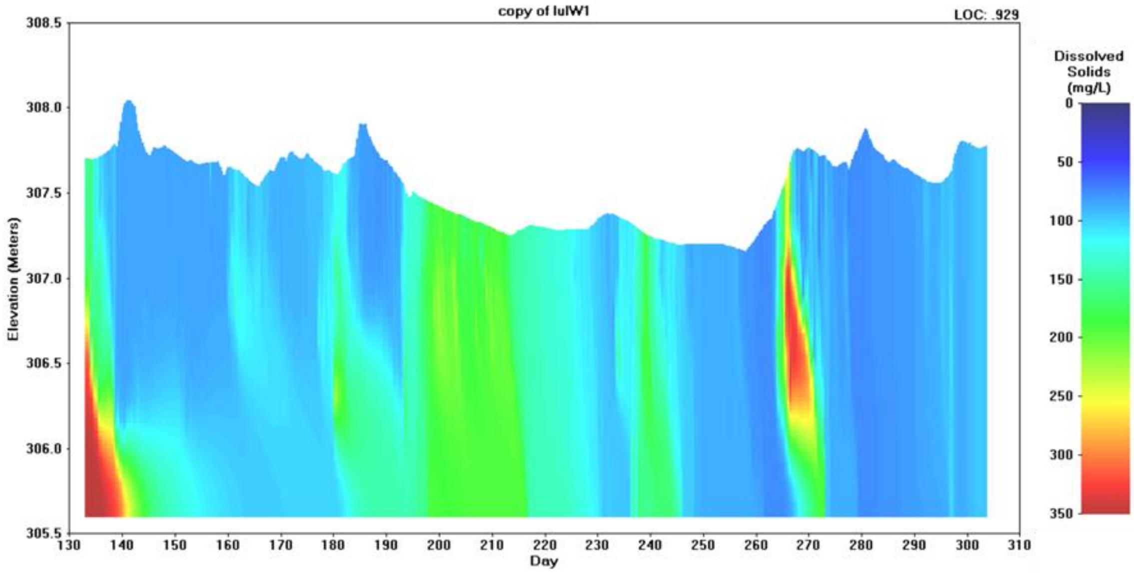

Figure B.3: Time-depth chart of the concentration of TDS in the east basin of the CLM

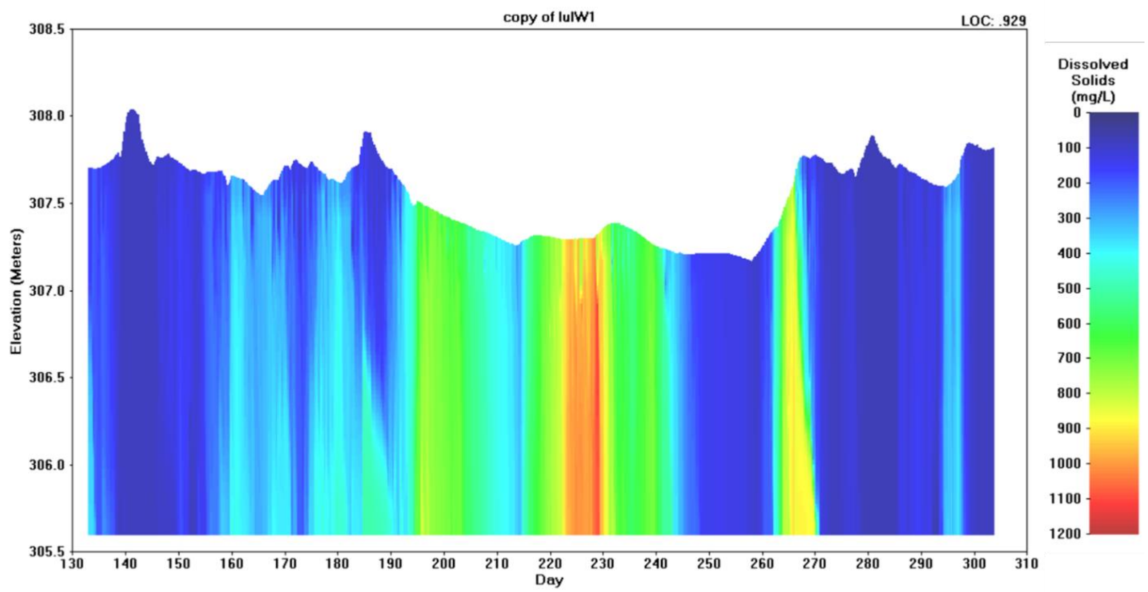

Figure B.4: Time-depth chart of the concentration of TDS in the east basin of the PLM

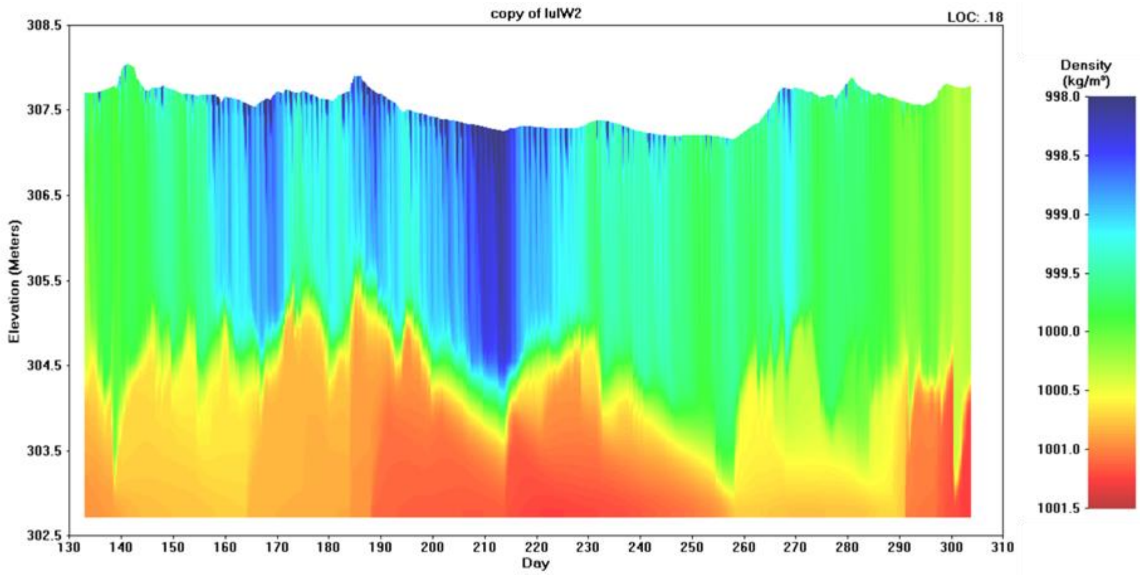

Figure B.5: Time-depth chart of water density in the west basin in the CLM

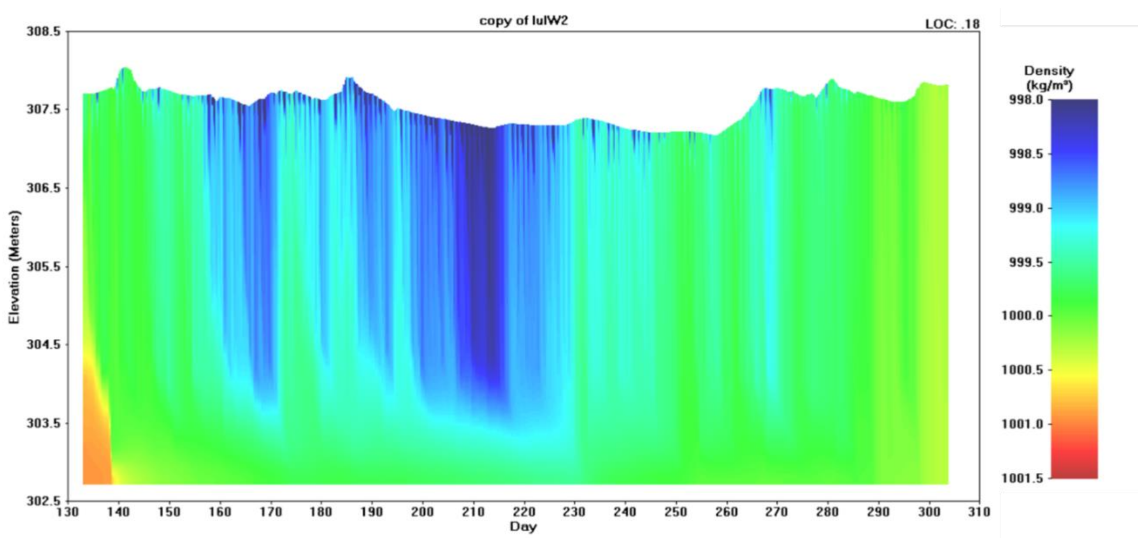

Figure B.6: Time-depth chart of water density in the west basin in the PLM

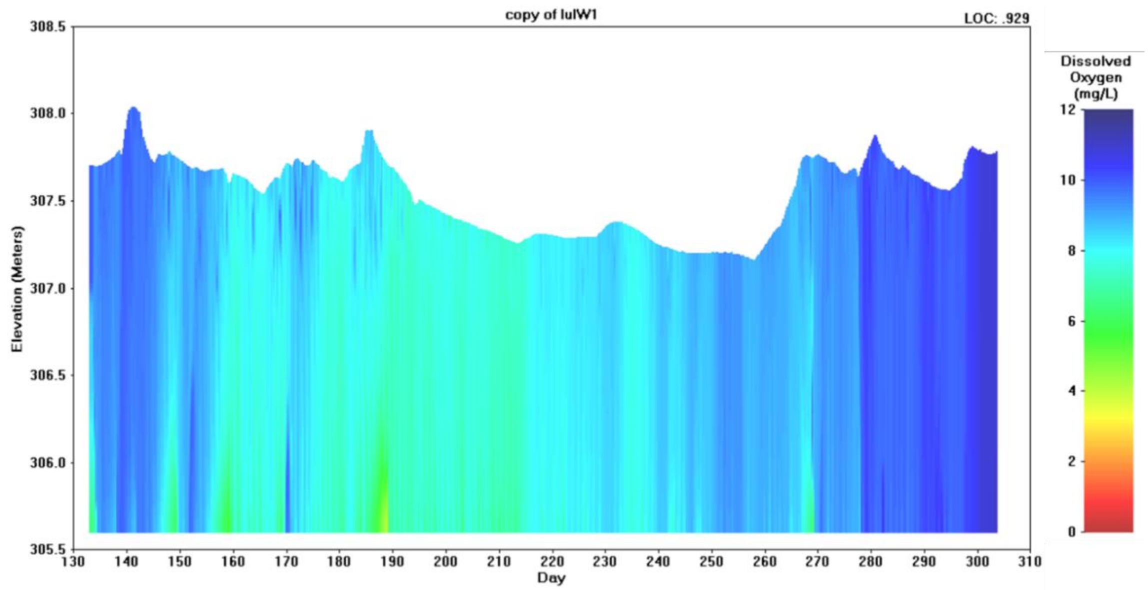

Figure B.7: Time-depth chart of water density in the east basin in the CLM

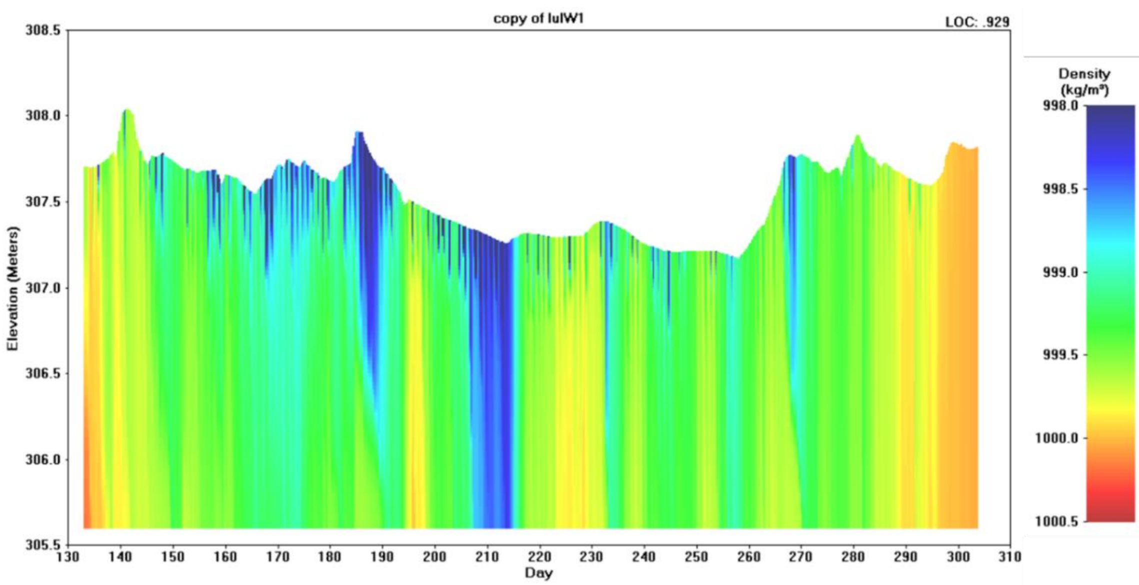

Figure B.8: Time-depth chart of water density in the east basin in the PLM

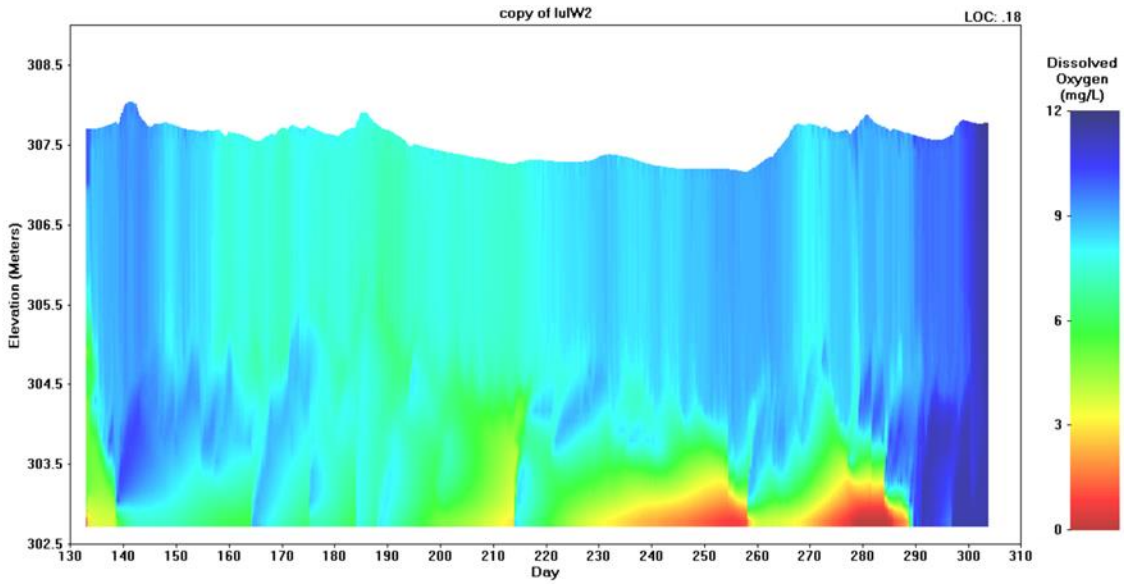

Figure B.9: Time-depth chart of the concentration of dissolved oxygen in the west basin in the CLM

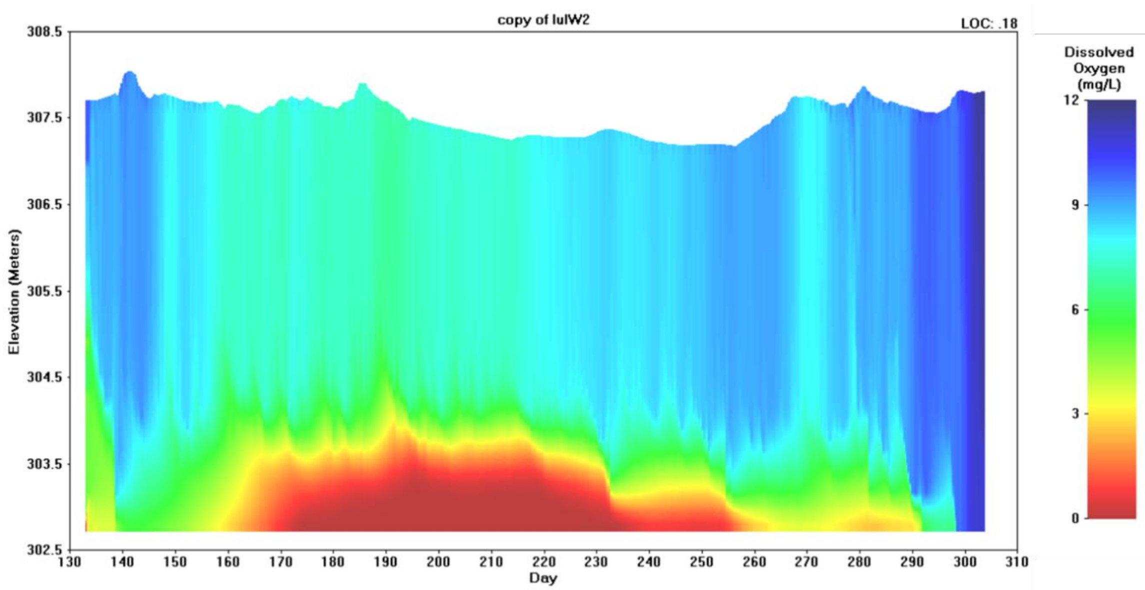

Figure B.10: Time-depth chart of the concentration of dissolved oxygen in the west basin in the CLM

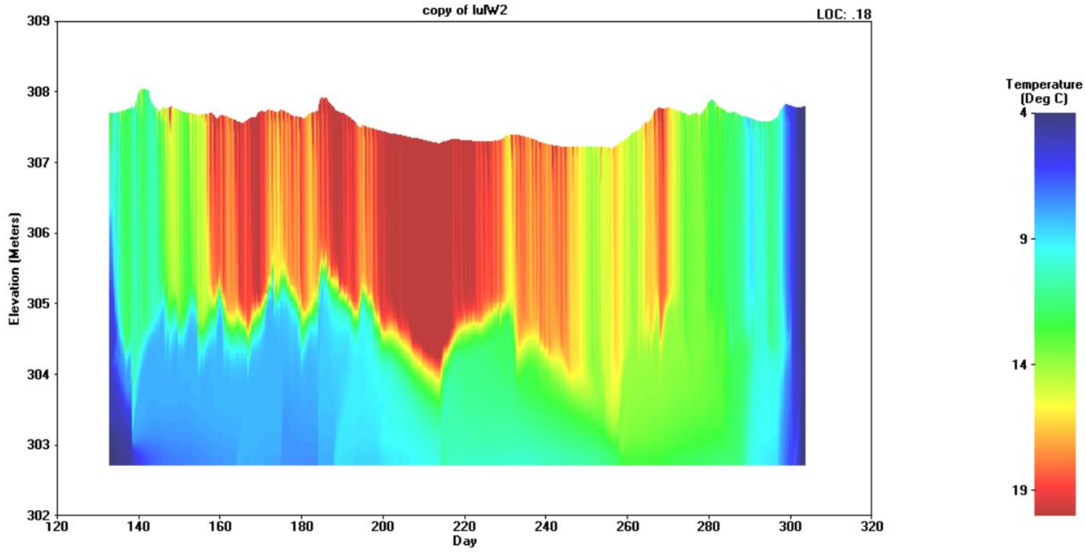

Figure B.11: Time-depth chart of the temperature in the west basin in the CLM

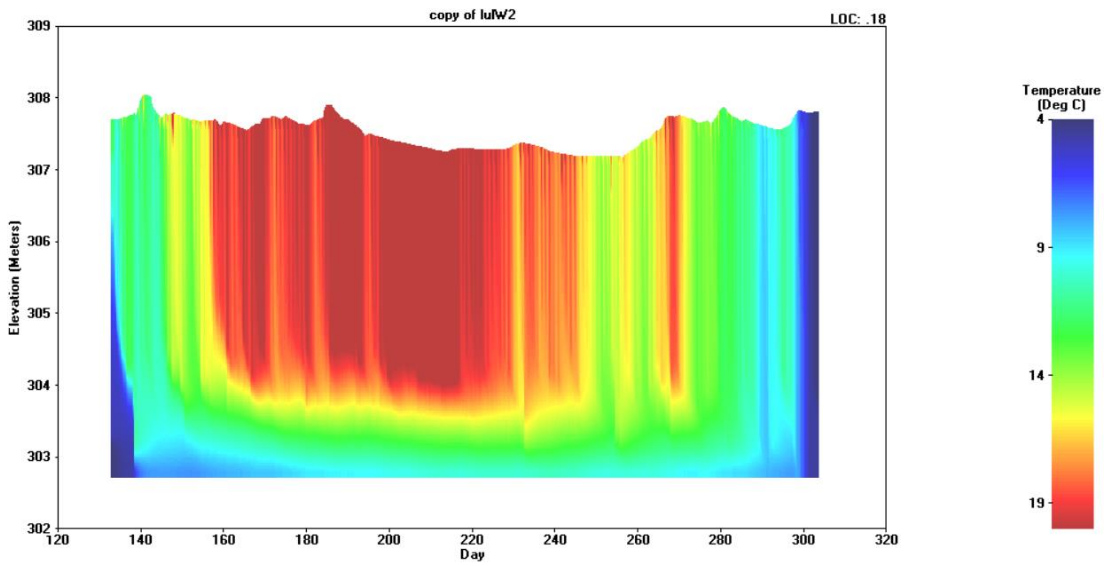

Figure B.12: Time-depth chart of the temperature in the west basin in the PLM

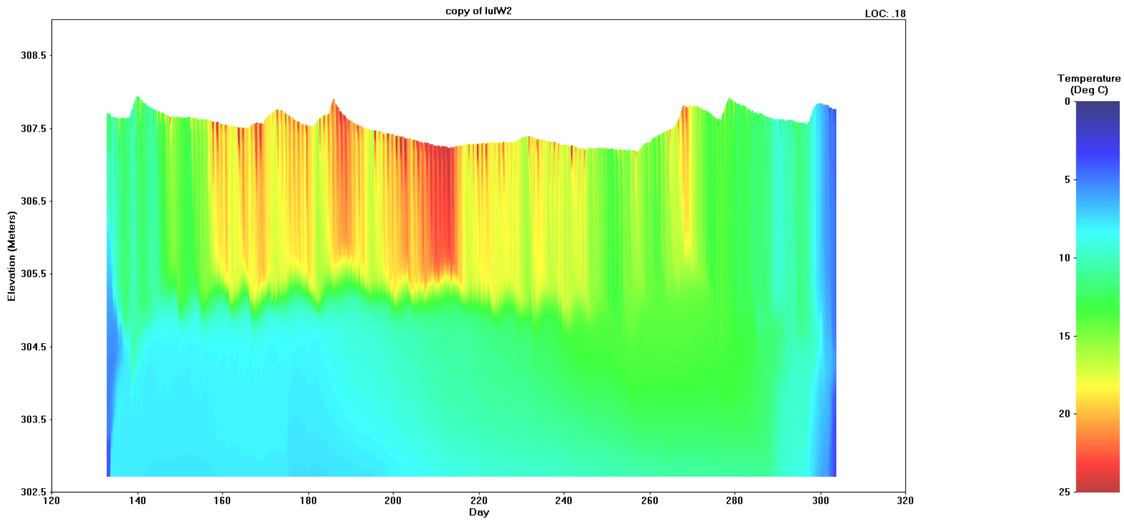

Figure B.13: Time-depth chart of temperature in the west basin in the CLM potential meromix model.

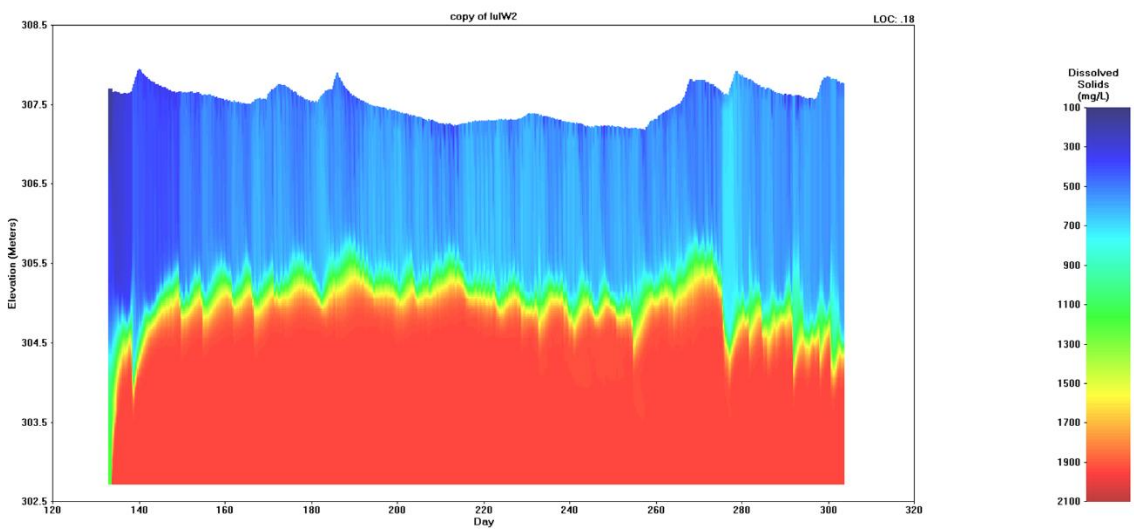

Figure B.14: Time-depth chart of TDS in the west basin in the CLM potential meromix model.

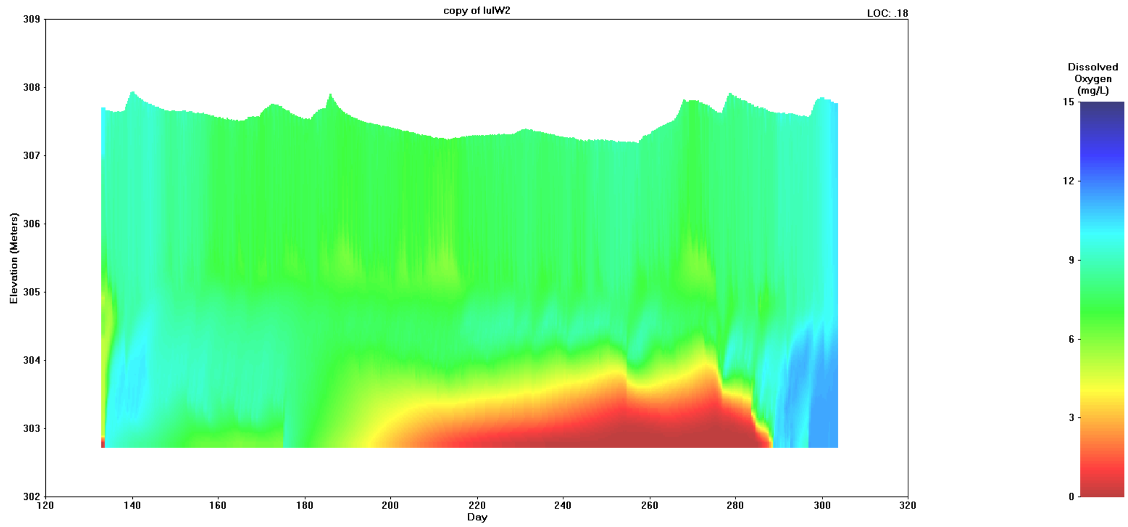

Figure B.15: Time-depth chart of dissolved oxygen in the west basin in the CLM potential meromix model.

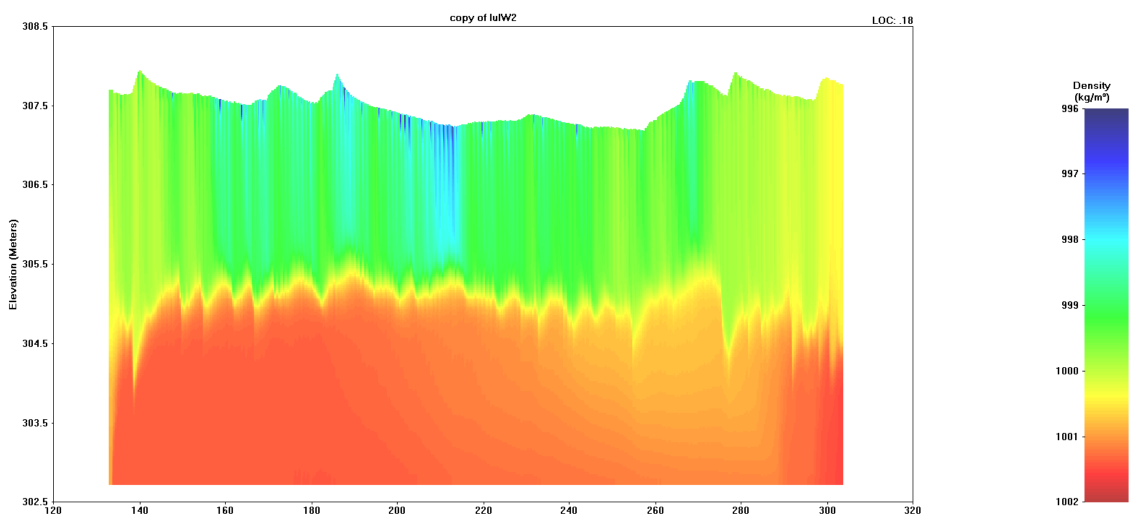

Figure B.16: Time-depth chart of density in the west basin in the CLM potential meromix model.

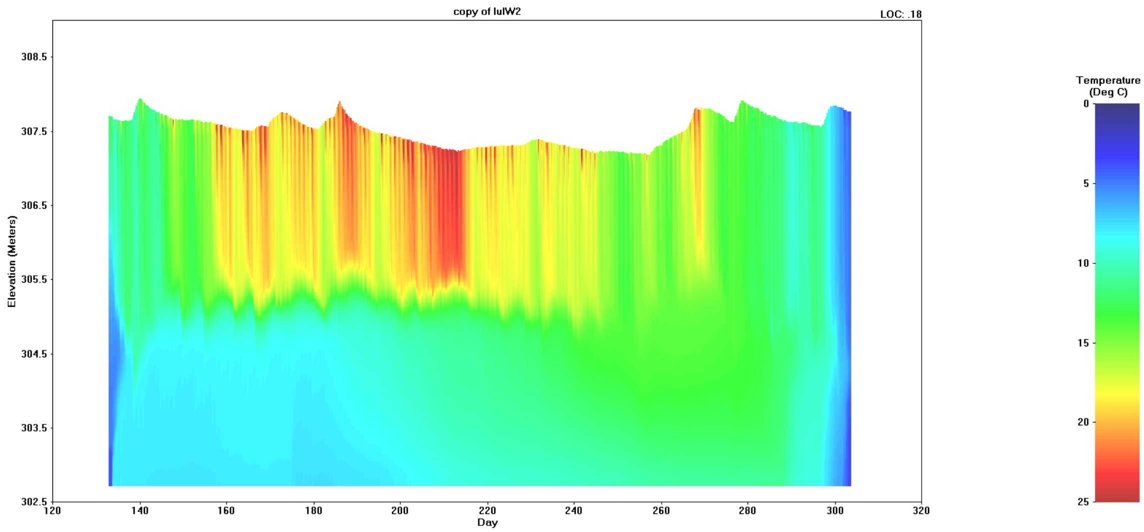

Figure B.17: Time-depth chart of temperature in the west basin in the PLM potential meromix model.

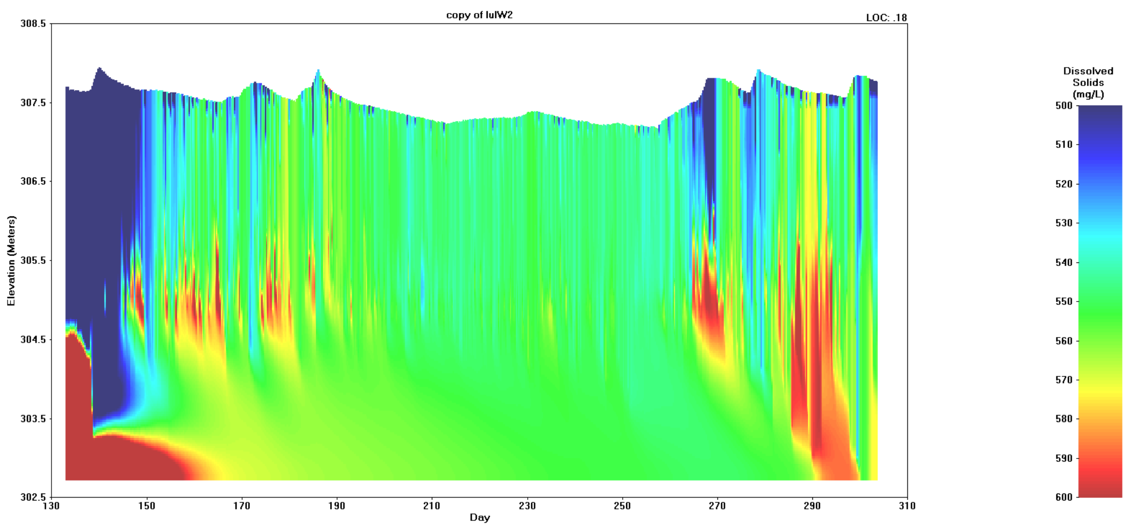

Figure B.18: Time-depth chart of TDS in the west basin in the PLM potential meromix model.

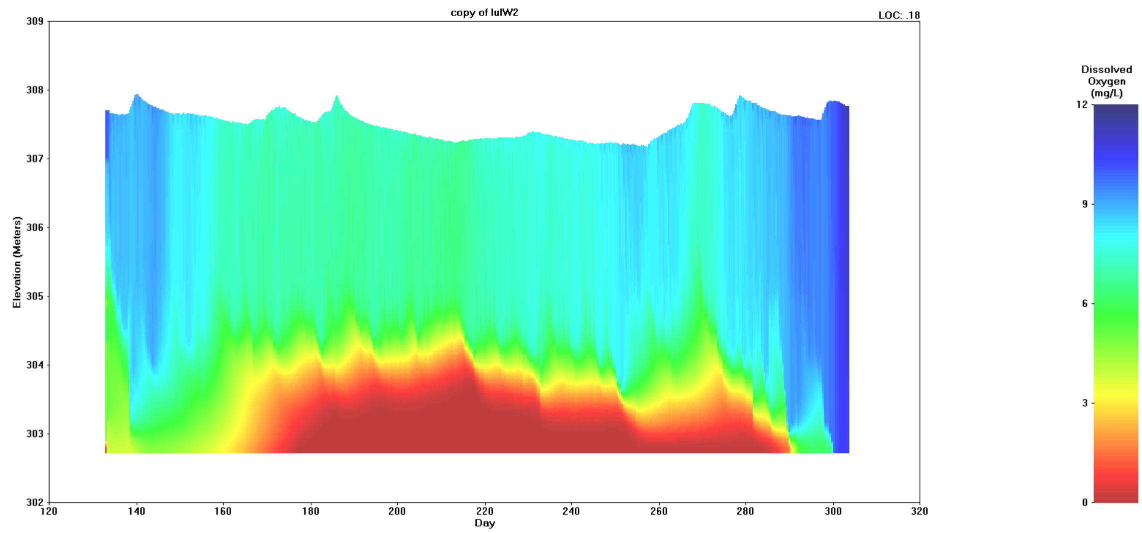

Figure B.19: Time-depth chart of dissolved oxygen in the west basin in the PLM potential meromix model.

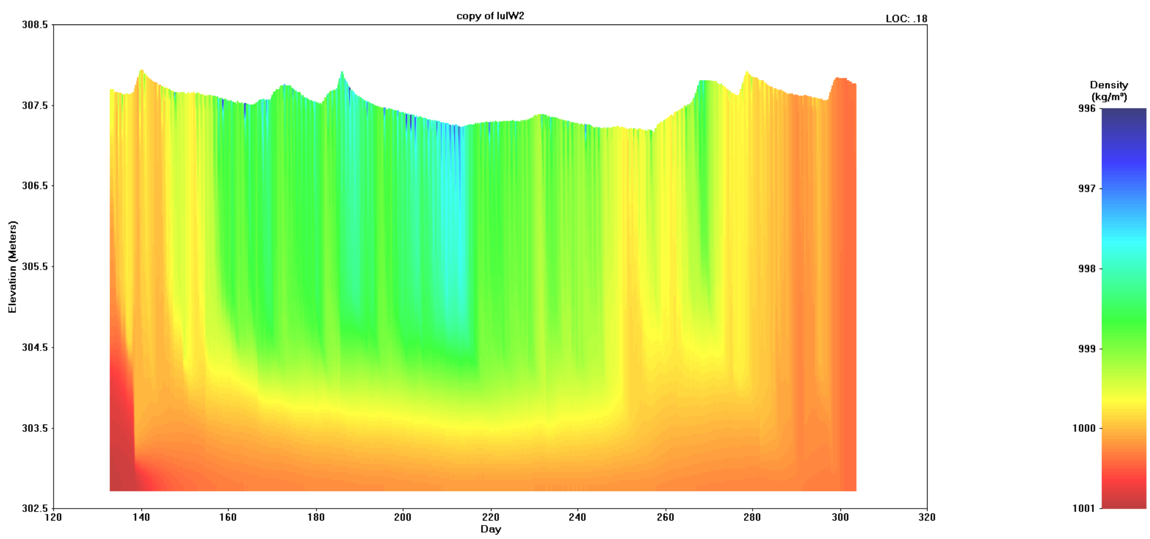

Figure B.20: Time-depth chart of dissolved oxygen in the west basin in the CLM potential meromix model.

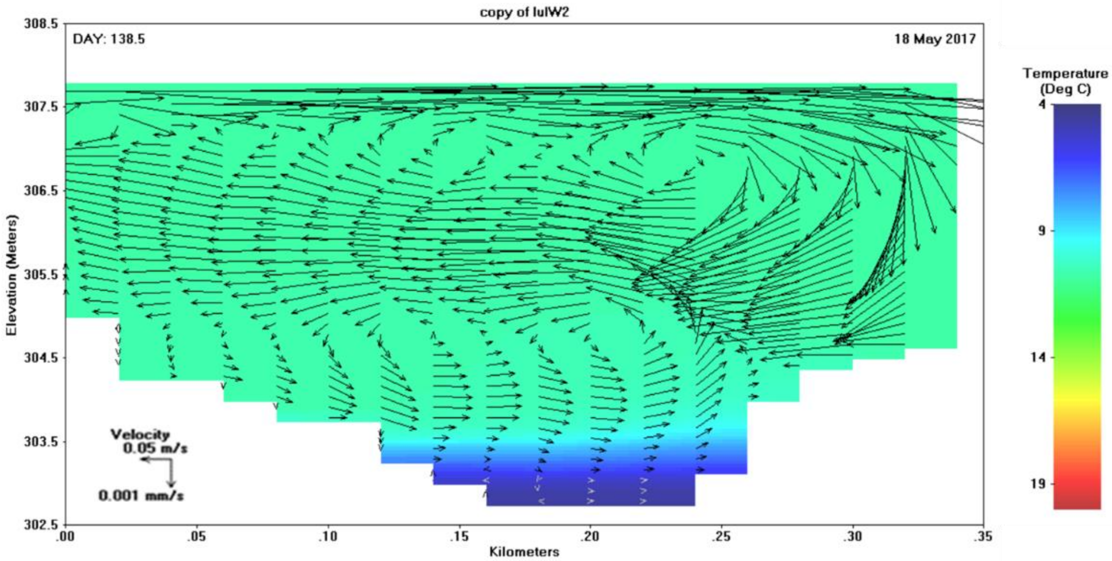

Figure B.21: May 18 velocity vectors of the CLM

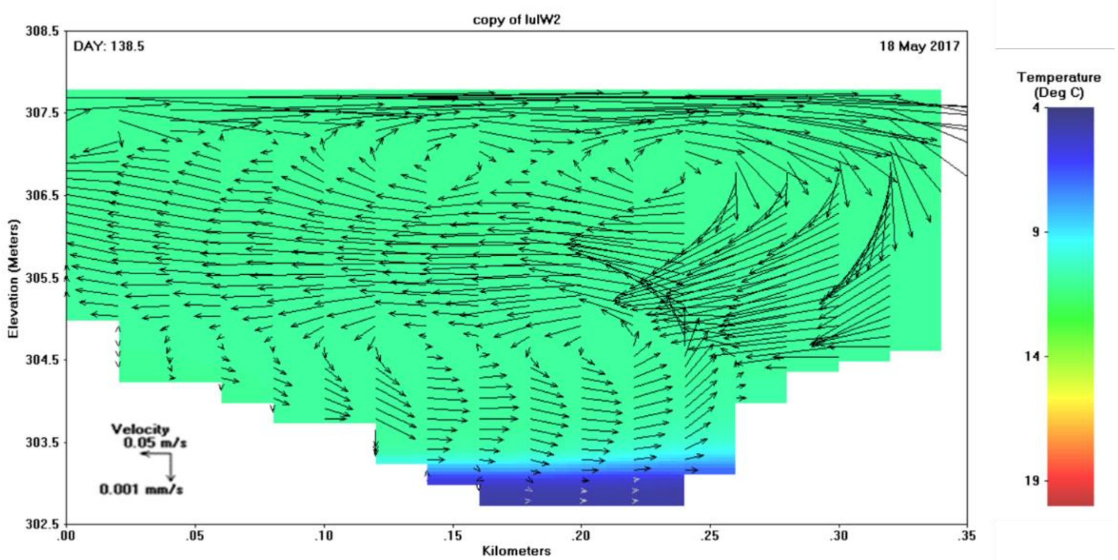

Figure B.22: May 18 velocity vectors of the PLM

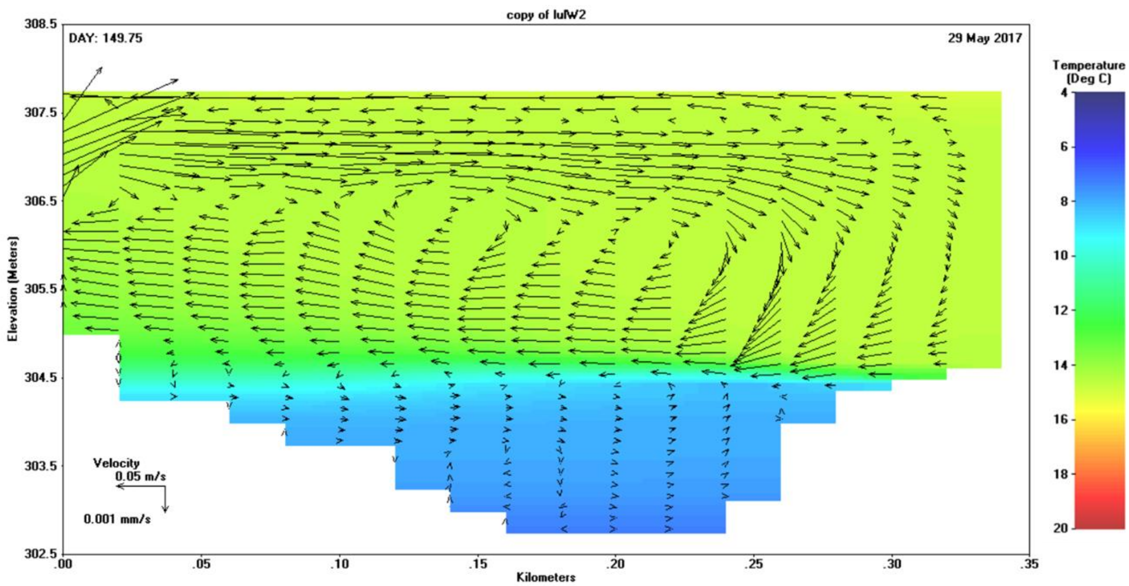

Figure B.23: Velocity vectors of CLM on May 29

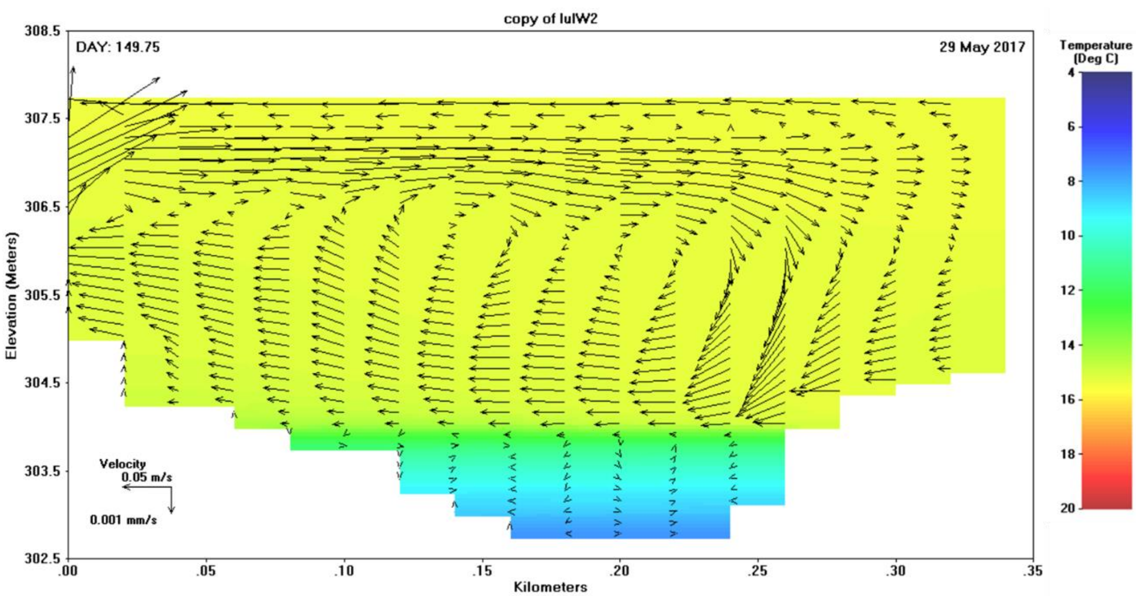

Figure B.24: Velocity vectors of PLM on May 29

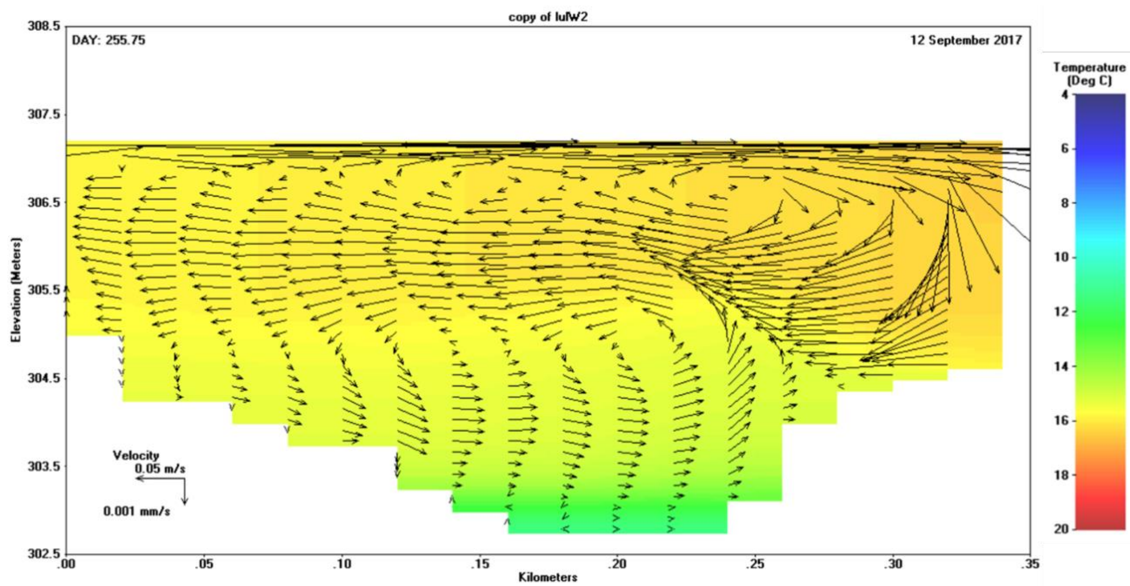

Figure B.25: Velocity vectors of CLM on September 12

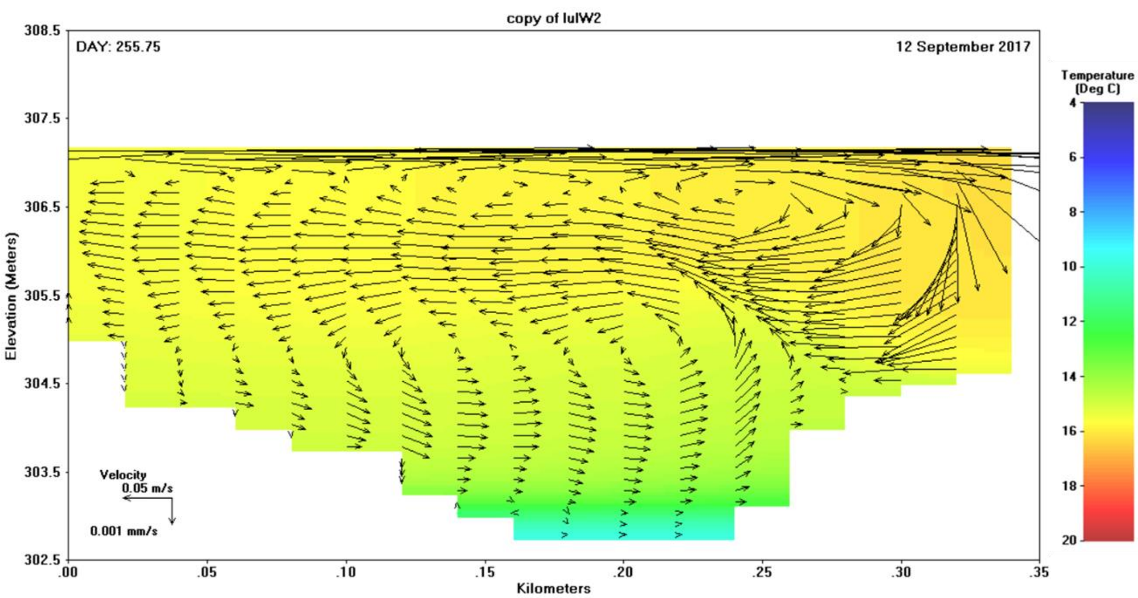

Figure B.26: Velocity vectors of PLM on September 12

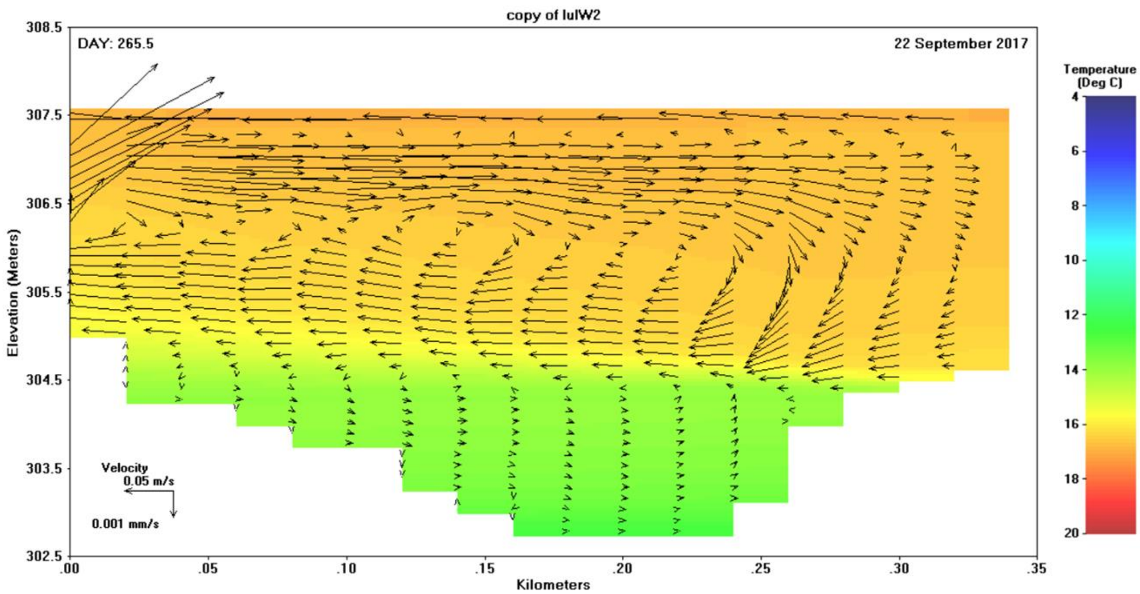

Figure B.27: Velocity vectors on September 22 in the CLM

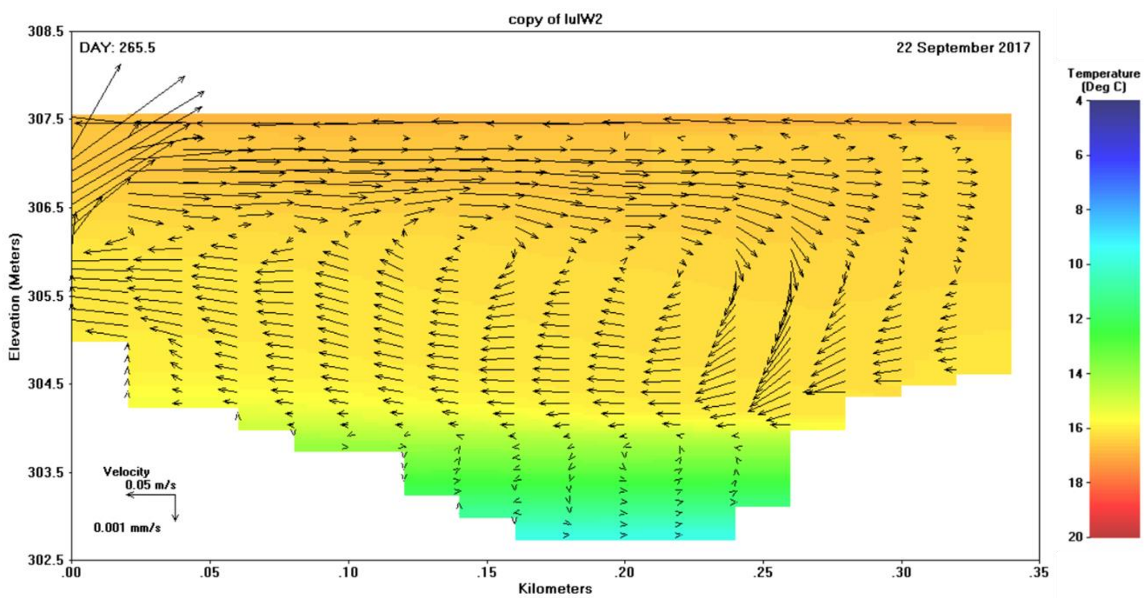

Figure B.28: Velocity vectors on September 22 in the PLM

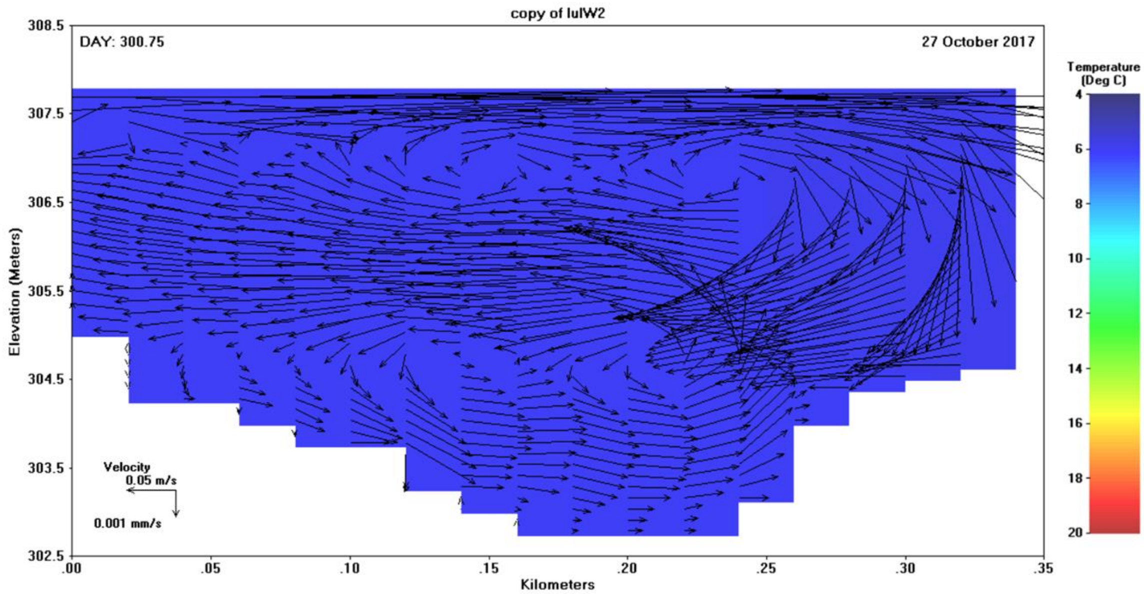

Figure B.29: Velocity vectors on October 27 in the CLM

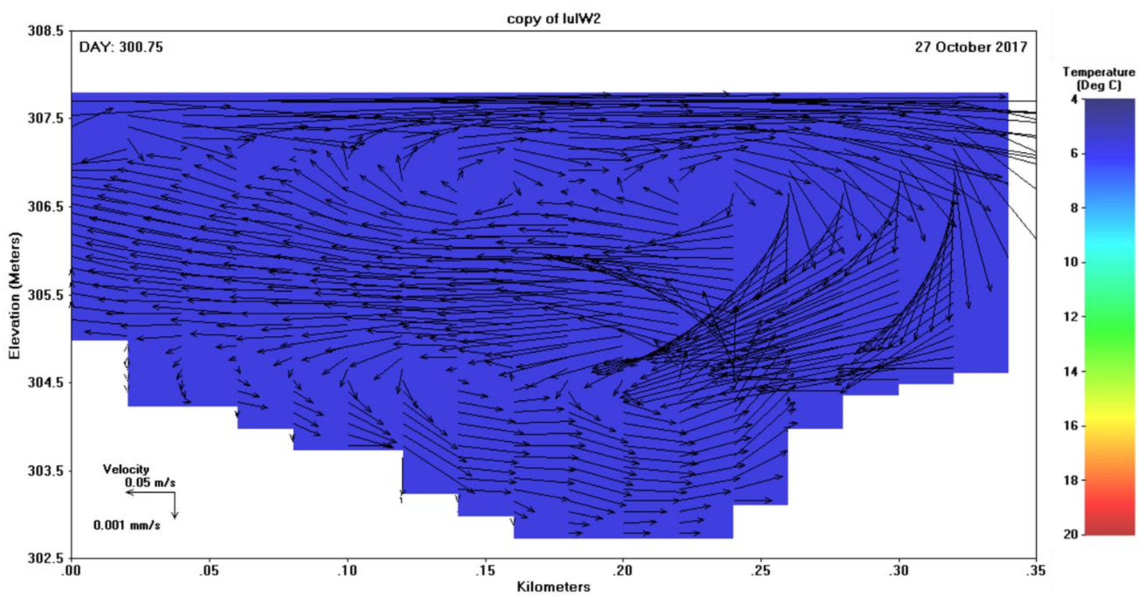

Figure B.30: Velocity vectors on October 27 in the PLM

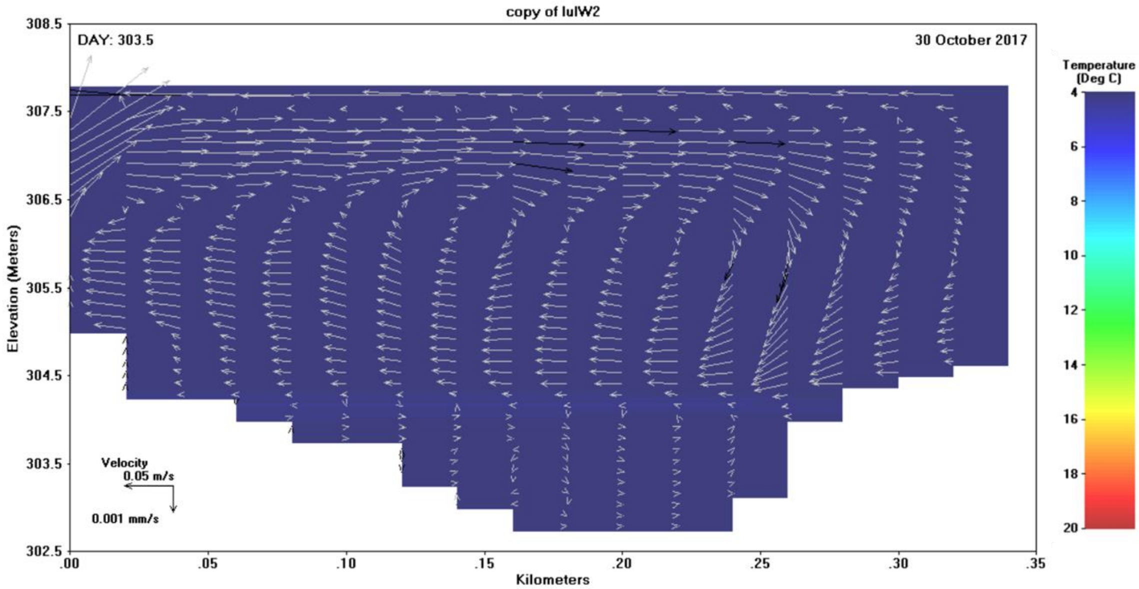

Figure B.31: Velocity vectors on October 30 in the CLM

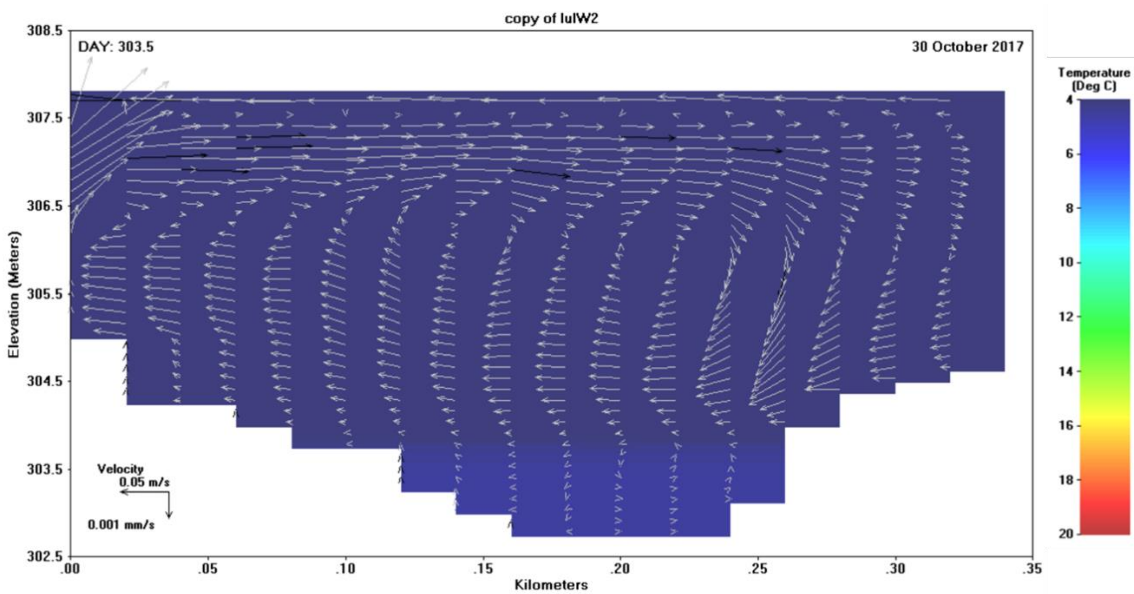

Figure B.32: Velocity vectors on October 30 in the PLM

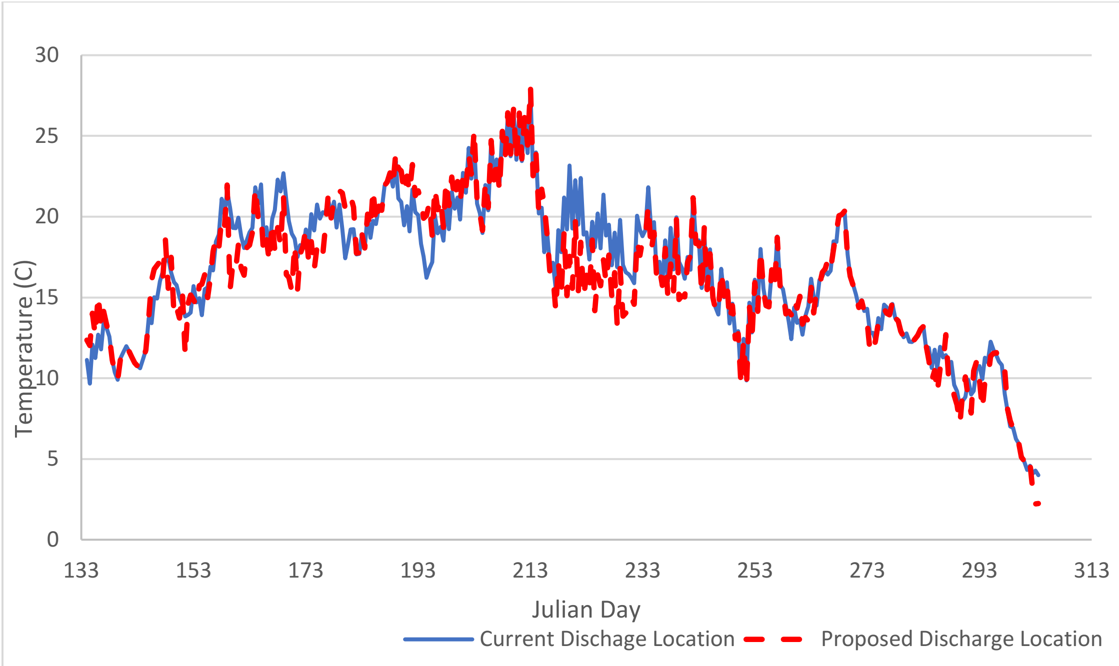

Figure B.33: Littoral temperature in the narrow channel for the CLM and PLM

Appendix C: Calibration Detail

CE-QUAL W2 was calibrated to effectively replicate the water quality and hydrodynamics of the lake. Calibration was performed, utilizing field determined water level, bathymetry, temperature, concentration of TDS and concentration of dissolved oxygen profiles. The concentration of TDS at the outflow of LUL was monitored and compared to model output values. Several modifications had to be made in order to simulate Lower Unnamed Lake. The main calibration adjustments were discussed below.

The CE-QUAL W2 model grid represented the field determined bathymetry well, with an AME of 6.1% (Figure 4.1). The uppermost 4 m (304.1 - 308 MASL) below the grid surface varies by < 1% and makes up 96.4% of the lake volume. The deepest 1.35 m (302.6 - 303.95 MASL) has a greater variation, with an error averaging 13%. The deep section is relatively small, as a result, errors in grid construction constitute a greater percent vitiation. The greatest error is within the two bottommost layers, 0.06 & 0.18 above the sediment. The CE-QUAL W2 grid containing 65% and 21% more volume, respectively at these layers. Error in the deepest layer was due to the CE-QUAL W2 grid requiring a minimum cell width of 5 m (Cole & Wells, 2017). The CE-QUAL W2 grid consists of rectangular cells. When the smooth lake bottom was constructed into a rectangular grid, the surface area of the sediment-water interface was increased. Increased surface area increases the friction factor at the sediment-water interface (Pentecost, 2016). The increased bottom friction results in a greater shear force of the overlying water, which reduces the velocity, inhibiting mixing, as variations in the sediment friction factor may result in significant variations of eddy hydraulic radius, up to 2 m above the sediment (Limerinos, 1970; Jarrett 1984). The additional friction due to grid error is responsible for the lowest 0.5 m not mixing during turnover observed in the field, on October 28th. Further calibration through refining Manning's coefficient of drag and refining grid resolution may resolve the issue. The bathymetry at the deepest section sloped down 1 m, along one 20 m segment. This sill may have overly influenced the large-scale eddy conditions, isolating the deepest section from the mixing layer during turnover (Lu & Wang, 2009).

One boundary condition requiring modification for calibration was the placement of Pond 102 discharge. CE-QUAL W2 injects tributary discharges into a single cell within a single segment. Due to the small cell heights required for high resolution (0.12m), unrealistically high velocity vectors were produced in periods of high discharge. The increased momentum would create turbulent eddies within the model. To avoid this, Pond 102 was discharged evenly into six segments, rather than one.

A stream gauging rating curve was used to produce model inflow rate from UUL and LUL outflow rate. The rating curve matched the field determined flow rates with an r^2 of 0.9952 & 0.9923 respectively (n=10) (Appendix Figure A.5 – A.11). Inflows from Pond 102 and 400 A were provided by Barrick Hemlo (Figure 4.3). The model water surface elevation was compared to the observed field water level (Figure 4.4). Under the original lake inflow and outflow rates, the water surface elevation of the model was far greater than what was observed, ending the model run year 1.8 m above what the field data suggested. It was evident that water was flowing out of the lake that was not accounted for.

The railway tracks on the south side of the lake sit atop several culverts, leading to a several small ponds and a wetland area. Photos of this can be found in Appendix A (Figure A.18-A.20). This would have been nearly imposable to effectively gauge and input into the model. The solution was to match the lake outflow rate to the field determined water surface elevation, an adjustment that is often applied to CE-QUAL W2

(Cole & Wells, 2013). Increasing the lake outflow rate may have influenced water momentum. Through drawing more water out of the end of the lake, at segment 65 within the model, water upstream is effectively pulled towards the outflow. Increasing velocity in turn, increases shear stress and may impact mixing dynamics (Kittrell, 1959). The decision was made to increase the outflow rate to match the field and model water surface elevation, as the discrepancy would have rendered the model useless, considering how shallow LUL is. It is also possible that there is exchange between the surface and ground water at LUL, but that was not monitored by this study (Lee, 1996).

Observed temperature profiles at the deepest section of the lake (16 U 577674 E 5393620) were compared to model output temperature profiles (Figure 4.7). The CE-QAUL W2 manual recommends an AME of < 1°C for the lake to be sufficiently calibrated (Cole & Wells, 2017). The most notable adjustment that was required for calibration was modifying the temperature of the Pond 102 discharge. The temperature was modified to be equal to the observed lake temperature at 304.5 MASL. This was done because CE-QUAL W2 instantly injects the discharge water directly into the cell with the corresponding density, in the center of the lake. As a result, the discharge water did not have time to lose heat to the sediment and overlying water column before reaching the hypolimnion causing the model to greatly overpredict hypolimnion temperature. The warmer water instantly injected into the cooler hypolimnion would cause the model to become unstable, as warmer parcels of water would cause turbulent eddies (Tsay, *et al.* 1992). I therefore determined that the most accurate way to replicate the conditions of LUL within the model was to set the discharge temperature to the temperature at 304.5 MASL, within LUL.

Hypolimnion temperature was overpredicted by the model early in the run year, on June 6 & 26, July 15th and August 5th (Figure 4.7). This was due to a limitation of CE-QUAL W2, as the model uses a set sediment temperature and coefficient of bottom heat exchange. The manual recommends using the mean annual air temperature for the sediment. This may work in larges lakes, where hypolimnion and sediment temperature is largely unchanged, but shallow lakes, such as LUL experience a variation in sediment temperature throughout the year (Fang & Stefan, 1996; Birge *et al.* 1927). Reducing the sediment temperature resulted in more accurate hypolimnion temperatures early in the year (May 12th - August 5th) but less accurate later in the year (September 9th – October 31st). I decided that it was more important to accurately model temperature later in the year, around turnover, as determining whether the lake may be prone to becoming meromictic was a key objective in this study. Future development of a dynamic sediment temperature input within the model would eliminate this dilemma.

The model was calibrated for the concentration of TDS by comparing model outputs to field determined profiles and lake discharge. The model tended to overpredict the concentration of TDS within the profiles and outflow, so it was evident that there was an inflow of low-TDS laden water that was unaccounted for. I returned to the lake in 2019 and found an additional inflow on the east end of the lake, near the lake inflow from UUL (16 U 578817 E 5393571) that was unaccounted for during model construction. The stream is fed by a wetland area, approximately 70 m east of the lake (Appendix A Figure A.16-A.17). The inflow was added to the model in segment 2, with a flow rate equal to five times the precipitation rate over the area of the lake. It is unlikely that this estimation is particularly accurate, but with it, reasonable concentrations of TDS within the lake and at the outflow were produced. The inflow chemical constituents were set to the same as the inflow from UUL. Additionally, it is possible that the stream gauging rating curve did not accurately account for the low flow period from UUL during the summer, as low flow periods are difficult to determine, often varying by an error of 5 – 10% (USGS, 2013). Increased flow rates from UUL at this time may have impacted modelled TDS concentrations.

The profiles and outflow concentration of TDS at the beginning and end of the year are reasonable. The profiles have a 17% AME and 12 % AME on June 8th and 26th, respectively (Figure 4.8). The error increased on the July 15th & August 6th profiles, resulting in an AME of 30% and 32%, respectively. The September 7th & October 6th profiles from the model were quite accurate, with an AME of 10% & 7%, respectively. The final profile sample date, October 30th, is immediately after turnover. There was a 28% error, as the lake had begun to re-stratify, while the model is still turning over during the match tolerance date of October 27th. The deepest 0.5 m however did not turnover in the model, while complete turnover was observed in the lake (Figure 4.8). The inhibition in mixing in the deepest 0.5 m was likely due to errors in the bathymetric grid artificially increasing frictional forces, as previously mentioned.

The model outflow TDS error followed a similar trend to the profiles, being fairly accurate early in the year, then overestimating in the summer and being quite accurate later in the model run year. From the beginning of the model run year to July 5th the outflow TDS had an error 29 ± 23% (Figure 4.9). The greatest error occurred during the summer (July 7th to September 5th), when the outflow TDS is 59 ± 33 % greater in the model. July 7th is marked by a rapid decrease in the concentration of TDS at the outflow. This corresponded with a high flow period from UUL (Fig. 4.3). The field determined outflow TDS was reduced to 131 mg/L, while the modelled TDS was only reduced to 309 mg/L, although the model and observed exhibited the same concentration on July 6th. It is likely that the inflow was under-predicted during the high flow period on July 7th, as a result in variable stage height, resulting in less low-TDS water diluting the high-TDS lake water within the model (USGS, 2013).

The model and field observed concentration of TDS at the outflow then tracked with a similar slope, increasing on average, 7.9 & 6.3 mg/L/day, respectively, until August 21rd, when the concentration of TDS plateaued in the field outflow. The plateau in the field outflow TDS is a result of Pond 102 not discharging at that time (Figure 4.3). The outflow TDS in the model reached a maximum of 830 mg/L on August 21, while the field observed outflow TDS was 660 mg/l at that time. After August 21st, the concertation of TDS in the model outflow was reduced, until it equaled the field outflow concentration on September 5th. The dilution in the model outflow was a result of in increase in flow rate from the added inflow at that time. The discrepancy in the concentration of TDS at the outflow during the summer months could be attributed to insufficiently modelling the high flow period on July 7th and under-estimating the inflow of low-TDS water at that time. The model tended to over-estimate the concentration of TDS in the deepest 1 m of the lake (< 303.6 MASL). This effect was evident, stating on July 15th and persisted throughout the model run year. The deviation increased to a maximum at the bottom of the lake. This was due to the variations in the model grid required to match the bathymetry of LUL. Deviations in the model grid work to increase the friction factor within the model, as previously mentioned. As a result, water discharged has a greater residence time and stability within the hypolimnion (Pentacost, 2016).

The CE-QUAL W2 manual suggested that dissolved oxygen profiles should have an AME less than 1 mg/L (Cole & Wells, 2013. Although the model did not include algae, all calibration dates were under 1 mg/L. The mean AME for all dates was 0.68 mg/L (Figure 4.9). On the June 8th the model overpredicted the depth of the saturation from the surface to the heterograde curve by ≈ 1 m. finish. Dissolved oxygen was well represented on September 7th and October 5th, during low flow periods for Pond 102 discharge. After turnover, on October 30th, the model dissolved oxygen remains as an isocline, fully saturated throughout the water column. However, within the Lower Unnamed Lake, hypolimnion dissolved oxygen is reduced to 8.3 mg/L, while the epilimnion had a concentration of 10.7 mg/L. The model did not account for an increased rate in oxygen consumption as a result of turnover (Galvez & Niell, 1992). The sediment in Lower Unnamed Lake consisted of a high proportion of organic matter, averaging 30% w/w, and low bulk density, averaging 0.14 g/cm^3. There were a large population of macrophytes, including *Equisetum sp*. and *Typha sp.* within the lake (Appendix A, Figure A.21). Macrophytes contribute autochthonous organic matter, which settles to the sediment and is then re-suspended during turnover, releasing nutrients and organic matter into the water column (Andersen & Olsen, 1994). This process results in an increased biological oxygen demand (Human *et al.* 2015). Sediment resuspension was one of, but not the only limitation in the CE-QUAL W2 model dissolved oxygen model of Lower Unnamed Lake. Future studies should include a detailed survey of the algal community to effectively include algae within the model.

Another source of error, which contributed to the discrepancies in hypolimnion dissolved oxygen was the distribution of inflows in CE-QAUL W2. Pond 102 discharge was assumed to be fully saturated. In the Lower Unnamed Lake, the discharge water flows over the littoral zone, over the sediment-water-interface, as the discharge water was more dense than the epilimnion. It is likely that at this time dissolved oxygen was consumed by the sediment. As a result, the discharge water would likely of have had a lower concentration of dissolved oxygen when it reached the hypolimnion (Matisoff & Gerald, 2005). The aforementioned process does not occur in CE-QUAL W2, as the model is laterally averaged. The model instantaneously input the discharge evenly, across the cell with corresponding density (Cole & Wells, 2013). Consequently, the concentration of dissolved oxygen in the model discharge water within the hypolimnion is greater than what was observed in the field.

The location of the point in which stormwater from Pond 102 was discharged into Lower Unnamed Lake was modified from the current location (16 U 577510 E 5393670), to the proposed location (16 U 578440 E 5393560), upstream on the east end of the lake. From herein, the current location model will be referred to CLM and the proposed location model will be referred to as the PLM. The current discharge location was located in the west basin of Lower Unnamed Lake, 0.15 km west of the deepest point in the lake of 4.5 - 5m (Figure 3.6). Water from the current location flowed from the discharge point, to the hypolimnion, causing the lake to be chemically stratified (Figure 4.8; Figure 4.14). The proposed discharge location is upstream, in the shallow channel of the lake, where depth averages ≈ 1 m (Figure.3.1). The proposed discharge is 0.75 km from the deepest point in the lake (Figure 3.6).

The PLM was set to the same initial conditions, including temperature, TDS, dissolved oxygen and nutrient profiles, inflow and outflow rates and weather conditions. The PLM contained two additional modifications: Pond 102 discharge temperature (^{o}C) and the coefficient of bottom heat exchange (CBHE) ($W\ m^{-2}\ {}^{o}C^{-1}$). The temperature of Pond 102 discharge was set to the field determined temperature, rather than the temperature at 304.5 MASL that the current discharge location was set to what was observed in the field, as it was assumed the discharge water wouldn't lose heat the sediment to the same degree as the CLM. To account for the thermal energy removed from the system in as a result of reducing 102 discharge temperature in the CML, the CBHE was increased from 0.3 to 1.0 ($W\ m^{-2}\ {}^{o}C^{-1}$), in the PLM. This assumption was done to maintain the temperature at the sediment-water interface, illustrated by Figure 4.12. When the CBHE of the PLM model was set to 0.3 ($W\ m^{-2}\ {}^{o}C^{-1}$), unrealistically high temperatures were produced at the sediment-water interface. After manipulation of the CBHE, the sediment temperature varied by a MAD of 1.05^{o}C, which is more realistic, as lake bottom sediment provides thermal inertia, therefore, temperature at the sediment-water interface should not be significantly impacted (Fang & Stefan, 1996).